Pontifícia Universidade Católica do Rio de Janeiro

João Henrique Paulino de Azevedo

Geospatial modelling for green hydrogen and derivatives production potential assessment

Tese de Doutorado

Thesis presented to the Programa de Pós-graduação em Engenharia Mecânica do Centro Técnico Científico of PUC-Rio, in partial fulfillment of the requirements for the degree of Doutor em Engenharia Mecânica.

Advisor: Prof. Sergio Leal Braga
Co-advisor: Florian Alain Yannick Pradelle
Co-advisor: Prof. Ulf Moslener

Rio de Janeiro

May 2025

PONTIFÍCIA UNIVERSIDADE CATÓLICA
DO RIO DE JANEIRO

João Henrique Paulino de Azevedo

Geospatial modelling for green hydrogen and derivatives production potential assessment

Thesis presented to the Programa de Pós-Graduação em Engenharia Mecânica do Centro Técnico Científico of PUC-Rio, in partial fulfillment of the requirements for obtaining the degree of Doutor em Engenharia Mecânica. Approved by the Examination Committee:

Prof. Sergio Leal Braga
Advisor
Departamento de Engenharia Mecânica - PUC-Rio

Prof. Florian Alain Yannick Pradelle
Co-advisor
Departamento de Engenharia Mecânica - PUC-Rio

Prof. Ulf Moslener
Co-advisor
UNEP Collaborating Centre für Climate and Sustainable Energy Finance
Frankfurt School

Prof. Edmar Luiz Fagundes de Almeida
Instituto de Energia da PUC-Rio – PUC-Rio

Prof. Rodrigo Flora Calili
Programa de Pós-Graduação em Metrologia - PUC-Rio

Eduardo Torres Serra
ES+PS Consultoria

Prof. Juan Jose Garcia Pabon
Instituto de Engenharia Mecânica - UNIFEI

Rio de Janeiro, May 12th, 2025

João Henrique Paulino de Azevedo

Graduated in Mechanical Engineering from the Pontifical Catholic University of Rio de Janeiro (PUC-Rio) in 2014 with a sandwich degree being held at the Australian National University (ANU). Master's in mechanical engineering with emphasis in Petroleum and Energy from PUC-Rio. He has more than 10 years of experience in the management and execution of projects aimed at energy generation, sustainability and education. Works as a researcher at PUC-Rio and FGV Energia, as well as a consultant for the World Bank and the Chamber of Electric Energy Commercialization (CCEE).

Bibliographic data

Azevedo, João Henrique Paulino de

Geospatial modelling for green hydrogen and derivatives production potential assessment/ João Henrique Paulino de Azevedo; Advisor Sergio Leal Braga; co-advisor Florian Alain Yannick Pradelle; co-advisor Ulf Moslener. – 2025.

147 f. : il. color. 29,7 cm

Tese (doutorado) - Pontifícia Universidade Católica do Rio de Janeiro (PUC-Rio), Departamento de Engenharia Mecânica, 2025.

Inclui bibliografia

1. Engenharia Mecânica – Teses. 2. Hidrogênio. 3. Energia renovável. 4. Potencial bruto. 5. Potencial técnico. 6. Modelagem geoespacial. I. Leal Braga, Sergio II. Pradelle, Florian Alain Yannick. III. Moslener, Ulf. IV. Pontifícia Universidade Católica do Rio de Janeiro. Departamento de Engenharia Mecânica 2025. V. Título.

CDD: 621

Acknowledgements

This study was financed in part by the Coordenação de Aperfeiçoamento de Pessoal de Nível Superior - Brasil (CAPES) - Finance Code 001. The authors thank Energy Assets do Brasil Ltda. for their financial support through their ANEEL R&D budget.

I owe my deepest gratitude to my family, for their unconditional love, care, and the educational and moral foundations they provided. Their constant encouragement and belief in me have been my greatest incentive. To my wife, Gisele, whose patience, affection, and tireless support have sustained me through every challenge; and to my son, João Vicente, whose arrival we eagerly anticipate.

I am profoundly thankful to my advisor, Prof. Sérgio Leal Braga, for his insightful guidance, rigorous standards, and unwavering confidence in my work; and to my co-advisor, Prof. Florian Alain Yannick Pradelle, for his thoughtful suggestions and generous mentorship.

Finally, I wish to acknowledge Ricardo Gedra at CCEE and Felipe Gonçalves at FGV Energia for their professional guidance and for opening doors to opportunities that have shaped my career. Your mentorship has been instrumental in my development as a researcher and engineer, and I am thankful for your kindness and expertise.

Abstract

Azevedo, João Henrique Paulino de; Leal Braga, Sergio (Advisor). **Geospatial modelling for green hydrogen and derivatives production potential assessment**. Rio de Janeiro, 2025. 147p. Tese de Doutorado – Departamento de Engenharia Mecânica, Pontifícia Universidade Católica do Rio de Janeiro.

This thesis develops and demonstrates two complementary geospatial tools—the GeoH$_2$-PAM framework for mapping gross, technical, and economic potential and the GeoH$_2$-FAT for site-specific techno-economic and environmental feasibility analyses—to assess the production potential of green hydrogen and its derivatives (ammonia and methanol) from renewable energy sources (solar photovoltaic, onshore wind, and offshore wind). High-resolution datasets for these resources are combined with eighteen environmental, technical, social, and economic constraints to transform theoretical (gross) resource estimates into realistic (technical) potentials. The framework employs production models for water electrolysis and subsequent chemical conversion, calibrated against region-specific data, while incorporating exclusion criteria such as capacity factor thresholds, infrastructural setbacks, and environmental protection zones. In the Brazilian context, the analysis reveals significant reductions in deployable capacity due to constraints, thereby exposing the divergence between idealized resource availability and practical implementation. Furthermore, a techno-economic evaluation using LCOE and LCOH metrics—and preliminary market-viability insights from GeoH$_2$-FAT—provides critical guidance for optimized site selection and policy decisions. This work thus contributes to advancing geospatial methodologies for renewable energy integration and supports the formulation of sustainable investment strategies that are essential for global decarbonization efforts.

Keywords

Hydrogen; Renewable energy; Gross potential; Technical potential; Geospatial modeling

Resumo

Azevedo, João Henrique Paulino de; Leal Braga, Sergio. **Modelagem geoespacial para a avaliação do potencial de produção de hidrogênio e derivados**. Rio de Janeiro, 2025. 147p. Tese de Doutorado – Departamento de Engenharia Mecânica, Pontifícia Universidade Católica do Rio de Janeiro.

Esta tese desenvolve e demonstra dois instrumentos geoespaciais complementares – o framework GeoH_2-PAM para mapear potenciais bruto, técnico e econômico e a ferramenta GeoH_2-FAT para análises de viabilidade técnico-econômica e ambiental site-specific – para avaliar o potencial de produção de hidrogênio verde e seus derivados (amônia e metanol) a partir de fontes renováveis (solar fotovoltaica, eólica onshore e eólica offshore). Conjuntam-se bases de dados de alta resolução para esses recursos com dezoito restrições ambientais, técnicas, sociais e econômicas, de modo a converter estimativas teóricas (brutas) em potenciais realistas (técnicos). O framework emprega modelos de produção por eletrólise da água e conversão química subsequente, calibrados com dados regionais, incorporando critérios de exclusão como limiares de fator de capacidade, recuos de infraestrutura e zonas de proteção ambiental. No contexto brasileiro, a análise revela reduções significativas na capacidade implantável devido a tais restrições, evidenciando a divergência entre disponibilidade idealizada e implementação prática. Além disso, uma avaliação tecno-econômica com métricas de Custo Nivelado de Energia Elétrica (LCOE) e Custo Nivelado de Hidrogênio (LCOH) – e insights preliminares de viabilidade de mercado a partir do GeoH_2-FAT – fornece orientações críticas para a seleção otimizada de sites e a formulação de políticas. Este trabalho contribui, assim, para o avanço de metodologias geoespaciais na integração de energias renováveis e apoia a definição de estratégias de investimento sustentáveis, essenciais para os esforços globais de descarbonização.

Palavras-chave

Hidrogênio; Energia renovável; Potencial bruto; Potencial técnico; Modelagem geoespacial

Table of Contents

List of figures

List of tables

List of symbols

Symbol / Acronym	Description	Units
AAS	American Amortization System	–
ACL	Free Power Market (Ambiente de Contratação Livre)	–
AWE	Alkaline Water Electrolysis	–
CAPEX	Capital Expenditure	$
CBIO	Decarbonization Credit (RenovaBio)	–
CCS	Carbon Capture and Storage	–
CF	Capacity Factor	– (dimensionless)
D_{ES}	Final energy demand	GWh
DNI	Direct Normal Irradiation	kWh/m^2
EEZ	Exclusive Economic Zone	–
EUSD	Electricity Distribution System Usage Charge	$/MWh
EUST	Electricity Transmission System Usage Charge	$/MWh
FC_{ES}	Conversion factor (tH_2 per unit energy)	tH_2/MWh
GeoH_2 FAT	Geospatial Hydrogen Feasibility Analysis Tool	–
GeoH_2 PAM	Geospatial Hydrogen & Derivatives Potential Assessment Model	–
GHI	Global Horizontal Irradiation	kWh/m^2
GIS	Geographic Information System	–
GSA	Global Solar Atlas	–

Symbol / Acronym	**Description**	**Units**
GWA	Global Wind Atlas	–
IEC	International Electrotechnical Commission	–
iREC	International Renewable Energy Certificate	–
IRR	Internal Rate of Return	%
ISF	Inverter Sizing Factor	–
LCA	Life Cycle Assessment	–
LCOA	Levelized Cost of Ammonia	\$/t NH_3
LCOE	Levelized Cost of Electricity	\$/MWh
LCOH	Levelized Cost of Hydrogen	\$/kg H_2
LCOM	Levelized Cost of Methanol	\$/t CH_3OH
LiDAR	Light Detection and Ranging	–
NNN	Number of energy source types	–
NPV	Net Present Value	\$
O&M	Operation & Maintenance	\$/year
OFW	Offshore Wind	–
ONW	Onshore Wind	–
OPEX	Operating Expenditure	\$/year
$P_{H_2,ES}$	Hydrogen potential per energy source	t H_2
PEM	Polymer Electrolyte Membrane electrolysis	–
PRICE	French Amortization System (equal installments)	–
PVOUT	Photovoltaic output	kWh/kWp
R_{ES}	Inventory of energy resource	GWh

Symbol / Acronym	**Description**	**Units**
RES	Renewable Energy Sources	–
SAC	Constant Amortization System	–
SMR	Steam Methane Reforming	–
SOEC	Solid Oxide Electrolysis Cell	–
SPV	Solar Photovoltaic	–
TAC	Credti Originating Fee (*Taxa de Abertura de Crédito*)	%
WRF	Weather Research and Forecasting model	–

"We cannot solve our problems with the same thinking we used when we created them."

Albert Einstein

1 Introduction

Accelerating climate change and the geopolitical vulnerabilities of fossil-fuel supply chains have made deep decarbonization a strategic priority for governments and industry alike. Recent scenario studies show that meeting the Paris-Agreement temperature targets will require cutting energy-related CO_2 emissions by 45–60 % before 2035, a goal that hinges on rapid electrification, large-scale deployment of variable renewables, and the parallel roll-out of low-carbon gases such as hydrogen and its derivatives [1,2]. Green hydrogen produced via electrolysis powered by solar and wind resources is especially attractive because it can substitute fossil hydrogen in fertilizer and refining sectors, provide a clean feedstock for synthetic fuels, and act as a long-duration storage medium that complements batteries in renewable-rich power systems [3]. Analysts estimate that green hydrogen could supply 10-20 % of final energy demand and avoid six gigatonnes of CO_2 yr^{-1} by mid-century—provided that production costs fall below ≈ USD 2 kg^{-1} and that suitable sites for large electrolysers are identified in time [4]

Brazil is unusually well placed to contribute to—and benefit from—this emerging hydrogen economy. The country possesses some of the world's highest-quality solar irradiance and onshore/offshore wind regimes, alongside a predominantly renewable power grid and an extensive network of deep-water ports that could support ammonia or methanol exports [5]. Turning these theoretical attributes into bankable projects, however, requires reconciling resource abundance with land-use competition, biodiversity protection, grid capacity, and socio-economic constraints. High-resolution geospatial analysis is therefore indispensable for pinpointing locations where ample renewable potential aligns with infrastructure and environmental suitability.

The evolution of Geographic Information Systems (GIS) from its early cartographic origins to the sophisticated spatial analysis tools available today has revolutionized the way renewable energy resources are assessed. Early mapping efforts, such as John Snow's cholera map [6], laid the foundation for spatial problem-solving, while subsequent developments by pioneers like Roger Tomlinson led to modern GIS applications in planning and environmental management [7]. In recent decades, the rapid improvement in data availability, remote sensing techniques, and computational power has fostered the emergence of high-resolution geospatial models capable of capturing the heterogeneous nature of renewable resources.

Renewable-energy technologies —notably solar photovoltaic (SPV) arrays and modern wind turbines—have advanced rapidly as high-resolution resource data, remote-sensing products, and GIS toolkits have matured [8–10]. These geospatial advances now support rigorous "gross-to-technical" potential studies that merge resource quality with land-use, topographic, and environmental exclusion layers, yielding more realistic estimates of deployable capacity [11–13]. At the same time, the strategic push for green hydrogen has spawned a parallel literature that couples such spatial resource layers with electro-hydrogen production models, permitting joint evaluation of renewable availability and the techno-economic feasibility of converting that energy into hydrogen (and downstream derivatives such as ammonia or e-methanol) [14–16].

Building on these advances, the present thesis introduces two complementary instruments. The GeoH$_2$-Potential Assessment Model (GeoH$_2$-PAM) converts global solar- and wind-resource rasters into maps of gross, technical, and economic potential for hydrogen, ammonia, and methanol, after applying eighteen environmental, social, technical, and economic exclusion layers. The GeoH$_2$-Feasibility Analysis Tool (GeoH$_2$-FAT) then drills down to the plant scale, simulating site-specific techno-economic and life-cycle-emission outcomes for alternative supply-chain configurations.

1.1 Motivation

Brazil possesses some of the world's most abundant solar and wind resources, yet translating this theoretical wealth into deployable green hydrogen projects requires navigating a complex landscape of land-use restrictions, environmental protections, and infrastructure limitations. Conventional resource assessments—which often consider only gross resource availability—tend to overestimate practical capacity by neglecting these real-world constraints. Furthermore, developers and policymakers lack both a strategic, territory-wide perspective on hydrogen potential and a detailed, site-level feasibility tool to evaluate specific project configurations.

From the systematic literature review (Section 2.1 and 2.2), it was not identified any previews studies that concurrently:

1. Generates one-kilometre–resolution maps for solar PV, onshore-wind, and offshore-wind hydrogen, ammonia, and methanol production potentials for Brazil while applying a uniform set of eighteen geospatial constraints;
2. Links those spatial results to pixel specific levelized cost surfaces (LCOE, LCOH, LCOA, LCOM); and
3. provides an open, modular GIS-connected feasibility platform (GeoH$_2$-FAT) that allows plant-scale capital- and operating-cost, financing, storage, transport, and cradle-to-grave life cycle analysis.

Accordingly, this thesis is motivated by three primary needs:

1. Use GeoH$_2$-PAM to move beyond idealized resource maps and quantify realistic (technical and economic) hydrogen and derivative potentials by integrating geospatial constraint layers.
2. Use GeoH$_2$-PAM to secure national and regional authorities with high-resolution, multi-layered potential maps that inform energy policy, land-use planning, and investment prioritization.
3. Use GeoH$_2$-FAT to provide developers with a flexible, site-specific tool that simulates techno-economic and environmental performance—covering production, storage, and transport—for tailored hydrogen project scenarios.

1.2 Objectives

The main objective of this thesis is to develop and validate geospatial modelling framework (GeoH$_2$-PAM) and a complementary feasibility analysis tool (GeoH$_2$-FAT) for assessing the production potential of green hydrogen and its derivatives from renewable energy resources. This original approach encompasses the entire spectrum from theoretical resource evaluation to the incorporation of practical technical and economic constraints, thereby bridging the gap between idealized resource assessments and deployable, sustainable energy solutions. Specific objectives include:

1. **Assemble and process renewable data for GeoH$_2$-PAM**: Gather solar PV, onshore wind, and offshore wind datasets, and convert them into capacity-factor layers suitable for input into the GeoH$_2$-PAM framework.
2. **Build production models within GeoH$_2$-PAM**: Develop mathematical routines that convert renewable power profiles into hydrogen output via electrolysis, and extend these to ammonia and methanol using appropriate conversion factors.
3. **Layer geospatial constraints in GeoH$_2$-PAM**: Identify and apply economic, environmental, social, and technical exclusion or setback layers to transform gross resource maps into realistic technical potential maps and calculate the potential for a giving area.
4. **Map economic potential with GeoH$_2$-PAM**: Compute Levelized Cost of Electricity (LCOE) and Levelized Cost of Hydrogen (LCOH) at each location and produce georeferenced cost maps.
5. **Develop GeoH$_2$-FAT**: Create a modular, plant-level tool that integrates Energy supply, Hydrogen production, Storage & Transport, and Financing into a single framework for techno-economic and environmental analysis.
6. **Validate GeoH$_2$-FAT** through case studies: Apply the tool to three scenarios (100 % PV, 100 % wind, and a 1/3 PV–1/3 wind–1/3 grid mix) at the Port of Pecém, running sensitivity tests on CAPEX, OPEX, resource availability, and financing to gauge impacts on LCOE, LCOH, IRR, and avoided-emissions revenue.

1.3 Scope of this work

To guide the reader through the development and application of the GeoH$_2$-PAM and GeoH$_2$-FAT tools, the structure of this thesis is organized into the following chapters, each addressing a key component of the work. The scope of this work is systematically delineated across the subsequent chapters, as follows:

Section 2 – Literature review: This section presents a comprehensive review of the extant literature on geospatial modelling for renewable energy and hydrogen production potential assessments. It critically examines previous methodologies, including those employed by prominent institutions such as the National Renewable

Energy Laboratory (NREL) and Brazil's Energy Research Office (EPE), thus establishing the theoretical and methodological foundations of the study.

Section 3 – Methodology: In this section, the detailed methodology developed for the present work is described. It outlines the acquisition and processing of high-resolution datasets for solar photovoltaic (SPV), onshore wind (ONW), and offshore wind (OFW) resource for GeoH_2-PAM, and then details the modular architecture of GeoH_2-FAT, covering its Energy, Production, Storage & Transport, and Financing blocks. The integration of 18 geospatial constraint layers—categorized into economic, environmental, social, and technical factors—is explained, alongside the mathematical models for hydrogen, ammonia, and methanol production.

Section 4 – Results and discussion: This section presents two complementary result streams. First, the application of GeoH_2-PAM to Brazil is detailed, featuring georeferenced maps and quantitative analyses that illustrate discrepancies between theoretical (gross), technical, and economic potentials for green hydrogen and its derivatives under varying constraint scenarios. Second, the capabilities of GeoH_2-FAT are demonstrated through three site-specific case studies—including 100 % solar, 100 % wind, and a hybrid mix—with sensitivity analyses of CAPEX, OPEX, and financing parameters.

Section 5 – Conclusions and future work: The final section synthesizes the main findings, discusses their significance for Brazil's hydrogen strategy. Furthermore, it outlines future research topics, including variable capacity-density analyses, alternative plant configurations, additional RES and constraint layers, higher-resolution and local datasets, and integration of certification and GHG-accounting frameworks.

2 Literature review

This section synthesizes the key advances and methodologies in geospatial modelling as they relate to both renewable energy resource assessments and hydrogen production potential. It begins by examining foundational work in GIS-based mapping of wind, solar, and biomass potentials, then turns to studies that specifically integrate these resources into hydrogen production frameworks. Next, it clarifies the evolving terminology used to classify resource potentials—from gross to market levels—and finally it contrasts global approaches with Brazil's national assessments.

In the following subsections, Section 2.1 presents a brief literature review on the use of geospatial modelling for renewable energy potential assessments, Section 2.2 provides a detailed review of research focused on geospatial modelling for hydrogen production potential mapping and assessment, Section 2.3 examines the terminology and classification schemes used to define and differentiate gross, technical, economic, and market resource potentials, and Section 2.4 outlines Brazil-specific considerations by comparing national-level estimates from the Energy Research Office (EPE) with the more granular frameworks employed by international bodies such as NREL.

2.1 Geospatial modelling for renewable energy potential assessment

Geospatial modelling has become a cornerstone for assessing the potential of renewable energy sources (RES) at multiple spatial scales, from continental to neighborhood levels. On early 1990s, [17] recognized the importance of Geographic Information Systems (GIS) in regional planning, including energy-related decision-making. By the late 1990s, GIS-based approaches were already being used to identify suitable sites and estimate biomass, wind, and solar potentials [8,18–21]. As noted by [22], publications integrating GIS and renewables have been growing rapidly thanks to improvements in data availability, remote sensing techniques, and computing power.

A primary strength of GIS lies in its capacity to bring together heterogeneous data sources—such as in situ measurements, reanalysis datasets, remote sensing products, Light Detection and Ranging (LiDAR), and high-resolution digital elevation models. This integration enables researchers to create detailed resource-availability maps for a variety of renewable energy types. For instance, biomass assessments have drawn on extensive satellite imagery, inventory data, and LiDAR to optimize the siting of biomass-based plants [23,24]. Studies in this field often involve mathematical programming or agent-based modelling to link potential biomass feedstocks with electricity or heat generation [25,26].

Wind and solar energy assessments have similarly benefited from GIS. Early work on solar energy potential produced large-scale "solar cadastres" by linking ground-station data with geostatistical interpolations or statistical methods [9,27]. Later approaches integrated satellite-derived solar irradiance maps, local meteorological data, and fine-resolution LiDAR-based elevation models to account for terrain effects and urban shading [28,29]. One challenge in such high-resolution approaches is computational cost, addressing complex environments often employ specialized algorithms and GPU-accelerated methods to handle large LiDAR datasets efficiently [30].

Wind-energy assessments, meanwhile, range from global to micro-scale analyses of wind speed and power density. Early global and country-level studies relied on geostatistics and sparse in situ measurements [31]. Later, more sophisticated wind atlases emerged, using computational fluid dynamics (CFD) and atmospheric mesoscale models—such as the Weather Research and Forecasting model (WRF)—to downscale reanalysis data and produce wind maps at finer resolutions [32]. Through GIS, researchers combine terrain slope, accessibility, predominant wind direction, and other factors to determine optimal siting of wind farms and turbines [10,33]. In particular, [34] developed a GIS-based decision support system that incorporated constraints such as resource availability, infrastructure costs, environmental limitations, and financial metrics to evaluate wind energy potential.

2.2 Geospatial modelling for hydrogen production potential assessment

Geospatial modelling plays a essential role in assessing the potential for hydrogen production by integrating geographical data with various technological and energy parameters. This approach enables the identification of optimal locations for hydrogen production facilities based on the availability of renewable energy resources, technological capabilities, and economic feasibility.

The trajectory of geospatial modelling for hydrogen production potential assessment has evolved significantly over the past decade, reflecting advancements in technology and a growing emphasis on sustainable energy solutions. Beginning in 2012 with Dagdougui [35] in Liguria, Italy, early studies focused on assessing both production and storage potential using Proton Exchange Membrane (PEM) electrolysis powered by solar photovoltaic (PV) and onshore wind. This foundational work set the stage for subsequent research that increasingly integrated diverse renewable energy sources and more sophisticated modelling techniques.

In 2014, Sigal et al. explored the production potential in Argentina by incorporating multiple renewable sources, including solar PV, onshore wind, and biomass, thereby broadening the scope of geospatial assessments [14]. Esteves et al. [36] further expanded this approach by evaluating hydrogen and ammonia production potential in Ceará, Brazil, using similar renewable energy combinations. This study was the first identified for Brazil and encompassing ammonia. Rahmouni et al. [37] continued this trend in Algeria, not only assessing production potential but also prospecting future demand, which emphasized the importance of aligning production capabilities with market needs.

The introduction of Alkaline Water Electrolysis (AWE) in Iran by Ashrafi et al. [38] and the subsequent studies in Morocco by Touili et al. [39] demonstrated a diversification in electrolysis technologies and power sources, enhancing the accuracy and applicability of geospatial models. By 2019, research had expanded both geographically and technologically. Nielsen and Skov [40] in Denmark developed investment screening models for national-scale power-to-gas plants, while Nematollahi et al. [41] conducted techno-economic assessments in Iran using solar and wind resources. Feitz et al. [42] broadened the geographical focus to Australia, evaluating production potential across various renewable sources and electrolysis technologies. These studies collectively highlighted the versatility and scalability of geospatial modelling in different regional contexts.

The year 2020 marked significant contributions from the USA and Algeria, with Connelly et al. [13] assessing a wide array of production technologies and power sources, and Messaoudi et al. [43] refining GIS-based multi-criteria decision-making methods for solar hydrogen production site selection. These advancements underscored the integration of comprehensive datasets and multi-faceted analytical frameworks in geospatial modelling.

In the subsequent years, from 2021 to 2023, the focus intensified on optimizing production potential and cost assessments across diverse regions. Almutairi et al. [44] and Herwartz et al. [45] investigated the economic aspects of hydrogen production in Afghanistan and Germany, respectively, while studies in Ghana, Ireland, Yazd (Iran), Algeria, and Kenya [15,46–49] employed advanced geospatial approaches to delineate production potentials and identify optimal locations. These recent studies illustrate a maturation of geospatial modelling techniques, incorporating economic viability and cost-efficiency alongside technical assessments.

Recently, the International Energy Agency (2024), in its Global Hydrogen Review 2024 [3], presented a global map of hydrogen production costs derived from hybrid solar photovoltaic (PV), onshore wind, and offshore wind systems. These maps depict the LCOH at each location by incorporating hourly solar PV and onshore wind capacity factors, cost-optimal capacities for PV, wind, and electrolysers, and flexibility measures such as battery storage or curtailment—an analysis carried out using the ETHOS model suite of the Institute of Energy and Climate Research-IEK-3 at Forschungszentrum Jülich. In addition to LCOH values, the maps also show solar PV capacity share, ranging from 100% (exclusive solar PV) to 0% (purely wind-based), illustrating various hybrid system configurations. The assessment assumes optimal oversizing of renewable plants to minimize LCOH, applies a uniform cost of capital of 9%, and uses CAPEX ranges for solar PV (USD 380–1,300 kW^{-1}), onshore wind (USD 980–3,260 kW^{-1}), and offshore wind (USD 1,770–4,300 kW^{-1}). Water costs are excluded. Figure 1 illustrates this map.

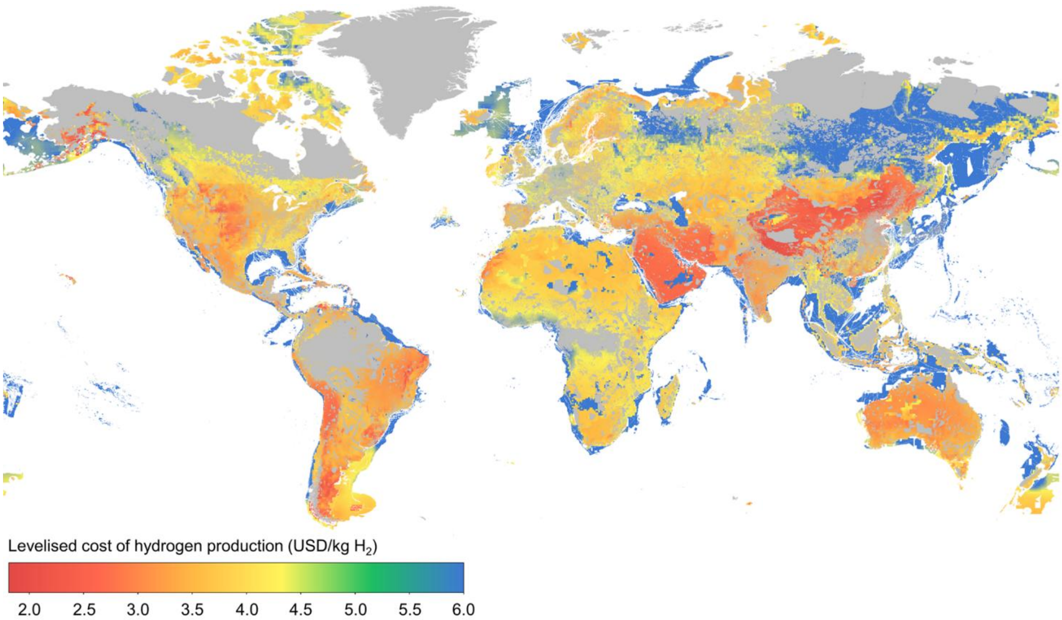

Figure 1 - Hydrogen production cost from hybrid solar PV and onshore wind, and from offshore wind in the Net Zero Emissions by 2050 Scenario, 2030.
Source: Retrieved from [3].

Another important recent initiative is from Agora [50–52]. The organization developed an in-house model—based on the PyPSA framework—for calculating and mapping the LCOH across Brazil, Europe, and Southeast Asia. In the European context, the work culminated in the “EU map of hydrogen production costs,” which identifies promising “hotspots” of low-cost renewable electricity and explores techno-economic factors such as plant oversizing, electrolyser operation strategies, and cost-of-capital variations between regions. Equally relevant for Brazil and Southeast Asia, the model highlights key drivers for early adoption—namely, direct sourcing of cost-effective electricity, optimizing solar PV-wind capacity shares, and siting electrolysers where abundant renewable potential meets industrial demand.

Table 1 presents relevant international experiences related to the determination of hydrogen potential through geospatial modelling, alongside the hydrogen production technologies addressed and the renewable energy sources used for the assessment.

Table 1 - Studies found in the literature that generated georeferenced maps of hydrogen production potential.

Reference	Year	Country/ Region	Production technologies	Power source	Findings
[35]	2011	Liguria, Italy	Electrolysis (PEM)	Solar PV and onshore wind	Production and storage potential
[14]	2014	Argentina	Electrolysis	Solar PV, onshore wind, and biomass	Production potential
[36]	2015	Ceará, Brazil	Electrolysis	Solar PV and onshore wind	Hydrogen and ammonia production potential
[37]	2016	Algeria	Electrolysis (PEM)	Solar PV and onshore wind	Production potential and

Reference	Year	Country/ Region	Production technologies	Power source	Findings
					demand prospecting
[39]	2018	Morocco	Electrolysis (PEM)	Solar PV	Production potential
[38]	2018	Iran	Electrolysis (AWE)	Onshore wind	Production potential with different turbines
[40]	2019	Denmark	Electrolysis (AWE and SOE)	Electricity grid	Potential locations for P2G plants
[41]	2019	Iran	Electrolysis	Solar PV and onshore wind	Production potential
[42]	2019	Australia	Electrolysis and coal gaseificaçao OR SMR with CCS	Solar PV, onshore wind and hydraulic	Production potential and potential locations
[13]	2020	USA	Electrolysis, coal, biomass and SMR with and without CCS	Nuclear, onshore wind, solar PV, biomass, hydraulic and geothermal	Production potential and potential locations
[43]	2020	Algeria	Electrolysis (PEM)	Solar PV	Production potential and potential locations
[44]	2021	Badakhshan, Afghanistan	Electrolysis (PEM)	Onshore wind	Production potential
[45]	2021	Berlin, Germany	Electrolysis (PEM)	Onshore wind	Production cost
[53]	2022	Europe	Biomass (bio-methane) with SMR and CCS	Biomass (different residues)	Production potential
[54]	2022	Eastern region of Marocco	Electrolysis (PEM)	Solar PV	Production potential
[55]	2022	Canada	Electrolysis (PEM)	Solar and o	Production potential and potential locations
[56]	2022	Piura, Peru	Electrolysis (PEM)	Solar PV and onshore wind	Production potential
[57]	2022	Urban zones in Mexico	Electrolysis (AWE and PEM)	Solar PV	Production potential and cost
[58]	2022	Punjab, Pakistan	Biomass gasification	Biomass (different residues)	Production potential
[59]	2022	Southern Thailand	Electrolysis (PEM)	Solar PV	Production potential and potential locations
[15]	2023	Ghana	Electrolysis (PEM)	Solar PV and onshore wind	Production potential and

Reference	Year	Country/ Region	Production technologies	Power source	Findings
					potential locations
[46]	2023	Ireland	Electrolysis (PEM)	Offshore wind	Production potential and cost
[47]	2023	Yazd, Iran	Electrolysis	Onshore wind	Production potential and potential locations
[60]	2023	Yazd, Iran	Electrolysis (PEM)	Solar PV	Production potential and potential locations
[48]	2023	Algeria	Electrolysis (AWE)	Onshore wind	Production potential, cost and location
[49]	2023	Kenya	Electrolysis (AWE and PEM)	Solar PV and onshore wind	Production potential, cost and location
[3]	2024	World	Electrolysis	Solar PV and, onshore and offshore wind	Production cost
[50–52]	2024	Brazil, EU and Southeast Asia	Electrolysis	Solar PV and onshore wind	Production cost

Legend: PEM = Proton Exchange Membrane; AWE = Alkalyne Water Electrolysis; SOEC = Solid Oxide Electrolysis; SMR = Steam Methane Reforming; CCS = Carbon Capture and Storage; PV = Photovoltaic

Source: Own elaboration through references indicated in the table.

2.3 Terminology for renewable energy potential assessment

A further aspect to consider alongside geospatial modelling is how renewable energy (RE) potentials themselves are classified in the literature. Over the past decades, various authors have proposed overlapping or conflicting categories such as “gross potential”, “theoretical potential,”, “geographical potential”, “technical potential,” “economic potential,” and “market potential”. However, there is little consensus on how these terms should be defined[61–64]. While some focus on resource-focused definitions (e.g., theoretical and geographic constraints), others introduce socio-political factors or economic barriers more explicitly. These divergences emphasize the complexity of comparing potential estimations across different studies.

For example, [64] highlights “realistic” and “realizable” potentials, drawing attention to social acceptance and regulatory issues that influence how much of a theoretical resource can actually be tapped. [61], by contrast, emphasize a multi-step funnel—moving from theoretical resources down through geographic, technical, economic, and market potential—but leave questions open about which costs, policy frameworks, or demand-side factors are factored into each step. Later work by [62] and [63] refines these concepts, referencing time dynamics ("mid-term potential") or market growth limits ("deployment potential"), yet no universal scheme has emerged. As these authors illustrate, classification of RE potentials is not just a scientific challenge—it also hinges on policy, economics, land use, and technological trajectories. Researchers undertaking geospatial modelling projects must therefore be clear on how they define and constrain resource potentials, especially when integrating factors such as socio-political acceptance and demand-side considerations.

Building on the varying definitions of RE potential outlined above, the U.S. Department of Energy (DOE) and its National Renewable Energy Laboratory (NREL) have been doing an extensive work on the matter of renewable energy resource assessment. As summarized by [11] and [65], this approach distinguishes four main categories of potential—gross resource potential, technical potential, economic potential, and market potential—each adding specific constraints and considerations. The first two (gross resource potential and technical potential) generally focus on physical resource availability and broad technical constraints, while the latter two (economic potential and market potential) incorporate economic, policy, and market factors to increasingly narrow the subset of feasible projects or installations. Figure 2 represents these categories.

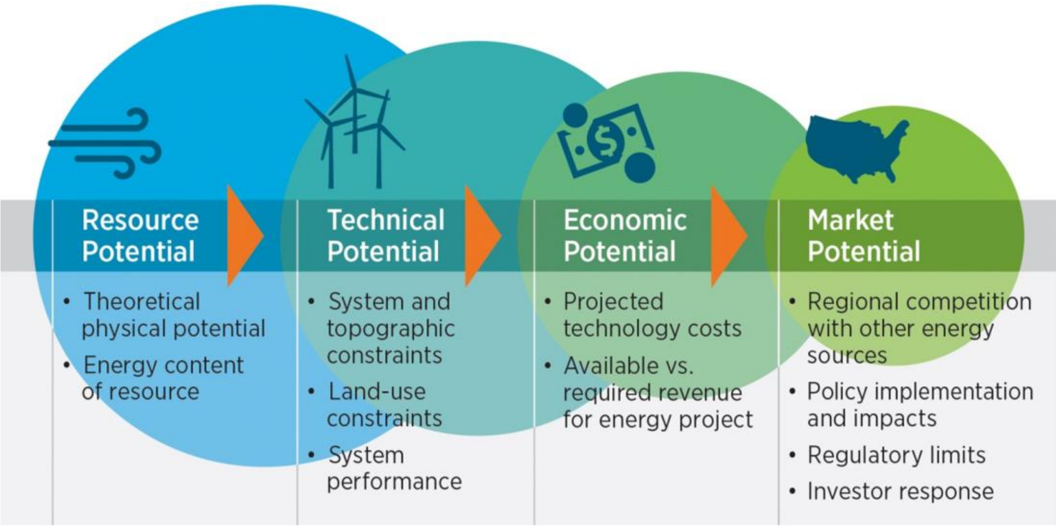

Figure 2 - Levels of renewable energy resource potential assessment used by NREL. Source: Retrieved from [11].

Gross resource potential or just gross potential refers to the theoretical amount of energy physically available within a given region, such as the incident solar energy striking the Earth's surface or the total wind resource at a certain turbine hub height. This top-level estimate excludes no land or topographic restrictions, providing a starting point to measure how much resource is theoretically present.

Technical potential constrains gross resource potential by including system performance parameters, land use limitations, and environmental and topographical constraints. For instance, typical NREL assessments account for wind turbine setbacks and terrain slope when estimating technical wind power capacity [66,67].

Technical potential effectively answers the question: "How much energy could we convert with current technologies, if we ignore economic or policy considerations, but account for physical siting and resource-quality issues?"

Economic potential adds a cost and revenue dimension: it is the portion of technical potential that is economically viable under a given set of cost assumptions —capital expenditures, operation and maintenance, financing) and revenue or avoided cost assumptions [11,67]. Economic potential thus captures whether the project's cost of generation (presented as LCOE) is less than or equal to the value of the electricity generated (often represented as levelized avoided cost of energy, LACE). When LCOE is lower than or comparable to LACE—possibly taking into account grid interconnection costs, carbon pricing, or other externalities—the resource is said to have positive net value [11]. Because of the inherent uncertainties in technology costs, system performance, electricity price trajectories, and policy conditions, the boundaries of economic potential can evolve over time. NREL's analyses often emphasize this dimension by constructing high-resolution geospatial "supply curves" that show how much capacity is economically viable at various price levels [65,67].

Market potential adds yet another layer by considering the actual share of resources likely to be deployed under policy frameworks, real-world constraints (e.g., project financing hurdles, regulatory approval processes, investor decision-making, public acceptance, or competing technologies), and overall market dynamics. Although market potential estimates can be informed by capacity expansion and dispatch models, such as NREL's Regional Energy Deployment System (ReEDS), they remain scenario-dependent and are not strictly a function of cost and resource quality alone [11,68].

In this thesis, GeoH_2-PAM is employed to quantify both gross and technical resource potentials—assessing available land area and corresponding power capacity, and then translating these into hydrogen, ammonia, and methanol yields—and to map economic potential via LCOE and LCOH. GeoH_2-PAM's economic outputs then inform downstream analyses, while GeoH_2-FAT builds on these maps to perform site-specific techno-economic and environmental simulations, offering preliminary insights into deployment feasibility and nascent market viability. Although full market-potential modeling lies beyond GeoH_2-PAM's scope, GeoH_2-FAT's case studies provide early indicators of investor returns and policy impacts. During the course of this research, the author also contributed to the book The Hydrogen Economy: Transition, Decarbonization, and Opportunities for Brazil (Portuguese: *A Economia do Hidrogênio: Transição, Descarbonização e Oportunidades para o Brasil*), where broader economic and market aspects of hydrogen project development in Brazil are examined in depth.

2.4 Considerations for the potential assessment in Brazil

The Energy Research Office (EPE), under the Ministry of Mines and Energy (MME) in Brazil, plays a critical role in assessing the country's energy and hydrogen resource potential. This section provides an overview of the methodologies and data used by EPE for energy resource potential estimation, focusing on renewable energy sources and hydrogen production potential.

According to the EPE report on energy resources potential for 2050 horizon [5], the evaluation was divided into non-renewable and renewable energy sources. The energy potential for each source is expressed in millions of tons of oil equivalent (Mtoe) over the period 2015–2050, as shown in Table 2:

Table 2 - Brazilian resource potential according to on 2050 horizon.

Energy Source	2015–2050 Potential (Mtoe)
Non-Renewable	
- Petroleum	9,047
- Natural Gas	2,926
- Mineral Coal	7,157
- Uranium	2,411
Subtotal (Non-Renewable)	21,542
Renewable	
- Biomass	531
- Hydroelectric	74
- Onshore Wind	30
- Offshore Wind	1,356
- Onshore Photovoltaic (PV)	43
- Solar Thermal	57
- Offshore PV	5,247
- Ocean Energy	34
Subtotal (Renewable)	7,371
Total	28,913

Source: Adapted from [5].

In relation to the renewable energy sources, which are the focus of this study, the potential for biomass was estimated based on various sources such as forest residues, sugarcane, and agricultural waste. The study highlights that significant gains in productivity are expected without requiring deforestation. Key considerations include intensifying livestock production and increasing forest management efficiency. The projected potential for biomass is 531 million tonnes of oil equivalent (Mtoe) by 2050, making it a significant contributor to the renewable energy matrix.

For hydroelectric energy, Brazil's vast hydrographic network offers substantial potential. The study identified that while 108 GW of the 176 GW inventory had been exploited by 2018, future development faces socio-environmental and logistical challenges, particularly in the Amazon and Tocantins-Araguaia basins. Despite these constraints, hydroelectricity remains a cornerstone of Brazil's renewable strategy, with an estimated additional potential of 74 Mtoe.

In the case of solar thermal energy, the study explored several technologies, including parabolic trough and solar tower systems with storage. The potential for solar thermal energy was projected to reach 57 Mtoe by 2050, making it a viable complement to other renewable sources, particularly for applications requiring thermal energy storage.

The ocean energy potential was calculated based on wave and tidal resources along Brazil's extensive coastline. The total potential for ocean energy was estimated at 34 Mtoe, reflecting the early stage of technological development in this sector but highlighting its long-term promise.

The assessment of ONW and OFW potential included the revision of previous estimates using updated wind measurement techniques. Onshore wind potential is estimated to exceed 440 GW, while offshore wind could reach 1,780 GW. The offshore wind estimates were divided into categories based on distance from the coast and water depth, with 57 GW within 10 km of the coastline and up to 606 GW in deeper waters between 50 to 100 meters. The combined potential for wind energy by 2050 is projected at 1,386 Mtoe.

The photovoltaic solar potential was evaluated for both onshore and offshore installations. Onshore photovoltaic potential was found to be significant, with an estimated potential of 43 Mtoe based on areas with high solar irradiance. Offshore solar potential was also assessed, resulting in an estimated potential of 5,247 Mtoe in Brazil's exclusive economic zone.

To estimate the technical potential for hydrogen production, EPE applies a comprehensive methodology that involves calculating the balance of available energy resources after meeting final energy demand and using specific conversion factors for each type of energy resource. The total technical potential for hydrogen production ($P_{H_2}^{total}$) is determined by summing the hydrogen potential of each energy resource ($P_{H_2,ES}$):

$$P_{H_2}^{total} = \sum_{i=1}^{N} P_{H_2,ES} \tag{2.4.1}$$

Where the hydrogen potential for each energy resource $P_{H_2,RES}$ is given by:

$$P_{H_2,ES} = (R_{ES} - D_{ES}) \cdot FC_{ES} \tag{2.4.2}$$

Where ES represents each type of energy source, including both renewable and non-renewable sources, and N is the total number of energy source types considered. The term $P_{H_2,ES}$ refers to the hydrogen potential for each energy resource, which is calculated by subtracting the final energy demand from the total available inventory and multiplying the result by the corresponding conversion factor. Specifically, R_{ES} denotes the inventory of energy resource in GWh, representing the total energy available for each type of resource by 2050, as determined from the energy resource inventory conducted in the National Energy Plan 2050 [69]. Meanwhile, D_{ES} represents the final demand for each energy resource in GWh, which corresponds to the cumulative demand projected for the period between 2020 and 2050 under the expansion scenario challenge [70]. For electricity, it was assumed that the entire demand would be met by renewable onshore sources, such as hydropower, solar, and wind energy. Other energy resources were adjusted according to the projected cumulative demand over the same period.

The conversion factor of energy resources into hydrogen FC_{ES} is a key parameter in estimating hydrogen production potential and is expressed in tons of hydrogen per unit of energy input ($tH_2\ /toe$ or $tH_2\ /MWh$). The factor varies according to the efficiency of the hydrogen production process associated with each energy resource. For renewable resources such as hydraulic, wind, and solar energy, the production route involves electrolysis, resulting in a conversion factor of 0.258 $tH_2\ /toe$. Biomass-based hydrogen production, whether from forest biomass, agricultural residues, or sugarcane bagasse, can be achieved through biomass gasification, with a conversion factor of 0.13 $tH_2\ /toe$. Alternatively, sugarcane bagasse can also be used in combined heat and power plants (CHP) coupled with electrolysis, yielding a lower factor of 0.059 $tH_2\ /toe$, or through anaerobic digestion followed by steam reforming in decentralized systems, with a factor of 0.036 $tH_2\ /toe$. Similarly, livestock residues are processed via anaerobic digestion and steam reforming in decentralized facilities, providing a conversion factor of 0.21 $tH_2\ /toe$. Nuclear energy enables hydrogen production through high-temperature electrolysis in nuclear thermal reactors, with a factor of 0.086 $tH_2\ /toe$. Lastly, hydrogen production from natural gas is conducted via centralized steam reforming, resulting in a conversion factor of 0.227 $tH_2\ /toe$.

Finally, Table 3 presents the results of the estimated annualized technical potential for hydrogen production based on the balance of energy resources available by 2050. The assessment considers both renewable and non-renewable resources, with offshore renewable resources standing out due to their significant contribution, particularly solar photovoltaic and offshore wind energy.

Table 3 – Hydrogen production potential in Brazil calculated by EPE methodology.

Energy Resource	**Hydrogen Potential (Mt/year)**
Renewable – Offshore (total)	1,715.3
- Offshore wind – 10 km distance	11.2
- Offshore wind – 50 km distance (excl. 10 km)	39.8
- Offshore wind – 100 km distance (excl. 50 km)	50.2
- Offshore wind – EEZ (excl. 100 km)	249.2
- Oceanic	8.5
- Offshore PV	1,356.1
Renewable – Onshore (PV, wind and hydropower)	18.1
Biomass	50.5
Nuclear	6.9
Fossil	60.2
Total	**1,851**

Source: Adapted from [70].

It is important to note that a comprehensive understanding of hydrogen potential assessments requires comparing different methodologies. As defined in Section 2.3 (Terminology for Renewable Energy Potential Assessment), the term technical potential carries specific meaning. To illustrate how definitions diverge in practice, Table 4 contrasts key aspects of Brazil's Energy Research Office (EPE) methodology with those of the U.S. National Renewable Energy Laboratory (NREL). This comparison makes clear how each organization defines and categorizes resource potentials—and how those choices directly influence estimates of hydrogen production capabilities.

Table 4 - Comparison between potential assessment concepts from EPE and NREL.

Terminology	**EPE/MME (Brazil)**	**NREL/DOE (USA)**
Gross Resource Potential	Not formally defined as a separate metric, but EPE acknowledges an implicit "*potencial total*" — the total energy resource that could, in principle, be converted to hydrogen before any siting, efficiency, or demand adjustments. Published studies often proceed directly to technical potential.	Defined as the total physical energy available in a region without any constraints (e.g., total wind speed at turbine height or total solar irradiation).
Technical Potential	EPE's technical potential for hydrogen represents the maximum output derivable from the surplus resource inventory after meeting domestic energy demand, applying current conversion efficiencies; no economic or market filters are applied.	NREL's technical potential is a subset of the gross resource potential after applying real-world constraints (e.g., land use, topography, environmental, and system limitations) and then converting the remaining energy to hydorgen with state-of-the-art efficiencies.
Economic Potential	A subset of technical potential where producing hydrogen is economically viable based on investment, O&M costs, and energy sales. Does not include market-specific risks.	Subset of technical potential where hydrogen production is lower than potential revenue, considering displaced energy and capacity costs.
Market Potential	Subset of economic potential that includes real-world barriers like information asymmetry, financing access, and investor perception. Often requires public policy support.	Subset of economic potential, determined after accounting for market dynamics, such as policy incentives, regulations, investor behavior, and competition with other energy sources.

Source: Own elaboration.

A key divergence between EPE's and NREL's approaches lies in how each stages the "funnel" of hydrogen-resource potential. NREL explicitly defines gross renewable resource potential as the total physical energy available in a region before any exclusions; its technical hydrogen potential is derived from that gross resource only after applying real-world siting constraints (land use, environmental buffers, topography) and then converting the remaining energy to hydrogen with state-of-the-art efficiencies.

By contrast, EPE does not publish a stand-alone gross figure. Instead, it presents a “technical” hydrogen potential that starts from the surplus renewable-energy inventory left after domestic demand is met and simply applies current conversion factors, without yet layering systematic spatial exclusions. This difference in terminology and filtering depth is critical for this thesis: adopting NREL’s more granular, funnel-style framework within GeoH$_2$-PAM allows a clear separation between theoretical, technically accessible, and economically feasible hydrogen scenarios, thereby strengthening the analysis.

While EPE’s methodology provides a valuable high-level benchmark, there remains significant room for refinement once geospatial constraints are mapped explicitly. By incorporating a novel geospatial modelling framework—one that layers land-use zoning, infrastructure proximity, biodiversity protections, and other exclusion criteria directly into the analysis—GeoH$_2$-PAM produces estimates that are far closer to real-world feasibility. Such enhanced methods are essential for guiding national energy policy, directing private investment, and accelerating Brazil’s transition to a sustainable hydrogen economy.

To translate these high-level, map-based insights into actionable project designs, the GeoH$_2$-FAT tool was developed. GeoH$_2$-FAT takes the spatial potentials generated by GeoH$_2$-PAM and applies them at the plant scale, simulating site-specific techno-economic performance (CAPEX, OPEX, LCOE, LCOH) and environmental impacts (LCA-based emissions) for tailored hydrogen production, storage, and transport configurations. In doing so, it closes the gap between nationwide resource assessments and on-the-ground investment decisions

3 Methodology

This section describes the methodology and key variables used in the Geospatial Hydrogen and Derivatives Potential Assessment Model ($GeoH_2$-PAM), which was developed to assess the gross, technical, and economic potential of green hydrogen and its derivatives from renewable energy sources. It also introduces Geospatial Hydrogen Feasibility Analysis Tool ($GeoH_2$-FAT), developed for techno-economic and environmental analysis of hydrogen production, storage, and transportation.

$GeoH_2$-PAM focuses on map-based resource assessment and does not perform detailed plant-level feasibility. To address this gap, $GeoH_2$-FAT was developed to simulate site-specific hydrogen production scenarios, generating technical outputs, financial indicators, and environmental metrics.

This section aims to describe the methodology and variables used in the geospatial model for the elaboration of the gross, technical and economic potential assessment of the production of green hydrogen and derivatives from renewable sources, and the georeferenced tool that was designed for economic and environmental feasibility analysis of green hydrogen production, storage and transportation.

3.1 Potential assessment model (PAM)

$GeoH_2$-PAM employs a sequential workflow—illustrated in Figure 3—to evaluate the gross, technical, and economic potentials of green hydrogen production from solar photovoltaic (SPV), onshore wind (ONW), and offshore wind (OFW). The computational model was implemented entirely in Python, while selected layer preprocessing and map visualizations presented in this work were carried out in QGIS software.

First, the renewable energy resources models used for green hydrogen production are described. The SPV resource model (Section 3.1.1) defines the PV dataset and converts long-term irradiance into capacity factors for hydrogen modeling. The ONW and OFW resource model (Section 3.1.2) utilize publicly available data and turbine power curves to calculate capacity factors for both onshore and offshore regimes. Subsequently, the Hydrogen production model (Section 3.1.3) transforms renewable power profiles into hydrogen yields using average electrolyzer efficiencies, which is then extended by the Ammonia production model (Section 3.1.4) through Air Separation Unit (ASU) and Haber–Bosch conversion factors, and by the Methanol production model (Section 3.1.5) integrating hydrogen with CO_2 capture. Thereafter, the Constraint application module (Section 3.1.6) applies eighteen geospatial exclusion layers spanning economic, environmental, social, and technical criteria to refine gross into technical potential. Finally, the Economic analysis module (Section 3.1.7) maps levelized costs (LCOE, LCOH, LCOA, LCOM) across the study area based on detailed CAPEX and OPEX assumptions. These interconnected stages feed into the Analysis and Results (Section 4), where the synthesized findings such as maps, graphs and tables for gross, technical and economic assessment, constraints overlapping and sensibility analysis are presented

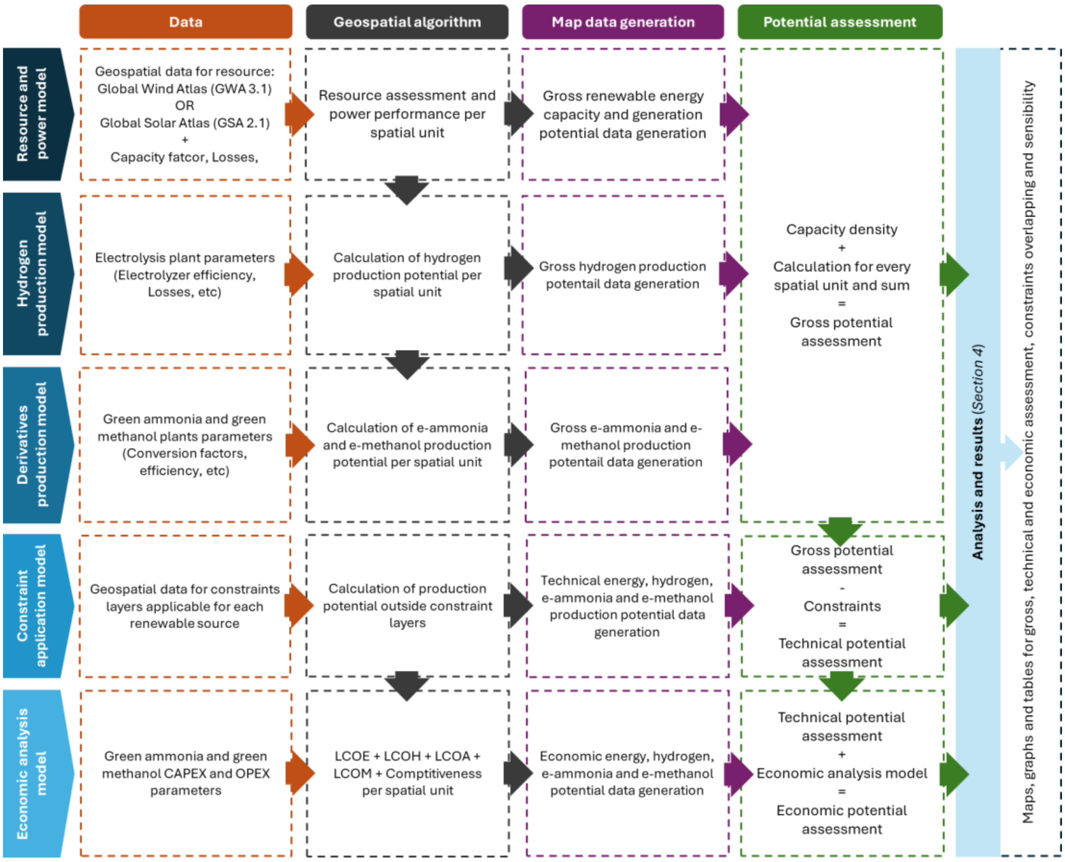

Figure 3 - Process flow diagram of GeoH$_2$-PAM's workflow.
Source: Own elaboration.

3.1.1 Solar photovoltaic resource

The performance of SPV systems depends on several critical factors, including the availability of solar radiation, ambient temperature, system design parameters (such as orientation and tilt), and the efficiency of individual components [71,72]. Among these, solar radiation is the most influential, as it directly impacts the energy conversion process. Accurate solar radiation data, typically measured as Global Horizontal Irradiation (GHI) or Direct Normal Irradiation (DNI), are crucial for estimating the energy yield of PV systems. Furthermore, variations in temperature, wind speed, and shading affect the efficiency of PV modules, requiring detailed modeling to account for losses during energy conversion [73]. In this context, Azevedo [74] constructed a detailed model for the assessment of SPV systems in Brazil, providing relevant insights into the country's solar energy potential. However, this thesis does not aim to explore the modeling of solar PV performance but rather focuses on the methodology for assessing hydrogen potential using widely available and easily accessible updated databases.

In 2017 an updated version of the Atlas Brasileiro de Energia Solar, which provides high-resolution solar radiation data for Brazil, incorporating more than 17 years of satellite-derived data, was published [75]. This second edition represents a significant improvement in the accuracy of solar resource assessment through the use of enhanced parameterizations in the BRASIL-SR radiative transfer model. The atlas also includes analyses on the spatial and temporal variability of solar resources and presents scenarios for employing various solar technologies. Additionally, it serves multiple sectors beyond energy, such as meteorology, agriculture, and architecture, making it a comprehensive tool for evaluating solar potential in Brazil.

Despite that this thesis presents the potential assessment results for Brazil, the aim of the author is to construct a generalized model the serves for any region in the globe. The model constructed in this thesis could use any available resource. However, it is preferable to have a global dataset that is continuously updated. For that reason, the solar resource data and PV system performance modeling used in this work are based on the dataset provided by Solargis, developed under the Global Solar Atlas (GSA) project managed by the World Bank and funded by the Energy Sector Management Assistance Program (ESMAP). This database includes high-resolution, long-term satellite-derived solar radiation data (GHI, DNI, and Diffuse Irradiation), along with meteorological parameters such as air temperature and terrain elevation. The data are processed using advanced models and validated against ground measurements to ensure accuracy [76].

The GSA 2.0 provides GIS data layers and downloadable maps at a resolution of 30 arc-seconds (nominally 1 km), offering reliable solar and PV potential data for regions worldwide. For specific locations, additional high-resolution data at 9 arc-seconds (approximately 250 m) are available, allowing detailed assessments of PV energy generation potential.

The PVOUT dataset from GSA 2.0 serves as a primary input for modeling hydrogen production from photovoltaic energy. This dataset provides the long-term average of daily totals of photovoltaic (PV) power potential in units of kWh/kWp, representing the potential energy output of a 1 kWp solar PV system operating under standardized conditions. Such a metric is vital for evaluating solar energy performance across diverse geographic locations. Additionally, the PVOUT dataset spans a long time series, covering the period from 1994/1999/2005/2007 to 2018, with updates extending to 2023, ensuring that it reflects recent climate variability and solar resource availability. Delivered in float format with a spatial resolution of 30 arc-seconds (approximately 1 km), the dataset enables detailed geospatial analyses of PV system performance over large areas. This high resolution supports precise energy yield estimations and helps identify optimal locations for deploying solar power projects. The modeled PV system in the dataset assumes free-standing c-Si modules mounted at the optimum tilt to maximize monthly energy production, making it particularly suitable for practical solar energy applications.

It is important to point out that the PVOUT dataset already accounts for a range of theoretical losses that affect the overall energy output of photovoltaic systems. The theoretical losses in PVOUT include various factors that influence photovoltaic system performance. These losses account for dirt and soiling (3.5%), direct current (DC) cabling losses (2.0%), mismatch losses (0.3%), and inverter conversion from DC to alternating current (AC) (2.0%). Additionally, transformer losses (0.9%) and AC cabling losses (0.5%) are considered, while downtime losses are assumed to be negligible (0.0%). The total theoretical loss in the GSA 2.0 calculation is estimated at 8.9%, providing a reliable baseline for energy yield estimation under standardized conditions. Therefore, no additional losses related to solar PV performance will be considered in this work.

The transformation of the original PVOUT dataset, provided in kWh/kWp, into Capacity Factor (CF) is performed to standardize the representation with other renewable energy resources. The Capacity Factor allows for the estimation of energy output by multiplying it with the installed power of the PV plant in kWp. Since the PVOUT dataset is represented as a raster file with values defined for each pixel (ii, jj), the conversion is applied on a pixel-by-pixel basis using the following generalized equations:

$$CF_{PV}(i,j)[AC] = \frac{PVOUT(i,j)[DC]}{h_{year}} \cdot ISF \qquad (3.1.1)$$

$$E_{PV}(i,j) = P_{PV\ Plant} \cdot CF_{PV}(i,j) \qquad (3.1.2)$$

Here, $PVOUT(i,j)$ represents the specific energy yield in $\frac{kWh}{kWp}$ for pixel (i,j), while h_{year} corresponds to the total number of hours in a year, typically 8760 hours for a non-leap year and ISF corresponds to the inverter sizing factor for DC to AC conversion which is equal to 1.4 in this work. The installed power of the photovoltaic plant is denoted by $P_{PV\ Plant}$ in kWp, and the resulting capacity factor for that pixel is given by $CF_{PV}(i,j)$. Finally, the estimated energy output in kWh for pixel is denoted by $E_{PV}(i,j)$. Figure 4 illustrates the SPV capacity factor map in % AC.

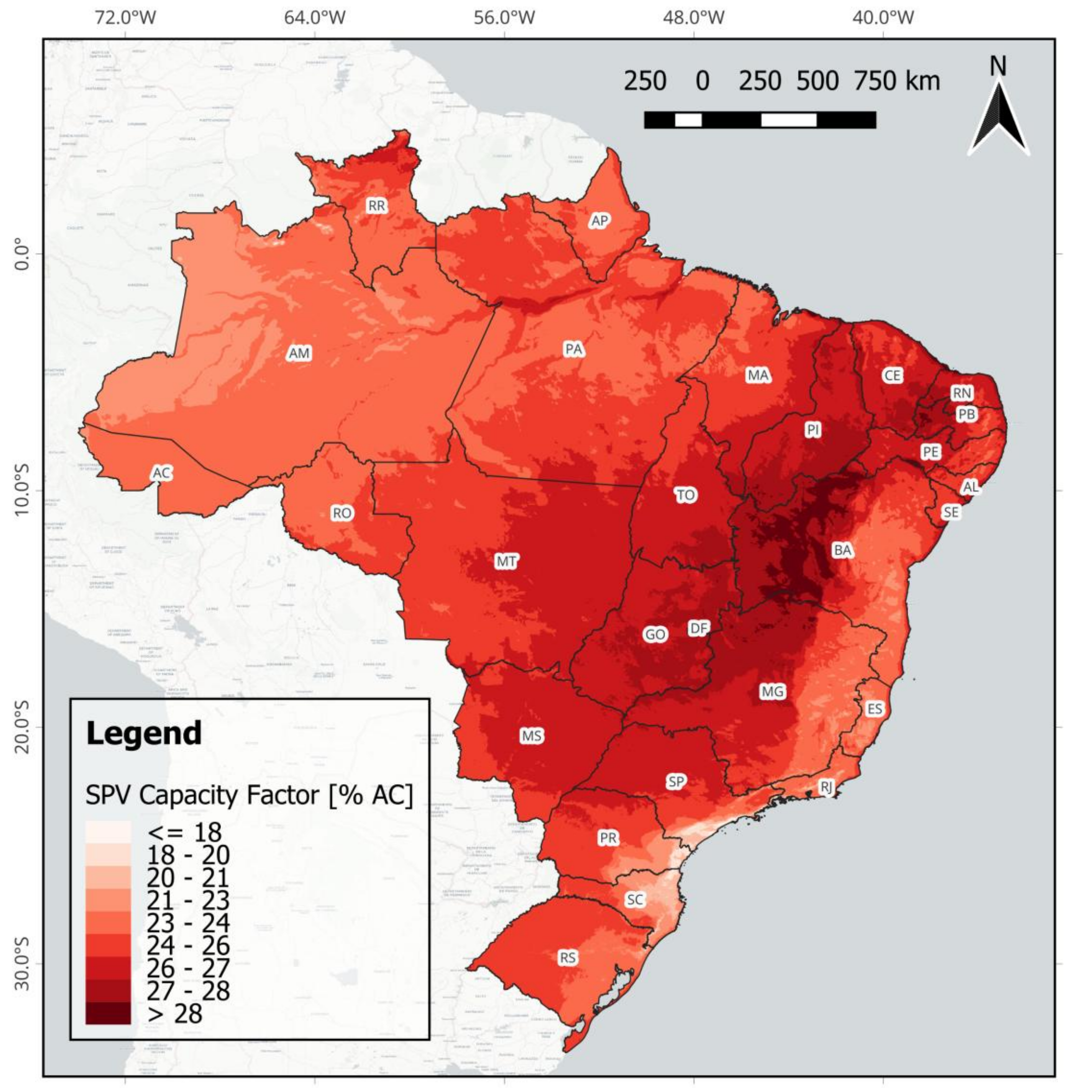

Figure 4 - SPV capacity factor resource map.
Source: Own elaboration with data from [76].

When assessing the gross and technical production potential, a sum is calculated for each valid spatial unit. However, an important variable to be defined in this calculation is the capacity density (sometimes referred as power density or deployment density, but in this work, it will be referred as capacity density) defined for the RES analyzed. Capacity density is the total amount of installed capacity power of a certain RES per unit of area. In the case of SPV, Bolinger and Bolinger (2022) [77] did in-depth research based on empirical observation with nearly complete sample of utility-scape SPV plants in the USA. The study shows that the capacity density benchmark is 87 MW_{DC}/km^2 for fixed-tilt and 59 MW_{DC}/km^2 for tracking plants. For reasonability, the author chooses to use a mean between fixed tilted and tracking plants, resulting in the value of 73 MW_{DC}/km^2 or 52 MW_{AC}/km^2 when using the ISF of 1.4.

3.1.2 Onshore and offshore wind resource

In 2017, the New Brazilian Wind Potential Atlas was launched by the Electric Power Research Center (*Centro de Pesquisas de Energia Elétrica* - CEPEL). Maps of the average annual wind speed are available for the heights of 30, 50, 80, 100, 120, 150 and 200 meters, onshore and offshore. However, offshore information only goes up to 70 km from the coast and the potential, in terms of installable capacity, has not been calculated [78].

According to Federal Law No. 8,617/1993, Brazil has the right to exploit offshore wind resources related to the Exclusive Economic Zone (EEZ), which refers to the range of up to 200 nautical miles (370,4 km) counted from the baselines on the Brazilian coast, which serve to measure the width of the territorial sea. Thus, the first step was to find a reliable database that could calculate the performance of an offshore wind turbine and provide data with a greater distance from the Brazilian continental coast. The chosen database was the Global Wind Atlas (GWA). The current version, GWA 3.1 [79], is a product of a partnership between the Department of Wind Energy of the Technical University of Denmark (DTU Wind Energy) and the World Bank Group, composed of the World Bank and the International Finance Corporation (IFC).

The datasets in GWA 3.1 comprise microscale wind data with grid intervals of approximately 250 meters. These data are produced by dynamically downscaling ERA5 data (2008–2017) from a grid spacing of approximately 30 km to a resolution of 3 km using the Weather Research and Forecasting (WRF) model. The DTU Wind Energy generalization methodology is applied to WRF results, which are then reduced with the WAsP model to a final resolution of 250 meters. The GWA provides georeferenced maps of wind speed, air density, Fact K and A of the Weibull distribution for altitudes of 10, 50, 100,150 and 200m, among others covering areas up to 200 km from the Brazilian coast [79].

To estimate a wind turbine's annual energy output, the capacity factor is calculated by convolving the long-term wind speed distribution at 100 m above ground level (AGL) with turbine-specific power curves. The gross capacity factor layers provided by GWA 3.1 are derived from wind speed distributions at 100 m AGL convolved with the power curves of three turbines—Vestas V112-3.45 MW, Vestas V126-3.45 MW, and Vestas V136-3.45 MW (with rotor diameters of 112 m, 126 m, and 136 m, respectively)—representing IEC Classes I, II, and III. This methodology, ensures that the turbine-specific performance is systematically evaluated for each modeled location, assuming standard air density (1.225 kg/m³) [80]. This classification is based on the technical standard IEC 61400-1 [81]. Table 5 reveals the basic parameters for turbine classification.

Table 5 - Basic parameters for wind turbine classes.

Wind turbine class		I	II	III	S
V_{ref}	(m/s)	50	42.5	37.5	Values specified by the designer
A	I_{ref} (-)	0.16			
B	I_{ref} (-)	0.14			
C	I_{ref} (-)	0.12			

Source: Retrieved from [81].

In Table 5, the parameter values apply at hub height and V_{ref} is the extreme 10-minute average wind speed with a 50-year recurrence period used to define wind turbine classes and derive design-related climatic parameters, A designates the category for higher turbulence characteristics, B designates the category for medium turbulence characteristics, C designates the category for lower turbulence characteristics and I_{ref} is the expected value of the turbulence intensity at 15 m/s.

Although IEC 61400-1 reports that offshore wind turbines fall under IEC-S Class, Draxl et al. (2015) [82] demonstrated that offshore turbines' power curves can closely align with IEC-1 Class turbines. As a result, the capacity factor data corresponding to IEC-1 Class turbines from GWA 3.1 is utilized in this study for offshore wind potential assessment. For simplification and consistency, the same IEC-1 Class capacity factor dataset is also applied to onshore wind, although it could be better explored in future works.

The author acknowledges the complexity of designing a real wind power plant, which involves solving a multi-variable optimization problem. Comprehensive works, such as the Wind Energy Handbook by Burton et al. (2021)[83], offer detailed methodologies for modeling wind turbine performance. The objective of this thesis is not to model wind turbine performance but to focus on geospatial modelling for potential assessment and map generation, which remains the central scope of this work.

The gross capacity factor methodology provides a consistent and reliable baseline for assessing turbine performance across the Brazilian Exclusive Economic Zone (EEZ), accounting for wind speed distributions at all modeled locations. This approach ensures compatibility between offshore wind conditions and modeling assumptions.

The GWA 3.1 provides gross capacity factor maps, which represent the ratio of actual energy produced to the maximum possible energy output without accounting for wake losses or other system inefficiencies [84]. Figure 5 shows the capacity factor map for IEC-1 Class turbines, combined with the 200-nautical-mile line of the Brazilian EEZ.

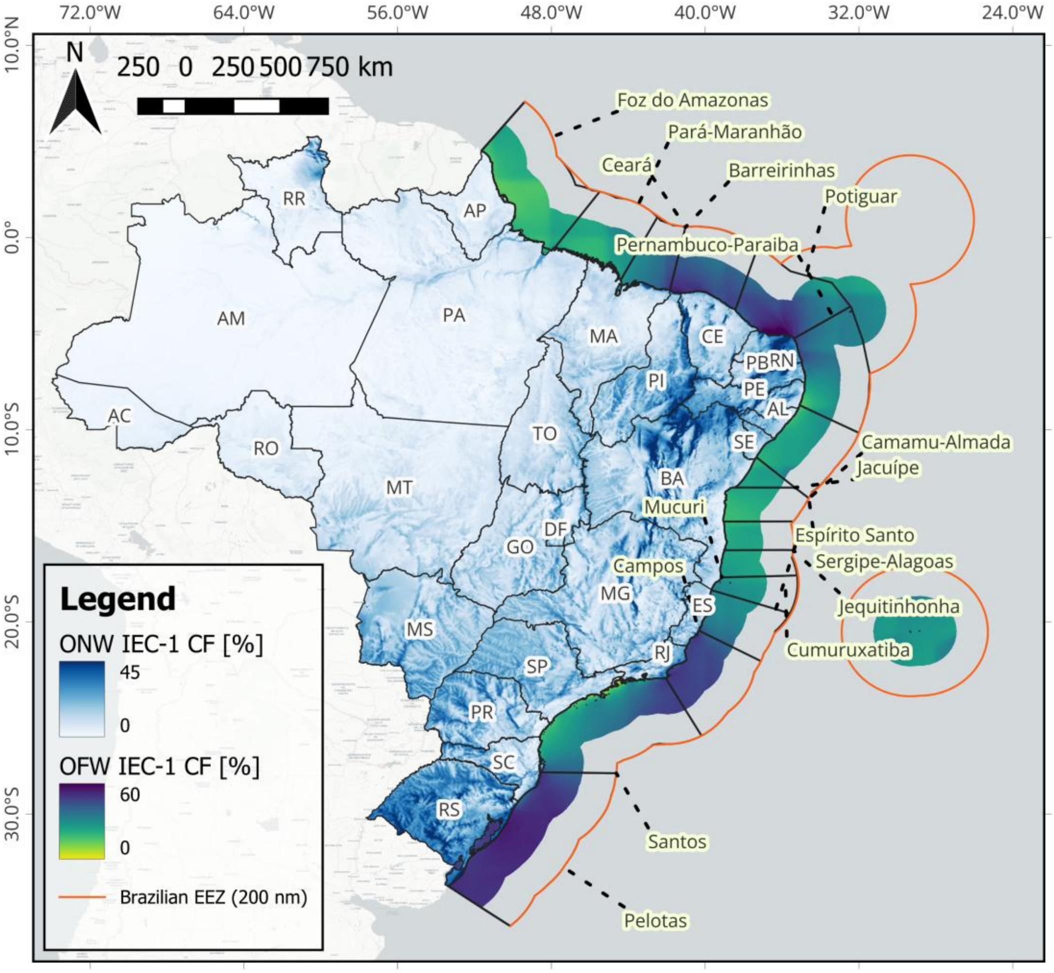

Figure 5 - GWA 3.1 IEC-1 Capacity Factor wind resource dataset.
Source: Own elaboration with [79] and [85] database.

To calculate the area required to install the turbines in a wind farm, it is necessary to consider that the turbines need to be spaced to decrease wind wake effects. IRENA [86] recommends minimum distances of seven rotor diameters in the predominant wind direction and five rotor diameters in the perpendicular direction. Based on this and to align with the GWA 3.1 capacity factor data, the Vestas V112-3.45 MW™ turbine, with a rotor diameter of 112 m, is used as a basis for estimating energy production in a specific area [87]. Using these spacing specifications, the installed capacity density is calculated as 7.86 MW/km^2.

Despite this calculated value, Enevoldsen and Jacobson [88] had analyzed data from existing onshore and offshore wind farms worldwide and observed an installed capacity density range from 3.3 to 20.2 MW/km^2, with a mean of 7.2 MW/km^2 for offshore wind farms. Additionally, the authors reviewed five other estimations of installed capacity density, reporting a mean value of 7.36 MW/km^2. For OFW and ONW map generation and visualization, this study adopts a capacity density of 7.2 MW/km^2 for consistency with observed values.

Moreover, factors such as minimum spacing between wind farms, interconnection limits, cable constraints, and incomplete utilization of the analyzed area may lead to overestimation of capacity density. For that reason, Borrmann et al. [89] suggested applying a correction factor of 25.2%, what would result in a reduced capacity density of 5.4 MW/km² for total potential calculations. This is the capacity density that will be used for ONW and OFW potential assessment in this thesis.

However, the literature does not reach a consensus on the most appropriate capacity density for assessing ONW and OFW potential. NREL/DOE have been constantly using a value of 3 MW/km² [11,90,91]. A recent study from Dai and Scown (2025), demonstrated that the capacity density in the USA ranges from 1.70 MW/km² to 3.88 MW/km² for existing wind farms. The value is lower in agricultural areas (2.73 ± 0.02 MW/km²) and higher in other land cover types (3.30± 0.03 MW/km²). Advanced studies suggest novel approaches to consider a variable and endogenous capacity density predictions for ONW according site-specific characterization [12,92]. Lopez et al [12] adopted a capacitty density of 4 MW/km² for OFW and a endogenous approach for ONW which resulted in two forms of capacity density based: included area capacity density had a median of 7.6 MW/km² and the convex hull capacity density had a median of 2.4 MW/km².

In Brazil, a study form EPE [93] estimated the OFW potential by applying a capacity density assumption for each region. Specifically, the same capacity densities adopted in the Bahia Wind Atlas (3.75 MW/km²) and the Rio Grande do Sul Wind Atlas (2.60 MW/km²) were used to calculate the installed capacity from the exploitable area. Because wind resources in the Northeast and North differ from those in the Southeast and South, a density of 3.75 MW/km² was applied to Northern and Northeastern states, whereas 2.60 MW/km² was applied to Southeastern and Southern states. The study further highlights that continued technological advances in wind turbine design and a deeper understanding of offshore wind resources have the potential to increase these density values, thereby raising overall wind energy potential in Brazil.

It is recognized, however, that future research should explore variable site-specific capacity densities, since the optimal layout and turbine spacing depend heavily on local wind regimes, terrain characteristics, and plant design configurations.

Regarding the availability factor of wind turbines, Pfaffel et al. [94] calculated time-based availability results from SPARTA and WInD-Pool show comparable figures of 92.5% and 92.2%, respectively. Therefore, an availability factor of 92% is adopted for this study for OFW and ONW.

Even with recommended turbine spacing, there is a power loss due to airflow interference. This results in an array efficiency that depends on spacing configurations and turbine design. Bosch et al. [95] and Eurek et al. [96] suggest that an array efficiency of 90% is sufficient for resource assessment models.

The calculations are performed for each spatial unit *(i,j),* of the georeferenced map. The annualized technical potential of OFW and ONW power generation can be computed using the following formula [92]:

$$E_{Wind}(i,j) = CF_{GWA\,3.1}(i,j).A.\delta.\eta_{af}.\eta_{aef}.h_{year} \quad (3.1.3)$$

Where, E_{Wind} is the technical potential for wind energy (MWh/year), A_k is the available land area (km^2) in a spatial unit, δ is the capacity density (MW/km^2), η_{af} is the availability factor, η_{aef} is the array efficiency factor, and $CF_{GWA\,3.1}$ is the localized capacity factor from the GWA 3.1 Class IEC-I GIS data.

3.1.3 Hydrogen production model

Currently, there are two mature technologies of electrolyzers: PEM (Polymer Electrolyte Membrane) and AWE (Alkaline Water Electrolysis). Table 6summarizes some electrolyzers models with their respective manufacturers and characteristics.

Table 6 - Technical data of commercial electrolysers.

Model	Manufacturer	Technology	Production capacity [kg/h]	Energy consumption [kWh/kgH$_2$]	Specific capacity [kg/h/kW]
HyLYZER® -4.000-30	Cummins	PEM	330.8	51.0	0.017
HyLYZER® -1.000-30	Cummins	PEM	82.7	52.0	0.017
HyLYZER® -500-30	Cummins	PEM	41.4	61.7	0.017
SiLYZER 200	Siemens	PEM	18.6	62.0	0.015
SiLYZER 300	Siemens	PEM	18.6	62.0	0.015
HySTAT® - 100	Cummins	AWE	8.3	57.5	0.017
HyProvide - A90	Green Hydrogen	AWE	8.1	53.6	0.017
Nel A3880	Nel Hydrogen	AWE	320.9	53.2	0.017
Nel M4000	Nel Hydrogen	PEM	330.8	54.8	0.017

Source: Own elaboration from manufacturers datasheets.

From Table 6, the average energy consumption of an electrolyzer was calculated, resulting in a value of 56.42 kWh/kg H_2. Therefore, this value will be used in this work to elaborate the map of hydrogen production potential.

The electrolyzer efficiency in this study is based on the mean energy consumption values provided by manufacturers, as shown in Table 3. While this approach ensures consistency and simplicity for georeferenced analysis, it does not account for dynamic efficiency variations under fluctuating power inputs. Advanced modeling approaches, such as those outlined in Rezaei et al. [97], highlight the benefits of incorporating dynamic operational conditions and efficiency curves for electrolyzers.

Recent studies, such as Rezaei et al. [98], have demonstrated that electrolyzer efficiency can vary significantly with input power from renewable energy sources, particularly under intermittent conditions. However, this work employs the mean efficiency values provided by manufacturers to maintain consistency across the georeferenced analysis of multiple locations. While this simplification is sufficient for assessing broad hydrogen production potential, it does not capture the operational dynamics of electrolyzers in real-world scenarios.

The choice of using mean efficiency values reflects the scope of this work, which focuses on a spatial assessment of hydrogen production potential rather than detailed operational optimization. Nonetheless, future studies should consider adopting dynamic modeling techniques, such as those demonstrated in recent literature, to improve the accuracy of hydrogen production estimates. These enhancements would allow for a more comprehensive understanding of the interaction between fluctuating renewable energy inputs and electrolyzer performance, thus increasing the precision and applicability of hydrogen production models.

3.1.4 Ammonia production model

The ammonia production model is based in a green ammonia production plant. The process begins with the PEM Electrolyzer, which generates H_2 through water electrolysis powered by renewable energy sources. Concurrently, an ASU extracts nitrogen (N_2) from atmospheric air, providing the second essential reactant for ammonia synthesis. The hydrogen and nitrogen streams are subsequently fed into the Ammonia Haber-Bosch Synthesis system, where the two reactants undergo a catalytic reaction to produce ammonia (NH_3). The arrows indicate the directional flow of material and energy between the units, emphasizing the interconnected nature of the process. Figure 6 illustrates the process.

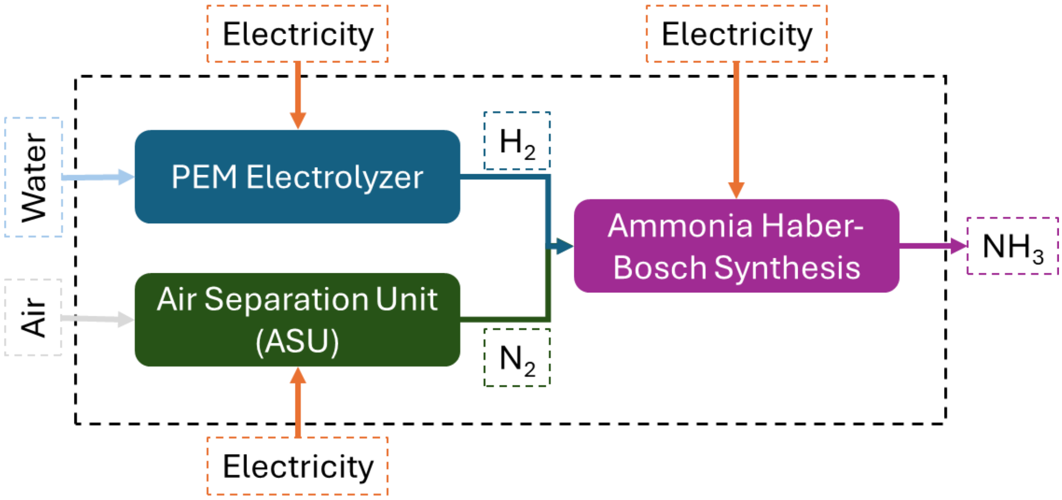

Figure 6 - Simplified process flow diagram of a green ammonia production plant. Source: Own elaboration.

To model the production of NH_3 from RES, it was made a research of the electricity consumption for the ASU and Haber-Bosch Synthesis. Them it was integrated with the hydrogen production model (Section 3.1.3), using real life conversion factors for N_2 and H_2 [99,100]. Equation 3.1.4 represents the equation for conversion of capacity-factor data from RES into NH_3.

$$NH_3(ii,jj) = \frac{CF_{RES}(ii,jj)P_{RESp}\, h_{year}}{\frac{\eta_{elec}}{\alpha} + \eta_{NH_3} + \frac{\eta_{ASU}}{\beta}} \tag{3.1.4}$$

Where CF_{RES} is the capacity factor of the renewable resource at pixel (ii,jj), P_{RESp} nominal (rated) power of the renewable source plant under consideration in kW, η_{elec} is the electrolysis plant electricity consumption in kWh/kgH_2, $\eta_{NH_3}$is the ammonia synthesis electricity consumption in kWh/kgNH_3, η_{ASU} is the air-separation unit electricity consumption in kWh/kgN_2, α is the H_2 to NH_3 conversion factor and β is the N_2 to NH_3 conversion factor. The literature assumptions used in this work for the production of NH_3 can be found in Appendix A.

It is worth noting that for the calculation of the gross and economic production potential, P_{RESp} represents the total nominal power calculated for a pixel. For that purpose, P_{RESp} is calculated as multiplying the correspondent capacity density adopted for the renewable source δ_{RES} and the area of a spatial unit A_{RES} of the capacity factor raster from the correspondent RES.

3.1.5 Methanol production model

The methanol production model is based on a green methanol (MeOH) production plant. The process begins with the PEM Electrolyzer, which generates hydrogen (H_2) through water electrolysis powered by renewable energy sources. Concurrently, a CO_2 Capture Unit captures carbon dioxide (CO_2), providing the second essential reactant for methanol synthesis. The hydrogen and carbon dioxide streams are subsequently fed into the Methanol Synthesis system, where they undergo a catalytic reaction to produce methanol (MeOH). The arrows indicate the directional flow of material and energy between the units, highlighting the integrated and interdependent nature of the process. Figure 7 illustrates the process.

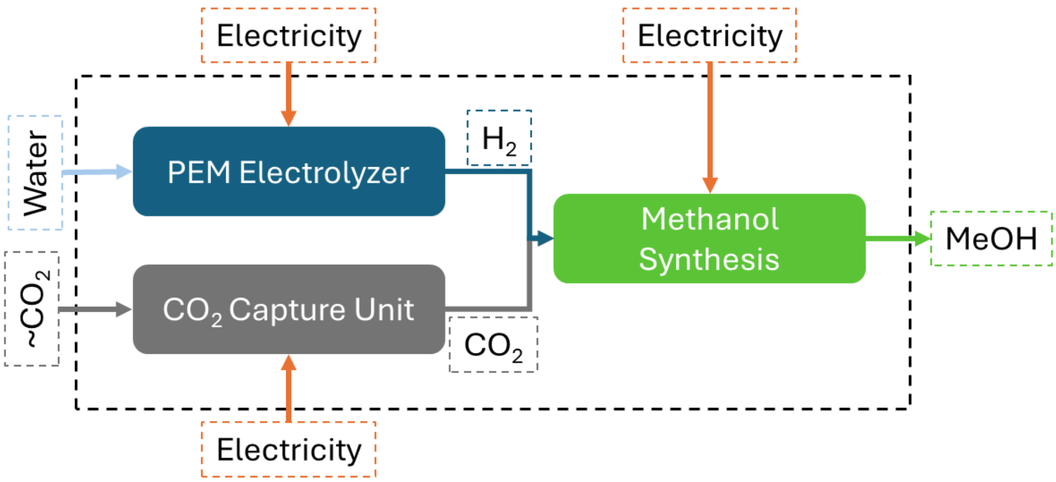

Figure 7 - Simplified process flow diagram of a green methanol production plant. Source: Own elaboration.

The following equation can be used for $MeOH$ production form RES:

$$MeOH(ii,jj) = \frac{CF_{RES}(ii,jj)P_{RESp}\,8760}{\frac{\eta_{elec}}{\gamma} + \eta_{MeOH} + \eta_{CC}} \tag{3.1.5}$$

Where η_{MeOH} is the MeOH synthesis power consumption in kWh/kgMeOH, η_{CC} is the CO_2 capture power consumption in kWh/kgMeOH and γ is the conversion factor representing the kg H_2 required per kg MeOH. The literature assumptions used in this work for the production of MeOH can be found in Appendix A.

As H_2 and NH_3, the calculation of the gross and economic production potential of MeOH, P_{RESp} represents the total nominal power calculated for a pixel. For that purpose, P_{RESp} is calculated as multiplying the correspondent capacity density adopted for the renewable source δ_{RES} and the area of a spatial unit A_{RES} of the capacity factor raster from the correspondent renewable source.

3.1.6 Constraints

The definition of constraints layers is a critical step for the calculation of technical and economic potential. There are multiple types of constraints and different considerations of each RES. Basically, the definition of these layers leads to the exclusion of land areas that are considered in the gross potential analysis. The challenge is to find and adequate this constraint into feasible geospatial data for the analysis.

For the development and assessment of technical and economic potential maps and calculation it was assumed several constraints. A comprehensive research was conducted, identifying 18 geospatial layers critical for conducting technical assessments of renewable energy and hydrogen production potential in Brazil. These layers were selected based on their direct influence on the deployment of SPV, ONW, and OFW energy systems, covering diverse aspects such as economic infrastructure, environmental protection, social impacts, and technical feasibility. To facilitate the analysis, the layers were classified into four types: Economic, Environmental, Social, and Technical. Each classification reflects the nature of the constraint and its potential impact on renewable energy and hydrogen projects. Specific exclusion criteria or setback distances were applied for each layer, ensuring that the resulting assessments are aligned with international best practices, local regulations, and sustainable development principles. The constraints indicated and applied in this work results are based in exclusion criteria observed in [12,13,101,102].

Of the 18 layers, four are classified as economic, reflecting infrastructure-related constraints such as navigation routes, pipelines, oil and gas fields, and transportation networks. Five layers are environmental, addressing key natural and conservation areas, including coastal setbacks, conservation units, priority biodiversity areas, archaeological sites, and water bodies. Four layers are social, covering sensitive areas such as urban regions, rural settlements, quilombola communities, and indigenous lands, where exclusion zones are crucial to avoid socio-environmental conflicts. Finally, five layers are technical, focusing on physical constraints such as capacity-factor restriction, slope, depth, distance from shore, and power transmission lines.

Together, these layers form a strong spatial dataset that enables a precise, holistic assessment of renewable energy and hydrogen potential across Brazil, helping to identify economic technically viable and socially environmental responsible development zones. Table 7 summarizes these layers and the constraints applied, while Appendix B provides a complete description and source of each geospatial dataset utilized for the assessment, including their specific maps and assumptions.

Table 7 - Summary of geospatial constraints layers applied for the technical and economic assessment of renewable energy and hydrogen production potential in Brazil.

		Constraint applied by RES		
Classification	**Layer**	**Solar PV**	**Onshore Wind**	**Offshore wind**
Economic	Navigation routes	N/A	N/A	Exclusion of high-density routes above 700 ships/year.
Economic	Oil & Gas pipelines	100 m setback exclusion	100 setback exclusion	500 setback exclusion
Economic	Oil & Gas fields	Exclusion	Exclusion	Exclusion
Economic	Transport infrastructure (Waterways, railways and highways)	50 m setback exclusion	300 m setback exclusion	300 m setback exclusion
Environmental	Coastal setbacks (viewshed setbacks)	N/A	N/A	Exclusion of 12 nautical miles (22 km) from the coast
Environmental	Conservation Units	Exclusion	Exclusion	Exclusion
Environmental	Priority Areas for Biodiversity Conservation	Exclusion	Exclusion	Exclusion
Environmental	Archaeological sites	Exclusion	Exclusion	N/A
Environmental	Water bodies	Exclusion	Exclusion	N/A
Social	Urban areas	Exclusion of urbanized areas, intraurban voids and other urban equipment	Exclusion of urbanized areas, intraurban voids and other urban equipment	N/A

		Constraint applied by RES		
Classification	**Layer**	**Solar PV**	**Onshore Wind**	**Offshore wind**
Social	Rural settlements	Exclusion	Exclusion	N/A
Social	Quilobola areas	Exclusion	Exclusion	N/A
Social	Indigenous land	Exclusion	Exclusion	N/A
Technical	Slope	Exclusions of slopes >75%	Exclusions of slopes >75%	N/A
Technical	Depth	N/A	N/A	< 60 m for fixed foundations and 60 to 1300 m for floating foundations Exclusion of depths > 1300 m
Technical	Distance from shore	N/A	N/A	Maximum of 200km from the shore in the EEZ.
Technical	Capacity Factor	Exclusion of areas <15% capacity factor	Exclusion of areas <20% capacity factor	Exclusion of areas <30% capacity factor
Technical	Power transmission cables	50 m setback exclusion	500 m setback exclusion	500 m setback exclusion

Source: Own elaboration.

3.1.7 Economic analysis

In order to generate georeferenced maps for an economic feasibility analysis, two important indicators were chosen: LCOE and LCOH. The equations used in this model for LCOE and LCOH are shown below:

$$LCOE(i,j) = \frac{\sum_{t=0}^{n}\left(CAPEX_{RES_t} + OPEX_{RE_t}\right)\left(\frac{1+f}{1+r}\right)^t}{\sum_{t=0}^{n}\frac{E_{RE_t}(i,j)}{(1+r)^t}} \left[\frac{USD\ \$}{kWh}\right] \quad (3.1.6)$$

Where n on the project life, t is the year, $CAPEX_{RES_t}$ and $OPEX_{RES_t}$ indicates the capital expenditure and operating expenses of the respectively renewable energy (solar, offshore wind or onshore wind), respectively, E_{WT_i} is the electricity output of the wind turbine, f is the inflation rate, and r is the nominal discount rate.

$$LCOH(i,j) = \frac{\sum_{t=0}^{n}\left(CAPEX_{RES+H_2}{}_t + OPEX_{RES+H_2}{}_t\right)\left(\frac{1+f}{1+r}\right)^t}{\sum_{t=0}^{n}\frac{M_{H_2}{}_t(i,j)}{(1+r)^t}} \left[\frac{USD\ \$}{kg\ H_2}\right] \tag{3.1.7}$$

Where $CAPEX_{RES+H_2}{}_t$ and $OPEX_{RES+H_2}{}_t$ indicates the capital expenditure and operating expenses of the respectively renewable energy source and electrolyzer plant, respectively, and $M_{H_2}{}_i(ii,jj)$ represent the hydrogen output of the electrolyzer in kilograms and $E_{RE}{}_i(ii,jj)$ the energy generated from the renewable plant for each pixel (ii,jj).

$$LCOA(i,j) = \frac{\sum_{t=0}^{n}\left(CAPEX_{RES+H_2+NH_3+ASU}{}_t + OPEX_{RES+H_2+NH_3+ASU}{}_t\right)\left(\frac{1+f}{1+r}\right)^t}{\sum_{t=0}^{n}\frac{M_{NH_3}{}_t(i,j)}{(1+r)^t}} \left[\frac{USD\ \$}{kg\ NH_3}\right] \tag{3.1.8}$$

Where $CAPEX_{RES+H_2+NH_3+ASU}{}_t$ and $OPEX_{RES+H_2+NH_3+ASU}{}_t$ indicates the capital expenditure and operating expenses of the respectively renewable energy (solar, offshore wind or onshore wind), electrolyzer plant, NH_3 production unit and air-separation unit at year t, respectively, and $M_{NH_3}{}_t(i,j)$ represent the NH_3 output in kilograms at year t.

$$LCOM(i,j) = \frac{\sum_{t=0}^{n}\left(CAPEX_{RES+H_2+MeOH+CC}{}_t + OPEX_{RES+H_2+MeOH+CC}{}_t\right)\left(\frac{1+f}{1+r}\right)^t}{\sum_{t=0}^{n}\frac{M_{MeOH}{}_t(i,j)}{(1+r)^t}} \left[\frac{USD\ \$}{kg\ MeOH}\right] \tag{3.1.9}$$

Where $CAPEX_{RES+H_2+MeOH+CC}{}_t$ and $OPEX_{RES+H_2+MeOH+CC}{}_t$ indicates the capital expenditure and operating expenses of the respectively renewable energy source, electrolyzer plant $MeOH$ production unit and carbon capture unit at year t, respectively, and $M_{MeOH}{}_t(i,j)$ represent the $MeOH$ output in kilograms at year t.

In this work, the LCOE for map generation is strictly related to the power generation at RES plant terminals, reflecting the total cost of electricity production excluding any connection to the grid. The LCOH for map generation is calculated from hydrogen production at the electrolyzer outlet, where all costs involved in hydrogen production, including the cost of electricity, are considered. Some refer it to relative LCOH [3]. The LCOA and the LCOM are calculated with the same logic for map generation.

For the CAPEX of hydrogen production by electrolysis, the curves of Figure 8 were obtained from several data from the literature for PEM technology [3].

Regarding OPEX, according to Matue et al. [103], the value should be set at 3% of CAPEX per year.

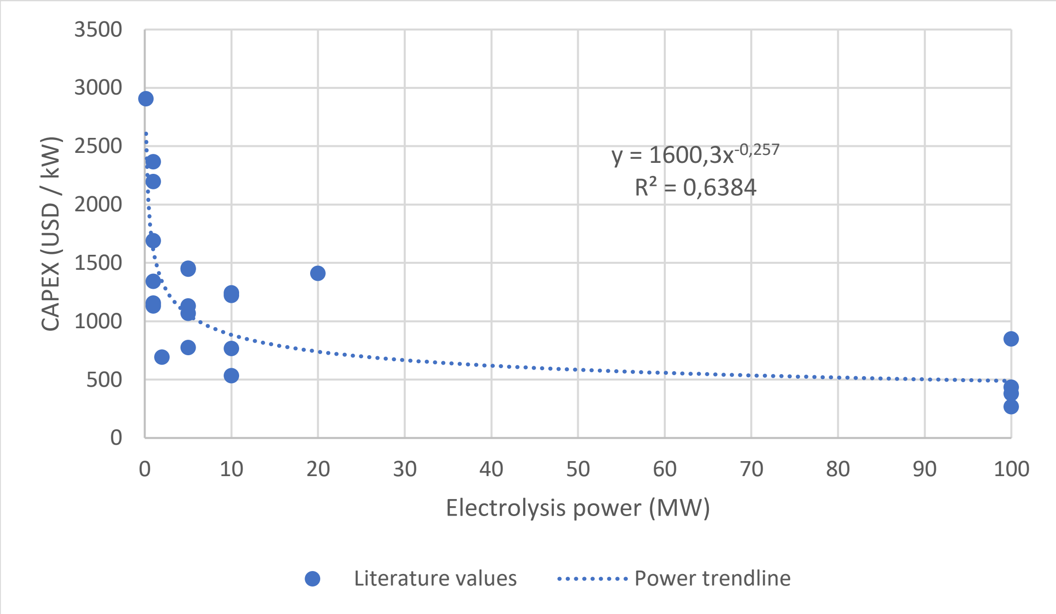

Figure 8 - PEM electrolyzer CAPEX power trendline.
Source: Own elaboration through literature data [104–109].

In the model, it is also considered the cost of overhaul of the electrolyzer, the rate of energy degradation of the wind turbine, the degradation of electrolyzer and the hydrogen loss due to leakage [110]. The values used in the simulations are summarized in Table 8. The detailed assumptions used in the PAM are described in Appendix A

Table 8 - Summary of the parameters used in the economic analysis for the calculation of LCOE and LCOH. Source: Own elaboration.

Parameter	*Value*	*Unit*	*Reference*
Offshore wind power plant	100	MW	-
Analysis period	20	Years	-
Nominal discount rate	8	% a.a.	-
Inflation rate	5	% a.a.	-
CAPEX offshore wind plant	3137	USD/kW	[111]
CAPEX electrolysis plant PEM	Figure 4	USD/kW	[104–109]
OPEX offshore wind plant	80	USD/kW/year	[111]
OPEX electrolysis plant PEM	3	% CAPEX/year	[112]
Overhaul value	60	% CAPEX	[110]
Time to overhaul	10	Years	[110]
Wind turbine degradation rate	1,6	%/year	[110]
Electrolyser degradation rate	1	%/year	[110]
Hydrogen leakage rate	0,1	%/year	[110]

Source: Own elaboration through references indicated in the table.

Additionally, the EPE reference does not explicitly state whether export cable costs are included in the CAPEX figure. Since the present study assumes an off-grid system, export cables are not required. It is possible that the CAPEX value includes grid-related costs, which may introduce inconsistencies with the off-grid configuration. Future refinements of the model should exclude such costs to better align with the system's assumptions and improve its applicability to off-grid configurations.

The simulated model corresponds to a 100 MW offshore wind plant with hydrogen production from off-grid PEM electrolysis. While this capacity is relatively small compared to typical offshore wind farm sizes, it was selected to align with the georeferenced modeling framework, which assesses the economic feasibility of offshore wind and hydrogen production across diverse locations. Larger wind farms, commonly deployed globally, could achieve economies of scale, potentially reducing project-specific CAPEX. Future studies could explore the impact of larger wind farm capacities on CAPEX and overall project economics.

Since the system is off-grid, there is no consideration of grid connection costs, and all electricity generated is directed to hydrogen production. Electrolyzers are assumed to be located on a single central platform rather than small stacks on individual turbine platforms. This configuration aligns with large-scale offshore hydrogen production concepts and optimizes cost assumptions by centralizing infrastructure. However, the model does not currently include additional costs associated with the offshore installation of electrolyzers, such as platform construction or integration with the wind farm. Furthermore, the model does not include costs related to compression, local storage, pipeline transportation, or other infrastructure for delivering hydrogen to its final point of use. These elements are outside the current scope but are recognized as critical for future comprehensive cost assessments.

The algorithm developed seeks to vary the power of the electrolysis plant in order to meet the technical requirements of each geographical point based on the capacity factor obtained from the GWA 3.1 data. The CAPEX of the electrolysis plant is then calculated according to Figure 8.

3.2 Feasibility analysis tool (FAT)

The GeoH$_2$-FAT was designed, aimed at doing economic-financial and environmental analysis of green hydrogen production projects in Brazil. The tool's architecture was constructed using Microsoft Excel software with VBA language and conceived in a modular structure, composed of four main building blocks and an integration block which are illustrated in Figure 9. The energy block (Section 3.2.1) represents the modeling of the electricity sources that supply the hydrogen plant. This plant, in turn, is comprised of the production and storage blocks (Section 3.2.2 and 3.2.3), as it represents the location where hydrogen is produced. The transport block (Section 3.2.3) is connected to the production and storage blocks, since hydrogen can be either directly transported or stored for later transport. The financing flow of the project is modeled in a separate block called the financing block (Section 3.2.4). Finally, the integration block (Section 3.2.5) is designed to consolidate the information and flows from all the blocks into a single location.

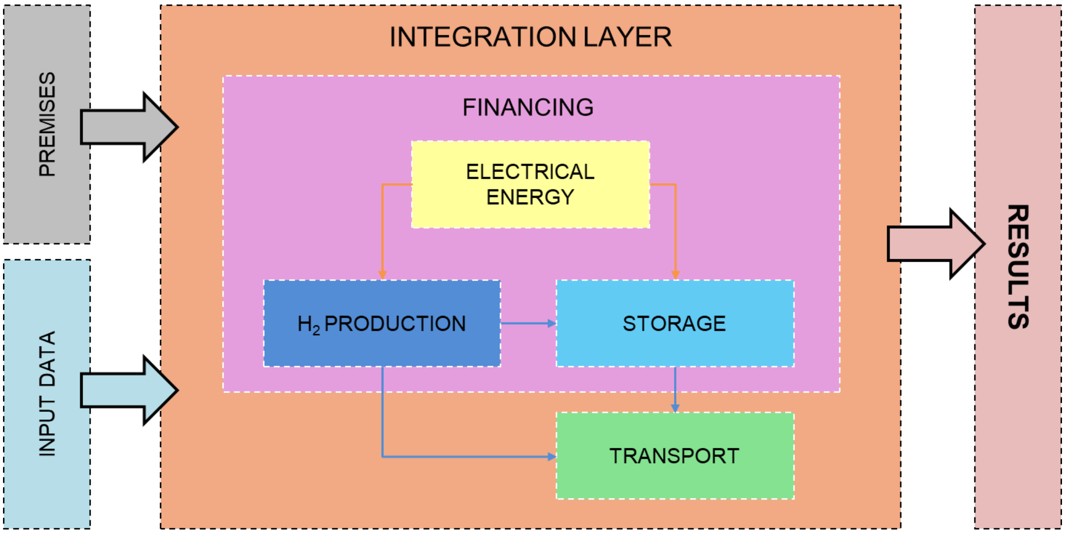

Figure 9 – Diagram representation of the designed GeoH$_2$-FAT.
Source: Own elaboration.

In summary, the construction blocks constitute the entire hydrogen chain, gathering the variables and equations necessary for the modeling, while the integration block consolidates the information from the construction blocks and initially verifies the technical consistency of the planned solution, providing economic-financial and environmental indicators for each analyzed case.

For the construction of each block, a comprehensive research of the technical, economic-financial, and environmental data necessary to define reference parameters was conducted. However, the tool also allows for user data input to develop scenarios to be simulated. All the default assumptions and user configurable data inputs are specified in Appendix C. This modular design enables greater scalability and versatility for the tool, allowing for the review and inclusion of specific blocks based on new electricity generation technologies or on advancements in hydrogen production, storage, or transportation, as well as new business models.

3.2.1 Energy block

The Energy Block is composed of sub-blocks that represent the possible configurations for electricity supply. These include: renewable electricity generation technologies (onshore wind and solar) and electricity procurement contracts in the wholesale electricity market (ACL).

The sub-blocks offer the following input options:

i) Sub-blocks related to local generation technologies (to be selected by the user):
    a. Solar
    b. Wind

ii) Sub-blocks related to electricity procurement:
   a. Self-generation, using wind and/or solar sources, which may be either local—i.e., located at the hydrogen production site—or remote, connected via the National Interconnected System (SIN).
   b. Electricity purchase from the ACL with I-REC certification.

Figure 10 presents the flowchart of the Energy Block, including its sub-blocks. The output data are derived from the integration of results across each module and their interconnections.

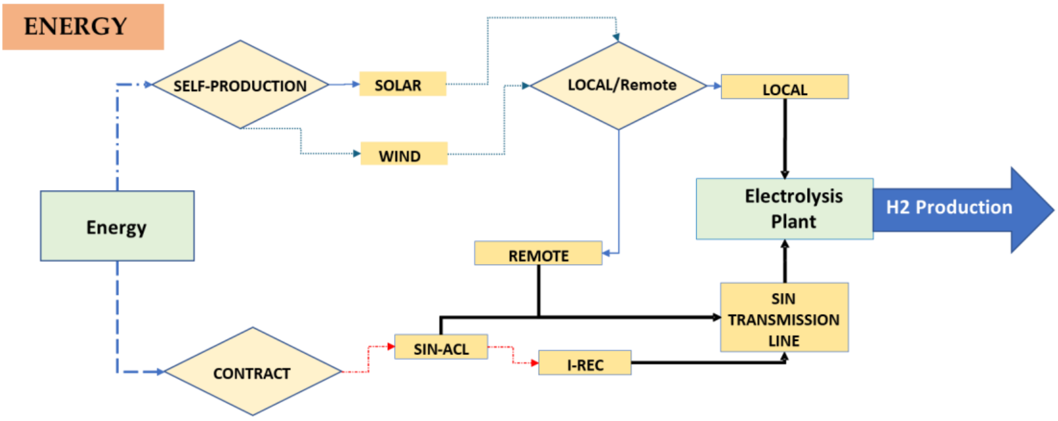

Figure 10 - Flowchart representing the energy block of the GeoH$_2$-FAT.
Source: Own elaboration.

For the purpose of simulating remote or local self-generation, the power capacity of the generation plant is initially defined based on the electrolyzer's demand. As shown in the flowchart in Figure 10, the self-generation plant may utilize either solar or wind resources. To simulate energy generation, the tool provides a selection of wind turbines and photovoltaic panels based on commercially available models, along with their respective technical specifications. From these technical specifications, the generation capacity of the plants can be calculated. The annual energy production (kWh/year) is then determined based on the type of panel or turbine selected and the availability of local resources.

In the case of solar energy, the tool uses data from the Brazilian Solar Energy Atlas 2017 [75]. For wind energy, the selected data source is the Global Wind Atlas (GWA)[79], which enables calculation of wind turbine performance based on the geographical location of the proposed wind farm.

For self-generation configurations, the LCOE in BRL/MWh is calculated based on CAPEX and OPEX data for the proposed generation plant, using reference values from EPE [111]. Among CAPEX components, equipment and auxiliary systems represent the most significant portion—approximately 70% of total investment costs for both wind and solar projects. Regarding OPEX, the document considers a range of BRL 40/MWh to BRL 60/MWh in solar energy auctions.

For cases involving electricity procurement contracts in the ACL (Free Contracting Market), costs are defined through bilateral contracts to be signed with independent power producers or self-producers. These contracts stipulate tariffs, durations, adjustment mechanisms, and other commercial terms, including the cost of I-REC certificates. The economic analysis is thus based on CAPEX and OPEX values for the selected generation technologies, or on the costs associated with electricity purchased from the ACL. The CAPEX and OPEX parameters incorporated into the tool are based on the “Generation Price Booklet” by EPE, which uses data from projects registered and approved in auctions between 2010 and 2020 [111].

The tool also incorporates connection costs to the SIN, which may include:

i) the **TUSD (Tariff for Use of the Distribution System)**, applicable when projects are physically connected to the distribution network; or
ii) the **TUST (Tariff for Use of the Transmission System)**, applicable when the connection is not directly to the Basic Transmission Network.

These tariffs cover the cost of making the energy transport infrastructure available and include sectoral charges applicable to energy consumers. All these cost components are also subject to applicable taxes (PIS/Cofins and ICMS), and the TUSD, TUST, and tax data have also been georeferenced within the tool.

3.2.2 Hydrogen production block

This section describes the composition and modeling approach for the green hydrogen production block. The system considers electrolyzers based on Alkaline and PEM (Proton Exchange Membrane) technologies. The hydrogen produced can be locally stored in compressed form for subsequent overland transport.

The H2 Production Block foundation is based in the same approach as the Hydrogen production model of GeoH$_2$-PAM (Sectio 3.1.3) and receives input from the energy block and from water consumption data. To estimate the annual hydrogen production (t/year), technical data from commercially available electrolyzers are used, as listed in Table 6. To assess CAPEX, a literature review was conducted focusing on electrolysis plants, considering both electrolyzers and auxiliary equipment. Figure 8 shows the results based on a synthesis of data from the literature.

The OPEX is divided into three main components:

i) Operation & Maintenance (O&M)
ii) Water cost, and
iii) Energy cost.

For water costs, a detailed mapping of industrial water tariffs was conducted based on the pricing practices of Brazilian water utilities across their concession areas. The tool uses industrial-category pricing, and Figure 11 displays the geographic distribution of these tariffs.

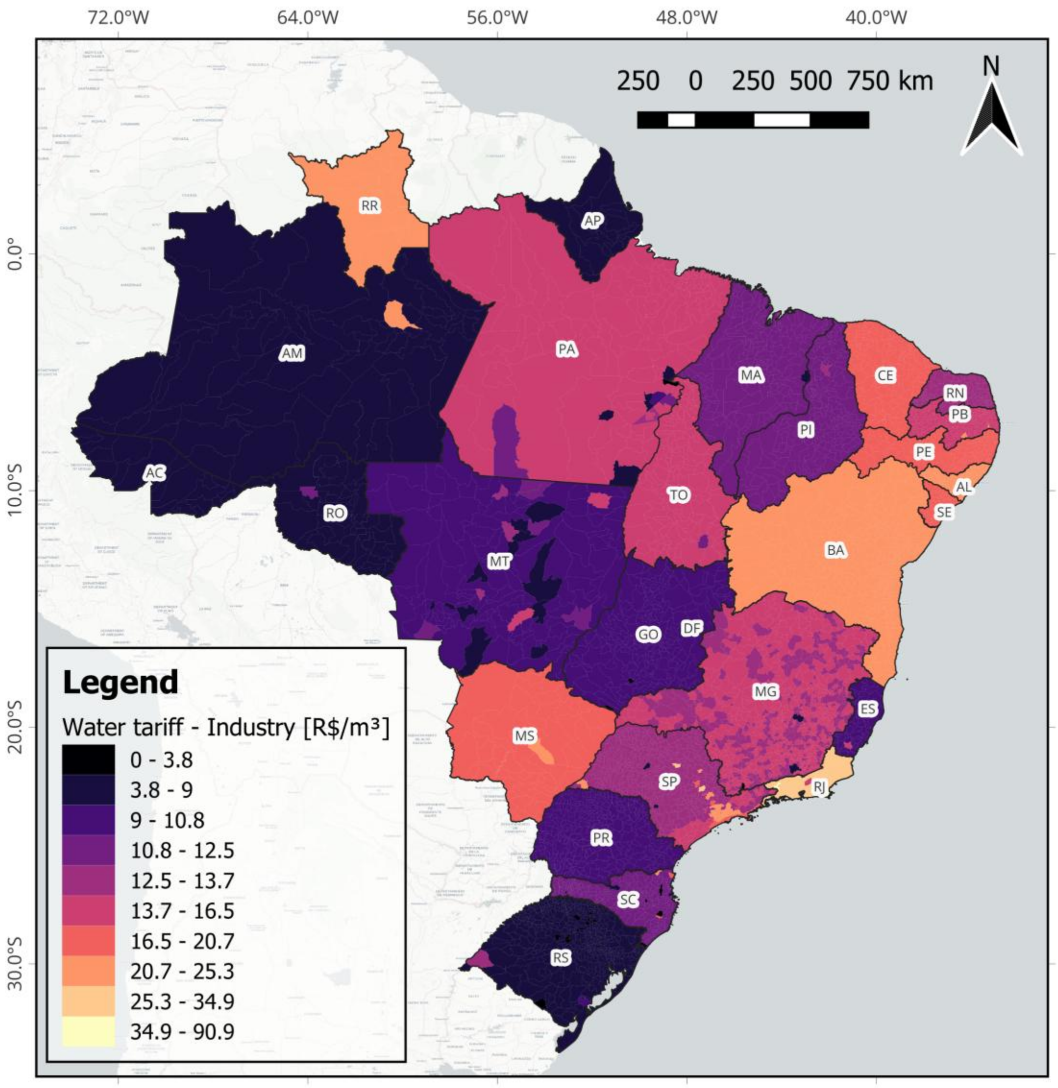

Figure 11 - Maps of water tariff for industry category in Brazil.
Source: Own elaboration from data gathered from water utilities in August of 2021.

Based on the data presented, it is possible to construct the entire H2 Production Block. The electrolyzer data provide key inputs such as the amount of hydrogen produced, the required power capacity, and the specific energy consumption needed for hydrogen generation. Once the electrolyzer power capacity is defined, both OPEX and CAPEX can be calculated, while the Energy Block supplies the electricity required for production.

3.2.3 Transport and storage blocks

This section provides a summarized description of how the hydrogen, ammonia, or liquid organic hydrogen carriers (LOHC) storage and overland transportation blocks are modeled in the proposed tool. The model considers transportation via pipeline (for compressed hydrogen) and truck transport (for compressed or liquefied hydrogen, ammonia, or LOHC). The transport mode and cost are adjusted according to the volume of the produced hydrogen and the distance to be transported. Table 9 shows how the cost (with corresponding mode) is calculated according to the two parameters mentioned.

Table 9 - Transport modes and costs based on distance and volume for the transport block.

		Distance [km]			
		1 a 10	10 a 100	100 a 1000	1000 a 10000
Volume [ton/day]	100 to 1000	0,05	0,08	0,34	1,79
	10 to 100	0,06	0,14	1,01	2,00
	1 tp 10	0,70	1,20	2,40	5,00
	0 to 1	0,70	1,20	2,40	5,00
Volume [ton/day]	100 to 1000	Pipeline	Pipeline	Pipeline	Pipeline /Ammonia
	10 to 100	Pipeline	Pipeline	Pipeline	Pipeline /Ammonia
	1 to 10	CGH2	CGH2	CGH2/LOHC	LOHC
	0 to 1	CGH2	CGH2	CGH2/LOHC	LOHC

Costs in 2019 USD/kg H2
Source: Adapted from [4].

Maritime transport scenarios are not included in this block, as these are assumed to fall under export activities, which are treated as a form of final use under the responsibility of the end consumer or client.

For storage costs this block presents particular challenges, as these stages currently represent critical bottlenecks in the development of the hydrogen economy, and up-to-date, consolidated data for comparing different logistics routes remain scarce in the literature. Table 10 shows how storage mode and costs are incorporated in the storage block.

Table 10 – Storage modes and costs incorporated in the storage block.

Storage Type	***Volume***	***Duration***	***Benchmark LCOS (USD/kg)***	***Potential Future LCOS (USD/kg)***	***Geographic Availability***
No storage	N/A	N/A	0.00	0.00	N/A
Salt caverns	Large	Months–weeks	0.23	0.11	Limited
Depleted gas field	Large	Seasonal	1.90	1.07	Limited
Rock caverns	Medium	Months–weeks	0.71	0.23	Limited
Pressurized tanks	Small	Days	0.19	0.17	Unrestricted
Liquid hydrogen	Small–medium	Days–weeks	4.57	0.95	Unrestricted
Ammonia	Large	Months–weeks	2.83	0.87	Unrestricted
LOHCs	Large	Months–weeks	4.50	1.86	Unrestricted
Metal hydrides	Small	Days–weeks	Not evaluated	Not evaluated	Unrestricted

Costs in 2019 USD/kg H2
Source: Adapted from [4].

Since there is a significant use of energy when storing hydrogen, research was made, and some assumptions were also incorporated in the tool. Table 11 summarizes these assumptions. The average energy use is applied according to the technology selected for the storage block.

Table 11 – Energy use for different hydrogen storage modes.

Energy Expenditure ($kWh/kg\ H_2$)	*Min.*	*Max.*	*Avg.*	*% of LHV Min.*	*% of LHV Max.*	*Reference*
Compression	0.70	1.00	0.85	2 %	3 %	[113]
Liquefaction	12.50	15.50	14.00	38 %	47 %	[114]
Methylcyclohexane (MCH) - LOHC	9.99	–	9.99	30 %	–	[115]
Ammonia	9.66	–	9.66	29 %	–	[115]

LHV = Low heating value
Source: Own elaboration through references indicated in the table.

3.2.4 Financing block

The financing block converts the techno-economic outputs of the model—CAPEX, OPEX, ramp-up profile, and annual hydrogen production—into a set of financial statements and performance metrics that determine bankability. By linking cash inflows (hydrogen sales, co-products, and potential decarbonisation credits such as CBIOs) with cash outflows (investment, operating costs, taxes, and debt service), the block returns the project's LCOH, Net Present Value (NPV), Internal Rate of Return (IRR), simple payback period, EBITDA-based margins, and Debt-Service Coverage Ratio (DSCR). These indicators are benchmarked against sponsor hurdles, lender requirements, and market references to support an investment decision.

This block encapsulates the project's cost structure, incorporating:

- Capital expenditure (CAPEX) for the facility;
- Financing conditions associated with each funding source—such as the Brazilian Development Bank (BNDES), the Funding Authority for Studies and Projects (FINEP), Banco da Amazônia (BASA), Banco do Nordeste (BNB), green bonds, and other instruments—covering interest rates, total tenor, grace period, loan size, and related terms;
- Sponsor equity, represented by the weighted average cost of capital (WACC);
- And the assumed hydrogen offtake conditions.

The $GeoH_2$-FAT embeds forward-looking financial projections. Using inputs for LCOH, CAPEX, OPEX, plant lifetime, and annual hydrogen production output—including ramp-up periods—it evaluates project performance across multiple revenue scenarios and boundary conditions. Given the influence of the hydrogen sales price on both LCOH and overall bankability, the model allows this parameter to be set either as a multiple of the calculated LCOH or as an exogenous value specified at each simulation run.

The financing block follows the methodology developed by NREL [116], the RETScreen software framework [117], and project finance principles [118]. The governing equations employed in the financial block are presented below.

Debt service is represented as a constant stream of regular payments extending over a fixed number of years or months—the amortisation term. This treatment of debt is especially relevant in project-finance modelling. The annual payment D can be computed using any of three internationally recognised repayment systems. The French Amortisation System, more commonly called the PRICE method, features equal instalments throughout the term; it is the most widely adopted approach, and its governing equation is:

$$D = Cf_d \frac{i_d}{1 - \frac{1}{(1 + i_d)^{N'}}} \tag{3.2.1}$$

where C represents the project's total initial cost or portion of CAPEX in financial close/construction start ($CAPEX_0$), f_d the debt ratio, $i_d$the effective interest rate on the debt, and N' the debt tenor or amortisation period. The annual debt service can be decomposed into a principal repayment (amortisation) $D_{p,t}$ and an interest payment $D_{i,t}$ in year t, such that:

$$D = D_{p,t} + D_{i,t} \tag{3.2.2}$$

$$D_{p,t} = D(1 + i_d)^{t-N'-1} \tag{3.2.3}$$

$$D_{i,t} = D\left[1 - (1 + i_d)^{t-N'-1}\right] \tag{3.2.4}$$

The Constant Amortization System (SAC) is characterized by equal principal-repayment portions and a decreasing interest component, which leads to progressively lower installments. It can be formulated as follows:

$$DD_{p,t} = \frac{Cf_d}{N'} \tag{3.2.5}$$

$$DD_{i,t} = i_d(N' - t + 1)\frac{Cf_d}{N'} \tag{3.2.6}$$

$$D_t = D_{p,t} + D_{i,t} = \frac{Cf_d}{N'}[1 + i_d(N' - t + 1)] \tag{3.2.7}$$

The American Amortization System (AAS), in turn, maintains a constant interest payment in each instalment for periods where $t < N'$ and settles the entire principal in the final year $N'$and it is expressed mathematically as follows:

$$DD_t = f(x) = \begin{cases} i_d Cf_d, & t < N' \\ Cf_d(1 + i_d), & t = N' \end{cases} \tag{3.2.8}$$

$$D_{p,t} = f(x) = \begin{cases} 0, & t < N' \\ Cf_d, & t = N' \end{cases} \tag{3.2.9}$$

$$D_{i,t} = i_d Cf_d \tag{3.2.10}$$

It should be emphasized that the closing outstanding balance, SF, is always equal to the previous year's balance minus the principal amortization.

$$SF_t = SF_{t-1} - D_{p,t} \tag{3.2.11}$$

where $SF_0 = Cf_d$, that is, the initial outstanding debt balance.

If a grace period is granted for debt repayment, the initial costs must first be compounded to their future value; only then can the instalments be determined. Accordingly:

$$C = C(1 + i_d)^{Nc-1} \tag{3.2.12}$$

where N_C denotes the length of the grace period. The "−1" term adjusts the formula for an arrears payment schedule, which is standard practice in loans and project financing.

Certain financial institutions customarily impose a credit-origination fee—known in Brazil as the *Taxa de Abertura de Crédito* (TAC)—calculated as a percentage of the loan principal. Although this practice has been prohibited since 2008 under CMN Resolution 3.517/07, lenders frequently rebrand the charge to circumvent regulatory scrutiny. By contrast, many institutions levy a registration fee (*tarifa de cadastro*), a fixed amount expressly authorized by Central Bank Resolution 3.919, issued in 2010.

All financial inputs can be altered, but the tools environment was set with default values that reflect prevailing conditions in the Brazilian renewable-energy market from BNDES Finem credit line [119]. Even though, the tool can be adjusted with forthcoming hydrogen-specific credit lines.

The cash-flow model records, year by year, all expenses (outflow) and revenues (inflow) generated by the project. In year 0, the pre-tax cash outflow $C_{out,0}$ equals the project's initial cost—that is, the share of the total investment that is financed directly and therefore not leveraged (i.e., not included in the debt component):

$$C_{out,0} = C(1 - f_d) \quad (3.2.13)$$

In subsequent years, the pre-tax cash outflow $C_{out,n}$ is calculated as:

$$C_{out,t} = \sum_{k}^{K} C_{OPEX_k}(1 + r_k)^t + D \quad (3.2.14)$$

where t denotes the year and the sum of $C_{OPEX_{k,t}}$ denotes any OPEX expense k that can occur in the plant, such operation-and-maintenance (O&M) of the hydrogen-production plant, O&M of the photovoltaic plant and the wind farm, storage costs, transportation costs for moving hydrogen or intermediates, water consumption and treatment costs, electricity transmission-system usage charges (EUST) and distribution-system usage charges (EUSD), fixed i-REC administration and variable i-REC transaction fees, the cost of electricity purchased from the ACL, etc., with r_k as the escalation rate applied.

For year 0, the pre-tax cash inflow $C_{in,0}$ equals the incentives, subsidies and/or grants, IG in year 0:

$$C_{in,0} = IG \quad (3.2.15)$$

In subsequent years, the pre-tax cash inflow $C_{in,t}$ is determined as follows:

$$C_{in,t} = R_{H2,t} + \sum_{k}^{K} R_k(1 + r_k)^t \quad (3.2.16)$$

$$CR_{H2,t} = P_{H2,t}Q_{H2,t} \quad (3.2.17)$$

where t is the year of analysis, $Q_{H2,t}$ is the volume of hydrogen sales, $P_{H2,t}$ is the price of hydrogen sales and R_{H2} is the revenue of hydrogen sales. The sum of R_k denotes any other revenue k that can occur in the plant, such as energy-sales, GHG or renewable energy credits, co-products sales such as oxygen, etc., with r_k as the escalation rate applied.

Thus, the pre-tax cash flow C_n for year n is simply the difference between the pre-tax cash inflow and the pre-tax cash outflow:

$$C_t = C_{in,t} - C_{out,t} \quad (3.2.18)$$

Asset depreciation arises primarily from physical wear or technological obsolescence, and its computation depends on the method adopted. Two approaches are considered in this study: the declining-balance method and the straight-line method. Annual depreciation charges feed directly into the model's income-tax and after-tax financial metrics. At the end of the project's life, the difference between the "end-of-life value" and the undepreciated capital cost is recognised as income if positive and as a loss if negative.

The declining-balance method accelerates depreciation, assigning a larger share of the cost to the early years of operation. In the first year (year 0), the capital-cost allowance CCA_0 is calculated on the portion of the initial capital expenditure that is fully incurred during the construction year:

$$CCA_0 = C(1 - \delta) \quad (3.2.19)$$

where δ is the base-depreciation fraction that specifies the portion of the initial cost to be capitalized and, therefore, eligible for tax depreciation; the remainder is treated as a full expense in the construction year (year 0). The undepreciated capital cost at the end of year 0, UCC_0, is then obtained from

$$UCC_0 = C - CCA_0 \quad (3.2.20)$$

In subsequent years, the capital-cost allowance is calculated as:

$$CCA_t = UCC_{t-1}d \quad (3.2.21)$$

where d is the depreciation rate and UCC_{t-1} is the undepreciated capital cost at the end of period $(t - 1)$, expressed as:

$$UCC_{t-1} = UCC_{t-2} - CCA_{t-1} \quad (3.2.22)$$

Finally, at the end of the project's service life (year N), the residual undepreciated capital cost is deemed fully expensed, and the capital-cost allowance for the final year is therefore set equal to that undepreciated balance:

$$CCA_N = UCC_{N-1} \quad (3.2.23)$$

so that the undepreciated capital cost at the end of that year is reduced to zero:

$$UCC_N = 0 \quad (3.2.24)$$

Under the straight-line depreciation method, the financial-analysis model assumes that the project's capitalized costs—defined by the tax depreciation base—are depreciated at a constant rate over the entire depreciation period. The share of initial costs that is not capitalized is expensed in the construction year, that is, year 0. Within this framework, the following equations are employed:

$$CCA_0 = C(1 - \delta) \tag{3.2.25}$$

For year 0 and for subsequent years within the depreciation period, the following equations are used:

$$CCA_t = \frac{C\delta}{N_d} \tag{3.2.26}$$

where N_d denotes the depreciation period.

The income-tax analysis allows the financial model to calculate the after-tax cash flows and resulting financial metrics. The applicable tax rate is the effective equivalent tax rate, that is, the rate at which the project's net income is taxed. The model assumes a single effective income tax rate, constant throughout the project's life and applied directly to the taxable net profit.

Taxable net profit is derived from the project's cash inflows and outflows, under the assumption that all revenues and expenditures are realized or incurred at the end of the respective year. The tax payment T_t for year t is computed as the effective income tax rate r_{IT} multiplied by the taxable net profit I_t for that year:

$$T_n = r_{IT}\, I_t \tag{3.2.27}$$

The taxable net profit for year one and subsequent years is calculated as follows:

$$I_t = C_t + D_{i,t} - CCA_t \tag{3.2.28}$$

In year 0, the taxable net profit is simply:

$$I_0 = IG - CCA_0 \tag{3.2.29}$$

Therefore, considering the previously defined pre-tax cash flows, asset depreciation, and income tax, the after-tax cash flow $\tilde{C}_n$ is calculated as follows:

$$\tilde{C}_t = C_t - T_t \tag{3.2.30}$$

Based on project data, the tool provides financial indicators, facilitating the project evaluation process. The net present value (NPV) of a project represents the value of all future cash flows discounted at a given discount rate in today's currency. It is calculated by discounting all cash flows, as shown below:

$$NPV = \sum_{t=0}^{N} \frac{\tilde{C}_t}{(1+r)^t} \tag{3.2.31}$$

where r is the discount rate and N is the project life (years).

The internal rate of return (IRR) is the discount rate that makes the project's NPV equal to zero, indicating the actual interest yield provided by the project's equity over its lifetime. It is obtained by solving the following equation for IRR:

$$NPV = 0 = \sum_{t=0}^{N} \frac{C_t}{(1+IRR)^t} \tag{3.2.32}$$

Note that C_0 is the net investment outlay (equity capital less incentives and subsidies) and is therefore recorded as a negative cash-flow at year 0. “Pre-tax IRR" uses pre-tax cash flows (C_n), whereas “after-tax IRR” uses after-tax cash flows ($\tilde{C}_n$).

The debt-service coverage (DSC) ratio compares the project's operational benefits with debt service payments, reflecting the project's ability to generate the cash flow required to meet its debt obligations. The DSC ratio for year n (DSC_n) is calculated by dividing the project's net operating income (net cash flows before depreciation, debt payments, and income tax) by the total debt payment (principal and interest):

$$DSC_t = \frac{max\left(C_t + D, COI_t - \tilde{C}_0\right)}{D} \tag{3.2.33}$$

where COI_n is the cumulative operating income for year n, defined as:

$$COI_t = \sum_{i=0}^{t} \tilde{C}_i \tag{3.2.34}$$

The term $C_t - D$ explicitly corresponds to the EBITDA (earnings before interest, taxes, depreciation, and amortization). Using the above formulation, the financial model calculates the debt-service coverage ratio for each year of the project and identifies the lowest ratio recorded over the entire debt repayment period, providing a conservative indicator of financial viability.

The LCOE and LCOH calculation are performed with similar equations as described in Section 3.1.7 which focus on potential assessment map generation. The cash flow described in this section is applied for their calculation in the financial block of the GeoH$_2$-FAT.

The financial variables reflect the hypothesized terms for each funding source—namely, their proportional share in the capital structure; pricing (interest or discount rates); disbursement modalities (schedule, grace period, amortization profile, and frequency); and whether funds are released *pari passu* with equity injections and project expenditures or under alternative arrangements. The resulting cash-flow outputs are subsequently imported into the integration block for the consolidated assessment of the overall plant.

3.2.5 Integration block

The Integration Block consolidates the main input data related to energy generation and/or purchase, as well as hydrogen production, storage, and transportation for simulating the chosen alternative. In addition, it conducts an environmental impact analysis. In this way, it integrates the results obtained from the building blocks discussed earlier in the chapter.

Within the Integration Block, it is possible to view the annual technical and financial flows throughout the plant's service life, such as energy consumption, hydrogen production, water consumption, and OPEX costs for production and power generation plants, among others. The block can operate under two modes:

1. **Constant Production Mode**: The annual hydrogen production is treated as a constant value, in accordance with the capacity specified for the hydrogen production plant. Maintaining this constant output requires higher electricity consumption over the years, due to inherent technological degradation.

2. **Constant Energy Mode**: A fixed amount of energy is set over the years. Under these conditions, hydrogen production decreases over time, stemming from equipment degradation.

It is noteworthy that, in the "Constant Production" mode, the block assesses whether the generated energy can satisfy the electrolyzer's demand, based on the production mode selected by the user and the project data. If insufficient, the tool signals this shortfall.

For the environmental impact analysis, the tool employs the methodology of Life Cycle Assessment (LCA). This methodology is widely used to measure environmental impacts and features various approaches. In this study, a cradle-to-grave approach was adopted, covering everything from the manufacturing of components and hydrogen production to final disposal.

In Brazil, the standard ABNT NBR ISO 14040 [120] supports LCA implementation, aiming to evaluate the magnitude and significance of potential environmental impacts linked to the subject under study. On this tool, only the impact category related to climate change—measured in CO_2-equivalent emissions—is considered in each block.

To implement LCA in the tool, a literature review was conducted on diverse applications of this tool. Drawing on those findings, a methodology was developed to quantify carbon dioxide equivalent (CO_2 eq) emissions for each block of the tool, with the Integration Block tasked with calculating emissions across the entire chain.

The modular approach of the tool permits impact assessment at three distinct boundaries:

i) Cradle-to-gate – from raw material extraction to the plant gate;
ii) Cradle-to-user's gate – extending to the user's location; and
iii) Cradle-to-grave – including final use in the mobility or power generation sector.

It is important to highlight that impacts are calculated under a cradle-to-grave perspective, starting with the extraction of raw materials, continuing through usage, and ending with final waste disposal (potentially involving recycling and/or final deposition).

Figure 12 presents a flowchart of the entire process, where the diamonds represent operational alternatives, and each blue arrow indicates the equivalent emissions calculated for each block. The output data are obtained by integrating results from each module and their interconnections.

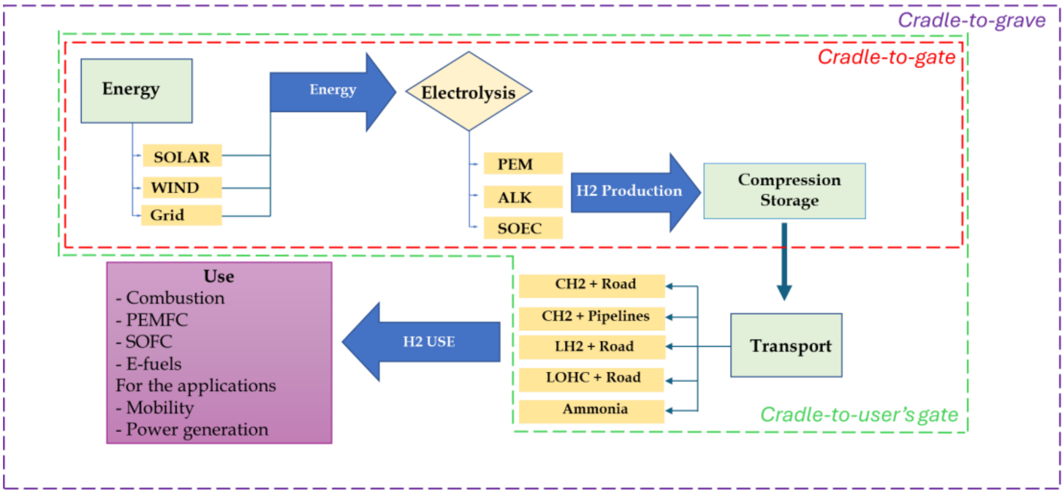

Figure 12 - Life cycle assessment flowchart applied in the developed tool.
Source: Own elaboration.

Hence, emissions can be calculated only up to the plant gate in the case of local production without transport or final use (cradle-to-gate), or from cradle to grave (cradle-to-grave) for more conventional fuels when referring to final use. Alternatively, a cradle-to-user's gate approach may be adopted by including transportation. The specific life cycle under analysis depends on the technologies chosen by the user in the tool's various blocks.

In each block, equivalent emissions are calculated in $kgCO_2eq$ per functional unit (FU). The functional unit is defined as 1 kWh for the power generation block or 1 kg of H_2 for the other blocks (hydrogen generation, storage, and transportation). Thus, the Integration Block determines the overall emissions impact across the entire production chain.

Extending this analysis to the use of this energy carrier, the tool considers end-use applications either in the mobility sector or electric power generation.

In mobility, comparative matrices were created for three types of use: (i) maritime passenger transport, (ii) maritime freight transport, and (iii) road transport. The reference functional units were 1 km traveled per ton of cargo transported (maritime) and 1 km traveled (terrestrial).

For the comparison results, the tool uses data collected from the literature [121–135] for combinations of fossil fuels (diesel, gasoline, heavy marine diesel oil, etc.) and renewable fuels (ethanol, green ammonia), applied in (the emission conversion factors can be found in Appendix D):

- Internal combustion engines (ICE), spark ignition (SI) or compression ignition (CI)
- Hybrid vehicles (Hybrid ICE)
- Battery electric vehicles (BEV), with a constant efficiency of 0.25 kWh/km for converting electrical energy into distance traveled [122]
- Fuel cell vehicles, either PEMFC or SOFC
- Gas turbines (GT)

For power generation, data from TURCONI et al. [136] on conventional technologies—coal, lignite, natural gas, petroleum, and biomass—were used to facilitate a cradle-to-grave comparison with power generation through fuel cells (PEMFC [137] and SOFC [138]).

Finally, an assessment is made of the potential for monetizing the environmental impacts produced or avoided. In the absence of a suitable mechanism for this purpose, an approach similar to RenovaBio's Decarbonization Credit (CBIO) calculator was employed to help meet decarbonization targets.

A CBIO is issued by biofuel producers and importers—duly certified by the ANP (National Agency of Petroleum, Natural Gas and Biofuels)—based on their invoices for sales and purchases. Meanwhile, fossil fuel distributors are assigned annual decarbonization targets by the ANP according to the share of fossil fuels they commercialize, and acquiring CBIOs is the only way to meet these targets. Each CBIO corresponds to one ton of CO_2 avoided. Brazil's stock exchange (B3) provides the environment for registering issuance, trading, and retirement requests for CBIOs, with financial institutions acting as registrars and/or representatives of CBIO-buying clients.

Following the CBIO operating logic for an initial economic assessment, data from the spreadsheet calculating equivalent emissions in hydrogen production—based on the user's selected configurations—were considered. The substitution of fossil fuels (coal, lignite, natural gas, and petroleum derivatives) was assumed to quantify avoided emissions and to calculate both the number of CBIOs and their economic value (either the annual average during the plant's operating lifetime in BRL or a weighted average per kilogram of H_2, in BRL/kg). An example of this calculation is demonstrated in Section 4.2.3.

Based on the outputs from the Integration Block and on the financial parameters in the Financing Block, the simulated project undergoes an economic-financial and environmental evaluation. In broad terms, the tool outputs: a technical assessment of the input data for the enterprise, signaling any nonconformities; operational and economic-financial parameters pertaining to the enterprise; and the project's emission values. Table 12 summarizes the main expected results from GeoH₂-FAT.

Table 12 - Expected main results from the $GeoH_2$-FAT.

Result	***Unit***
Hydrogen production	[ton H_2/year]
Electricity consumption	[MWh/year]
Water consumption	[m^3/year]
Power generation from the solar plant	[MWh/year]
Electricity consumption from ACL	[MWh/year]
Cost of electricity consumed from the ACL	[BRL/year]
Levelized production cost of the solar plant	[BRL/year]
Levelized production cost of the hydrogen plant	[BRL/year]
Levelized hydrogen storage cost	[BRL/year]
Levelized hydrogen transportation cost	[BRL/year]
Final levelized hydrogen cost	[BRL/year]
Annual water consumption cost	[BRL/year]
Overhaul cost of the hydrogen production plant	[BRL]
Financial costs	[BRL/year]
Cash flow and financial indicators, such as:	
Annual revenue	[BRL/year]
Annual profit	[BRL/year]
EBITDA	[BRL/year]
Project IRR	[%]
Shareholder IRR	[%]
NPV	[BRL/year]
Capital Structure – Debt/EBITDA	[%]
Debt Service Coverage Ratio (DSC)	[%]
Annual carbon emissions	[tCO_2eq]

Source: Own elaboration.

4 Results and discussion

This section aims to bring together the main results from the potential assessment model ($GeoH_2$-PAM) and the feasibility analysis tool ($GeoH_2$-FAT) that were developed in this thesis.

With respect to the $GeoH_2$-PAM, the simulations conducted for Brazil—evaluating the gross, technical, and economic potential of green hydrogen and its derivatives (green ammonia and green methanol) produced from SPV, ONW, and OFW—are detailed in Sections 4.1.1, 4.1.2, and 4.1.3. Regarding the $GeoH_2$-FAT, a base case was defined and results for three distinct case scenarios are presented. Case 1 (Section 4.2.1) reports the outcomes and sensitivity analysis for the CAPEX and OPEX of a plant powered 100 % by solar PV. Case 2 (Section 4.2.2) provides analogous results for a plant powered entirely by on-site wind. Finally, Case 3 (Section 4.2.3), comprising a 33 % solar, 33 % wind, and 33 % ACL (with I-RECs).

4.1 Potential assessment model (PAM) results

For each RES (SPV, ONW and OFW) the results encompass eight main outcome types: gross hydrogen production potential maps, technical hydrogen production potential maps, a constraint-overlap matrix illustrating how exclusion layers intersect, sensitivity analyses of gross versus technical potential under varying capacity-factor thresholds, state-by-state or sedimentary basins comparisons of constrained areas alongside gross and technical land/power potentials, detailed tables of per-state hydrogen and derivative production potential estimates, georeferenced economic potential presented as LCOE maps, and georeferenced economic potential presented as LCOH maps.

4.1.1 Solar photovoltaic (SPV)

This subsection presents the simulation results for utility-scale Solar PV (SPV) in Brazil, examining how spatial constraints and capacity-factor thresholds shape the differences between theoretical ("gross") and practically attainable ("technical") potentials for hydrogen production and its derivatives. As shown in Figure 13, vast areas throughout the country exhibit substantial solar irradiance, creating favorable conditions for hydrogen production and its derivatives. The subsequent analyses highlight how this initial gross potential is then curtailed by layers of environmental, infrastructural, and socio-economic restrictions, ultimately defining a more realistic "technical" potential.

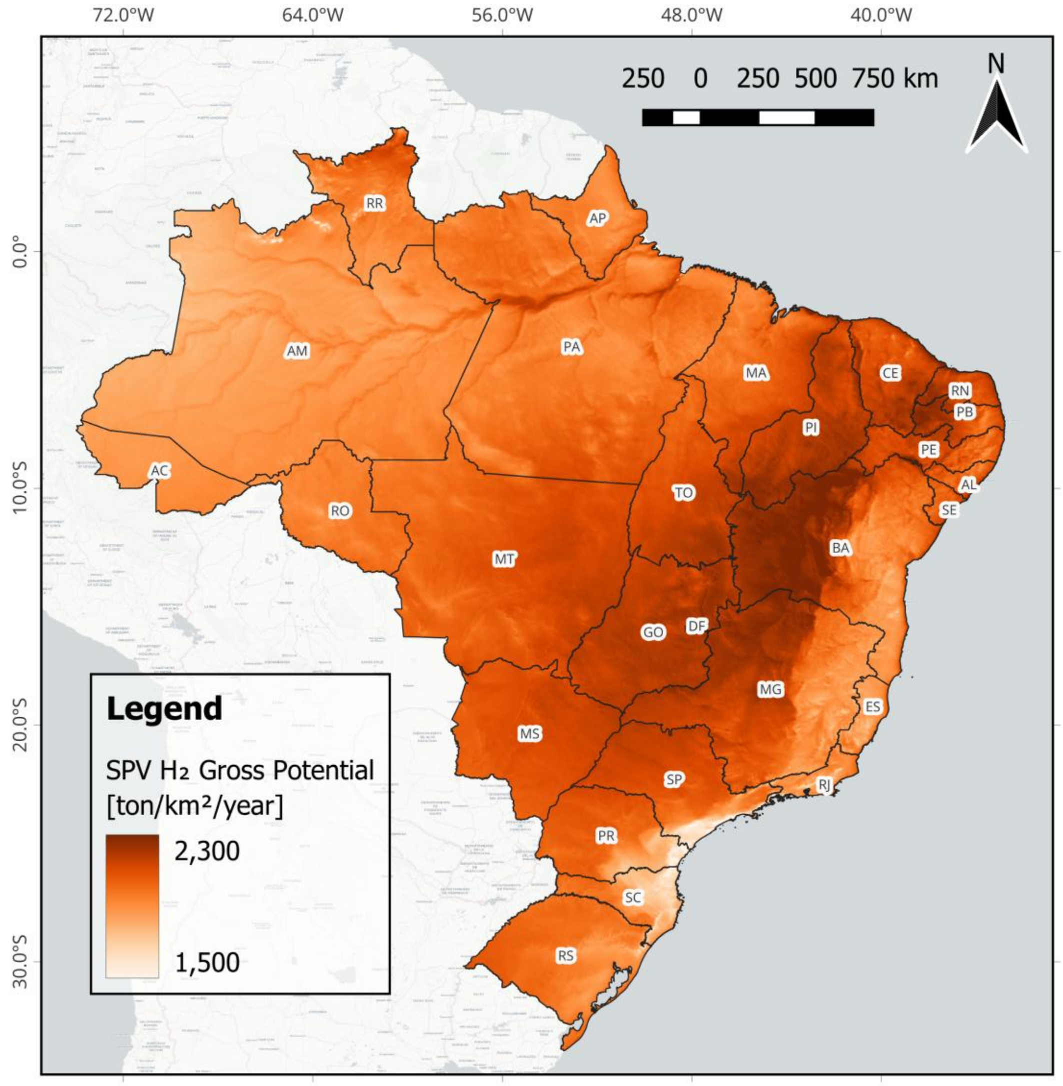

Figure 13 – Gross hydrogen production potential from utility-scale SPV.
Source: Own elaboration.

From the spatial distribution in Figure 13, it is evident that Brazil possesses a vast theoretical resource base for utility-scale Solar PV. However, as summarized in Table 13, once each major constraint is sequentially applied—ranging from infrastructure and environmental restrictions to social and heritage protections—the gross potential area of 8.475 (1,000 km²) and its corresponding capacity of 441.894 GW undergo substantial reductions. Notably, constraints such as "Priority Areas for Biodiversity Conservation" and "Rural settlements" cause notable declines, ultimately leading to a "technical" area of only 3.148 (1,000 km²) and 164.158 GW of power. These reductions similarly appear in projected energy output and hydrogen yields, underscoring how cumulative land-use limitations substantially diminish the country's exploitable solar resource when shifting from a purely theoretical framework to a realistic, constraint-driven perspective.

Table 13 – Brazil's gross and technical potential of energy, hydrogen and derivatives from SPV.

Mask Name	Area (1000 km²)	Power (GW)	Energy (TWh/year)	H2 (Mton/year)	NH3 (Mton/year)	MeOH (Mton/year)
Gross potential	**8.475**	**441.894**	**965.886**	**17.120**	**88.225**	**69.064**
Oil & Gas pipelines	8.468	441.557	965.151	17.107	88.158	69.012
Oil & Gas fields	8.393	437.640	956.303	16.950	87.350	68.379
Transport infrastructure	8.451	440.649	963.136	17.071	87.974	68.868
Conservation Units	6.944	362.098	795.802	14.105	72.690	56.903
Priority Areas for B. C.	5.950	310.239	675.414	11.971	61.693	48.294
Archaeological sites	8.474	441.860	965.808	17.118	88.218	69.059
Water bodies	8.322	433.944	948.366	16.809	86.624	67.811
Urbanized areas	8.425	439.318	960.245	17.020	87.710	68.661
Rural settlements	7.761	404.693	886.678	15.716	80.990	63.401
Quilombola areas	8.444	440.272	962.304	17.056	87.898	68.808
Indigenous lands	7.323	381.862	839.436	14.878	76.675	60.023
Slope	8.472	441.736	965.571	17.114	88.196	69.042
Capacity Factor	8.475	441.894	965.886	17.120	88.225	69.064
Power transmission cables	8.457	440.976	963.837	17.083	88.038	68.918
Technical potential	**3.148**	**164.158**	**365.152**	**6.472**	**33.353**	**26.109**

Source: Own elaboration.

A close inspection of the table reveals a significant discrepancy between the gross potential—the theoretical maximum without spatial or regulatory constraints—and the final "Technical potential," which reflects a more realistic estimate after all constraints are taken into account. In particular, the "Gross potential" area of 8.475 (1000 km²) and corresponding power of 441.894 GW drop markedly to 3.148 (1000 km²) and 164.158 GW in the "Technical potential," equating to reductions of approximately 63% in both land area and power availability. This decrease similarly manifests in the energy production column (from 110.261 GWh/year to 41.684 GWh/year) and in potential hydrogen yields (from 17.120 Mton/year to 6.472 Mton/year), again on the order of a 60–65% reduction.

Although many of the individual constraints—such as "Oil & Gas pipelines" or "Archaeological sites"—produce only marginal decreases compared to the gross baseline, others, notably "Conservation Units," "Priority Areas for B. C.," "Rural settlements," and "Indigenous lands," drive more substantial changes in the remaining exploitable area and energy output. For instance, "Priority Areas for B. C." decrease the available area from 8.475 to 5.950 (1000 km²), which constitutes a nearly 30% decline. With all the constraints applied, Figure 14 shows the technical potential of hydrogen production map.

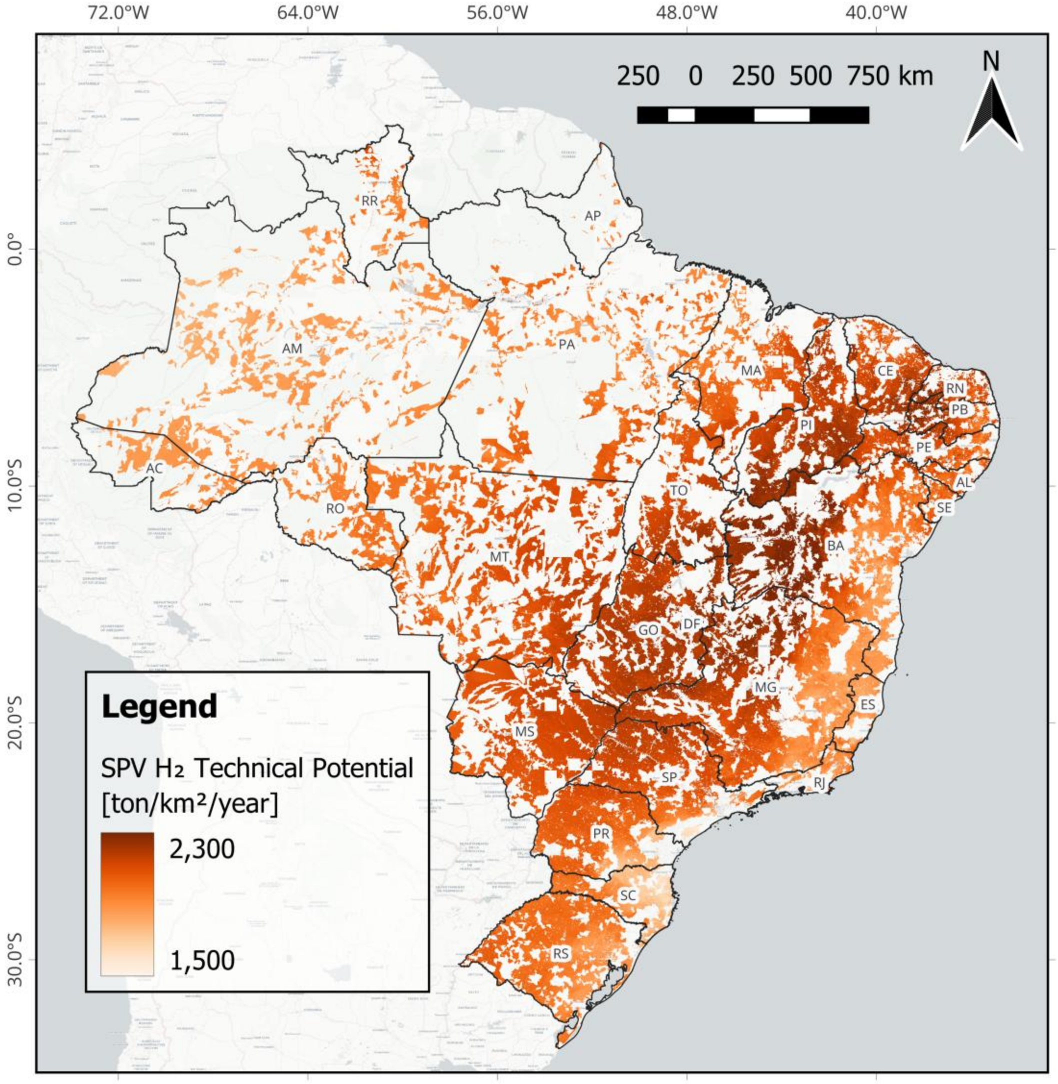

Figure 14 - Technical hydrogen production potential from utility-scale SPV.
Source: Own elaboration.

Overlapping areas arise because individual constraints often apply to the same geographic location. For instance, a single area might simultaneously fall within a biodiversity conservation unit, contain archaeological sites, and possess high slopes, each of which introduces its own limitations. As these constraints intersect, the portion of land viable for energy infrastructure or hydrogen production decreases, highlighting the importance of assessing each layer's spatial footprint in concert rather than in isolation. Table 14 shows the overlapping of constraints matrix when assessing technical potential of hydrogen production from SPV. It provides a concise depiction of how each constraint layer spatially intersects with every other layer, thereby illustrating the cumulative effect of overlapping restrictions on site suitability. The upper triangle (green cells) indicates the overlap between the row mask and the column mask as a percentage of the column mask's area, whereas the lower triangle (blue cells) represents the same overlap in terms of the row mask's area. Consequently, the asymmetry between corresponding green and blue cells highlights differences in the relative sizes of overlapping regions. For instance, "Oil & Gas fields" overlap only marginally with "Transport infrastructure" (1% in the lower triangle) because "Oil & Gas fields" occupy a smaller footprint overall, yet they comprise 0% of the total area of “Transport infrastructure” (upper triangle), signaling that these two layers do not extensively coincide. Observing which constraints, such as “Conservation Units,” “Priority Areas for Biodiversity Conservation,” or “Slope,” exhibit higher percentages across multiple columns reveals how widespread their geographic coverage can be. Meanwhile, the diagonal and final column remain at 100%, reflecting the fact that each mask fully overlaps with itself and that “Unified Solar PV Mask” logically encompasses all constituent constraints.

Table 14 - Overlapping of constraints matrix when assessing technical potential of hydrogen production from SPV.

	Oil & Gas pipelines	Oil & Gas fields	Transport infrastructure	Conservation Units	Priority Areas for Biodiversity Conservation	Archaeological sites	Water bodies	Urbanized areas	Rural settlements	Quilombola areas	Indigenous lands	Slope	Capacity Factor	Power transmission cables	Unified Solar PV Mask
Oil & Gas pipelines	100%	5%	3%	7%	37%	0%	1%	16%	2%	0%	0%	0%	0%	1%	100%
Oil & Gas fields	0%	100%	0%	3%	25%	0%	2%	1%	6%	0%	0%	0%	0%	0%	100%
Transport infrastructure	1%	1%	100%	9%	36%	0%	13%	7%	3%	0%	3%	0%	0%	0%	100%
Conservation Units	0%	0%	0%	100%	9%	0%	2%	0%	20%	1%	7%	0%	0%	0%	100%
Priority Areas for Biodiversity	0%	1%	0%	5%	100%	0%	3%	1%	8%	0%	1%	0%	0%	0%	100%
Archaeological sites	0%	2%	2%	11%	41%	100%	3%	4%	3%	1%	5%	0%	0%	3%	100%
Water bodies	0%	1%	2%	19%	44%	0%	100%	0%	6%	0%	4%	0%	0%	0%	100%
Urbanized areas	2%	1%	3%	7%	33%	0%	0%	100%	2%	0%	0%	0%	0%	0%	100%
Rural settlements	0%	1%	0%	43%	28%	0%	1%	0%	100%	0%	1%	0%	0%	0%	100%
Quilombola areas	0%	1%	0%	45%	29%	0%	2%	0%	9%	100%	0%	0%	0%	0%	100%
Indigenous lands	0%	0%	0%	10%	1%	0%	0%	0%	1%	0%	100%	0%	0%	0%	100%
Slope	0%	0%	0%	39%	29%	0%	0%	0%	1%	1%	12%	100%	0%	0%	100%
Capacity Factor	0%	0%	0%	0%	0%	0%	0%	0%	0%	0%	0%	0%	100%	0%	100%
Power transmission cables	0%	1%	1%	5%	35%	0%	0%	1%	4%	0%	0%	0%	0%	100%	100%
Unified Solar PV Mask	0%	2%	0%	29%	47%	0%	3%	1%	13%	1%	22%	0%	0%	0%	100%

Legend:
Upper Triangle (green): Overlap as a percentage of the column mask's area.
Lower Triangle (blue): Overlap as a percentage of the row mask's area.
Diagonal and last column (orange): Always 100% because a mask fully overlaps with itself

Source: Own elaboration.

Some constraints can be very sensible when assessing technical potential. Specifically, for SPV, the capacity factor restriction applied can radically modify the results. Brazil offers a high capacity factor for SPV, and the restriction of <15% applied in this thesis simply did not excluded any available area. However, if higher restrictions are applied, the results can be different. Figure 15 shows the technical e gross potential of hydrogen production from SPV in function of the SPV capacity factor restriction applied.

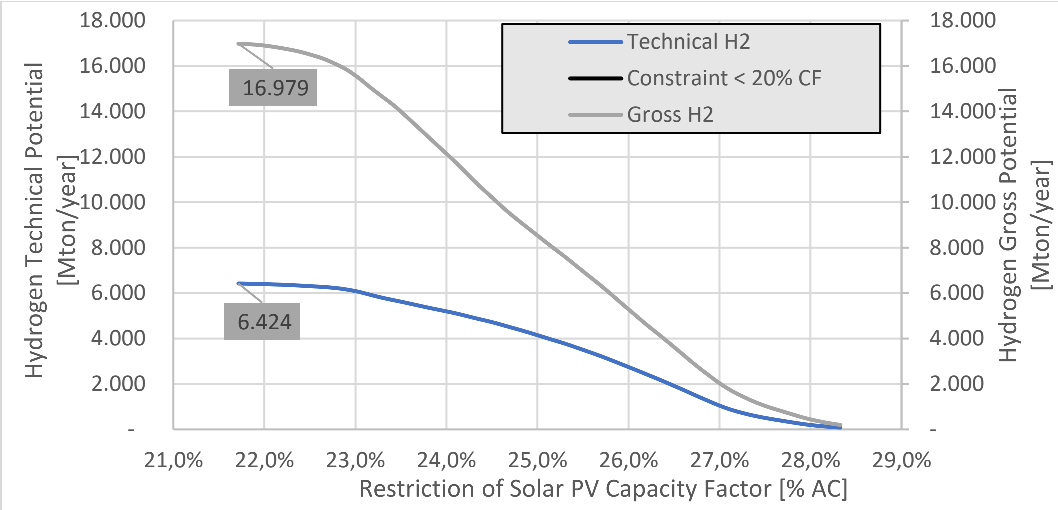

Figure 15 - Technical e gross potential of hydrogen production from SPV in function of restriction of capacity factor.
Source: Own elaboration.

A simulation of constraints considered, technical potential, gross potential and overlapping areas were also made for each state in Brazil. Figure 16 shows the area constrained for each constraint layer, technical and gross potential and overlapping areas for each state. The results reveal significant variation in land area constraints and technical potentials across Brazilian states, measured in 1000 km². Amazonas (AM) stands out with the highest total constraints, notably 460.82 from conservation units and 392.15 from priority areas for biodiversity conservation, reflecting its vast ecological reserves. Pará (PA) also has high constraints, particularly from conservation units (393.11) and indigenous lands (304.42), highlighting the state's rich environmental and cultural heritage. In contrast, smaller states like Alagoas (AL) and Espírito Santo (ES) exhibit the smallest constraints, with totals of 2.96 and 1.65 from conservation units, respectively, consistent with their more limited land availability. The lowest specific constraint is seen in Amapá (AP), where urbanized areas occupy only 0.16. Regarding technical potential, Minas Gerais (MG) leads with 368.23, followed by Mato Grosso (MT) with 327.46 and Bahia (BA) with 278.12, reflecting their expansive land areas and favorable renewable energy conditions. Meanwhile, Amapá (AP) and Distrito Federal (DF) exhibit the smallest technical potentials, with 4.18 and 0.06, respectively, highlighting the limitations of smaller or urbanized states. This analysis emphasizes the need for region-specific strategies to optimize renewable energy development while considering ecological and social priorities.

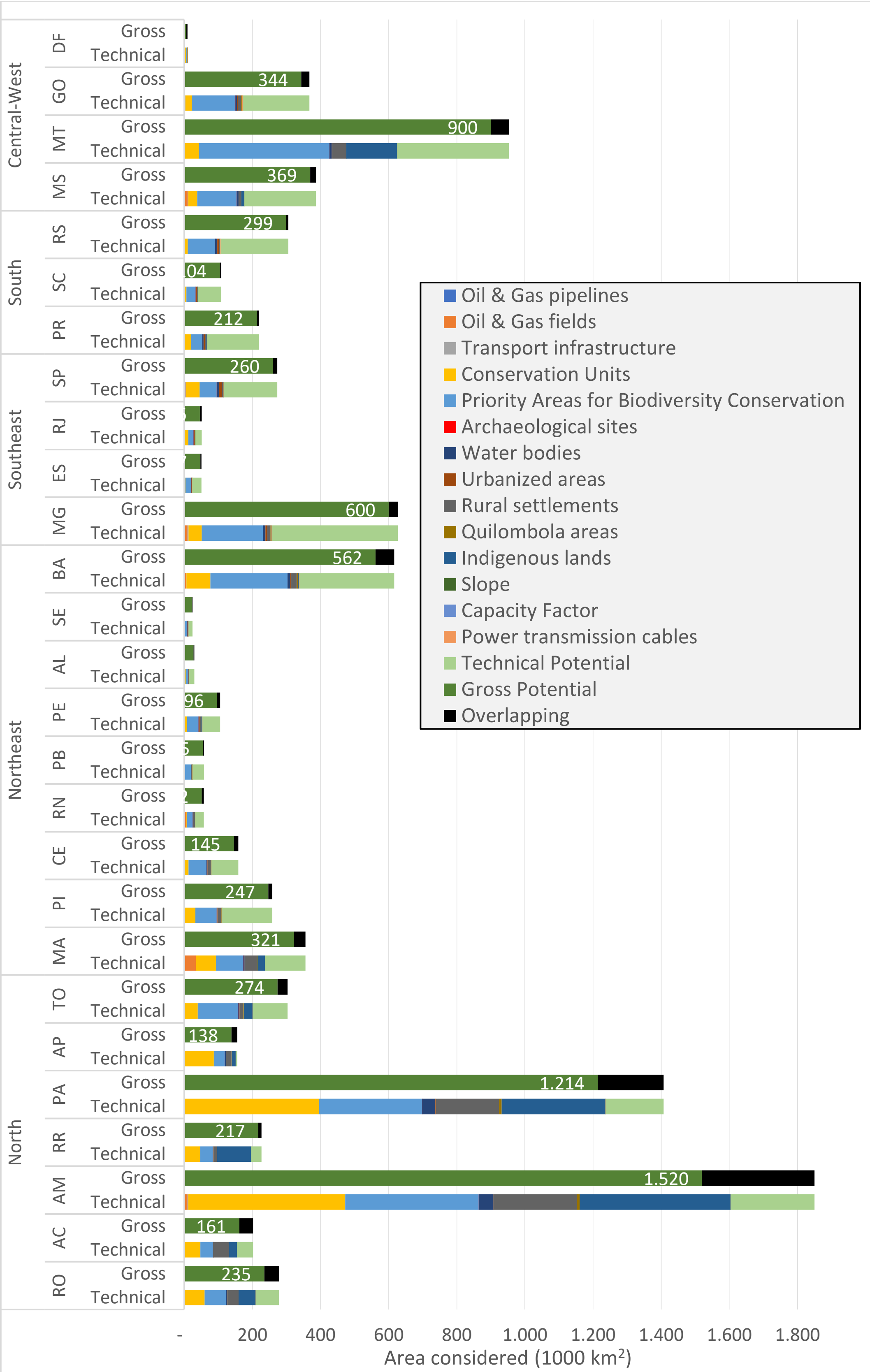

Figure 16 - Area constrained for each constraint layer, technical and gross potential and overlapping when assessing SPV for each state.
Source: Own elaboration.

However, this is just the area. The scenario can be different when talking about the production potential of green hydrogen and derivatives, because of capacity differences. Table 15 reveals the potential production of hydrogen and derivative for each state.

Table 15 - Potential production of hydrogen and derivative from SPV for each state in Brazil.

	Technical Potential			Gross Potential		
State	H2 (Mton/year)	NH3 (Mton/year)	MeOH (Mton/year)	H2 (Mton/year)	NH3 (Mton/year)	MeOH (Mton/year)
RO	133	686	537	461	2.374	1.858
AC	89	458	359	306	1.575	1.233
AM	460	2.372	1.857	2.849	14.680	11.491
RR	59	305	238	427	2.200	1.723
PA	337	1.738	1.361	2.414	12.438	9.737
AP	8	42	33	270	1.389	1.088
TO	218	1.124	880	582	2.999	2.348
MA	242	1.249	978	660	3.400	2.661
PI	322	1.662	1.301	540	2.785	2.180
CE	170	877	686	311	1.605	1.256
RN	55	283	222	111	573	449
PB	74	380	298	119	612	479
PE	109	563	441	203	1.045	818
AL	32	165	129	56	290	227
SE	24	124	97	45	231	181
BA	585	3.015	2.360	1.190	6.131	4.799
MG	763	3.933	3.079	1.253	6.456	5.054
ES	50	258	202	89	459	359
RJ	36	185	145	86	445	348
SP	326	1.681	1.316	533	2.748	2.151
PR	306	1.575	1.233	423	2.180	1.707
SC	125	643	504	191	986	772
RS	395	2.033	1.592	592	3.053	2.390
MS	444	2.288	1.791	777	4.006	3.136
MT	681	3.510	2.748	1.869	9.629	7.538
GO	428	2.204	1.725	751	3.871	3.030
DF	0	1	1	13	66	52

Source: Own elaboration.

Analyzing the hydrogen and its derivatives potential from SPV demonstrates notable variations when differentiating between the technical and gross potential across Brazilian states. When comparing technical versus gross potential, clear contrasts emerge across the Brazilian states. In terms of *technical* hydrogen output (H_2), Minas Gerais (MG) ranks highest at 763 Mton/year, followed by Mato Grosso (MT) at 681 Mton/year and Bahia (BA) at 585 Mton/year. However, these figures drop considerably from their respective *gross* potentials, illustrating how spatial constraints curtail the theoretical maximum. For example, Amazonas (AM) shows a gross hydrogen potential of 2.849 Mton/year but can only realize 460 Mton/year once these restrictions are applied. A similar pattern holds for ammonia (NH_3) and methanol (MeOH), with states such as MG, BA, and MT again leading in the technical estimates but still falling short of their gross capacities.

For the economic potential, the LCOE and LCOH were calculated for the constrained area. Figure 17 illustrates the estimated LCOE for utility-scale Solar PV across the constrained areas in Brazil, shedding light on the economic viability of projects once spatial, environmental, and social restrictions are applied. Regions with higher solar irradiance and favorable infrastructure conditions tend to exhibit lower LCOE, reflecting a stronger business case for Solar PV deployment. By contrast, areas with suboptimal solar resources or more pronounced development constraints often show higher LCOE values, indicating the need for supportive policies, improved transmission infrastructure, or targeted incentives

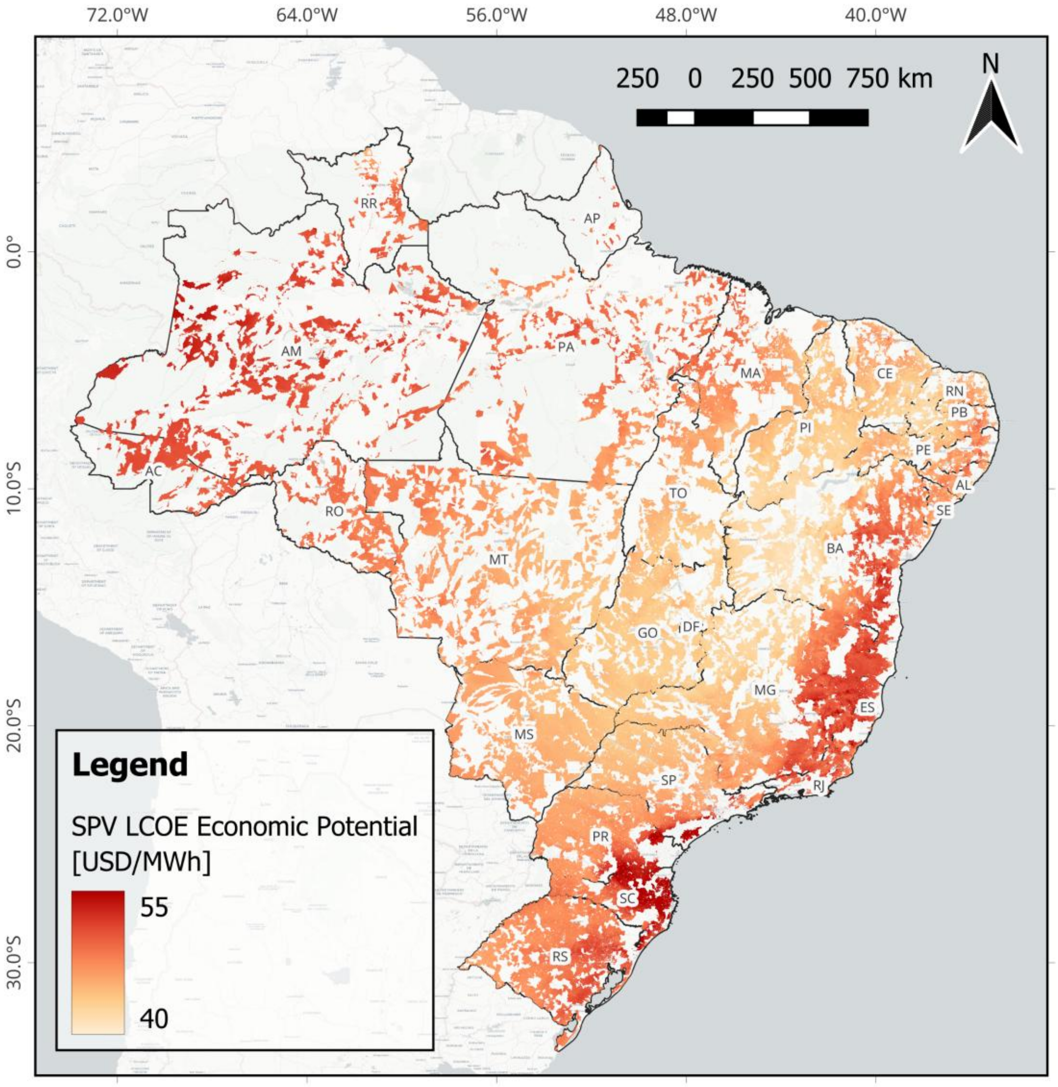

Figure 17 – Economic potential as LCOE of utility-scale SPV.
Source: Own elaboration.

The LCOH from utility-scale SPV varies considerably across Brazil, reflecting differences in solar resource quality, infrastructure availability, and land-use constraints. As illustrated in Figure 18, areas combining strong irradiance with fewer spatial limitations feature some of the lowest hydrogen costs, making them candidates for large-scale green hydrogen initiatives.

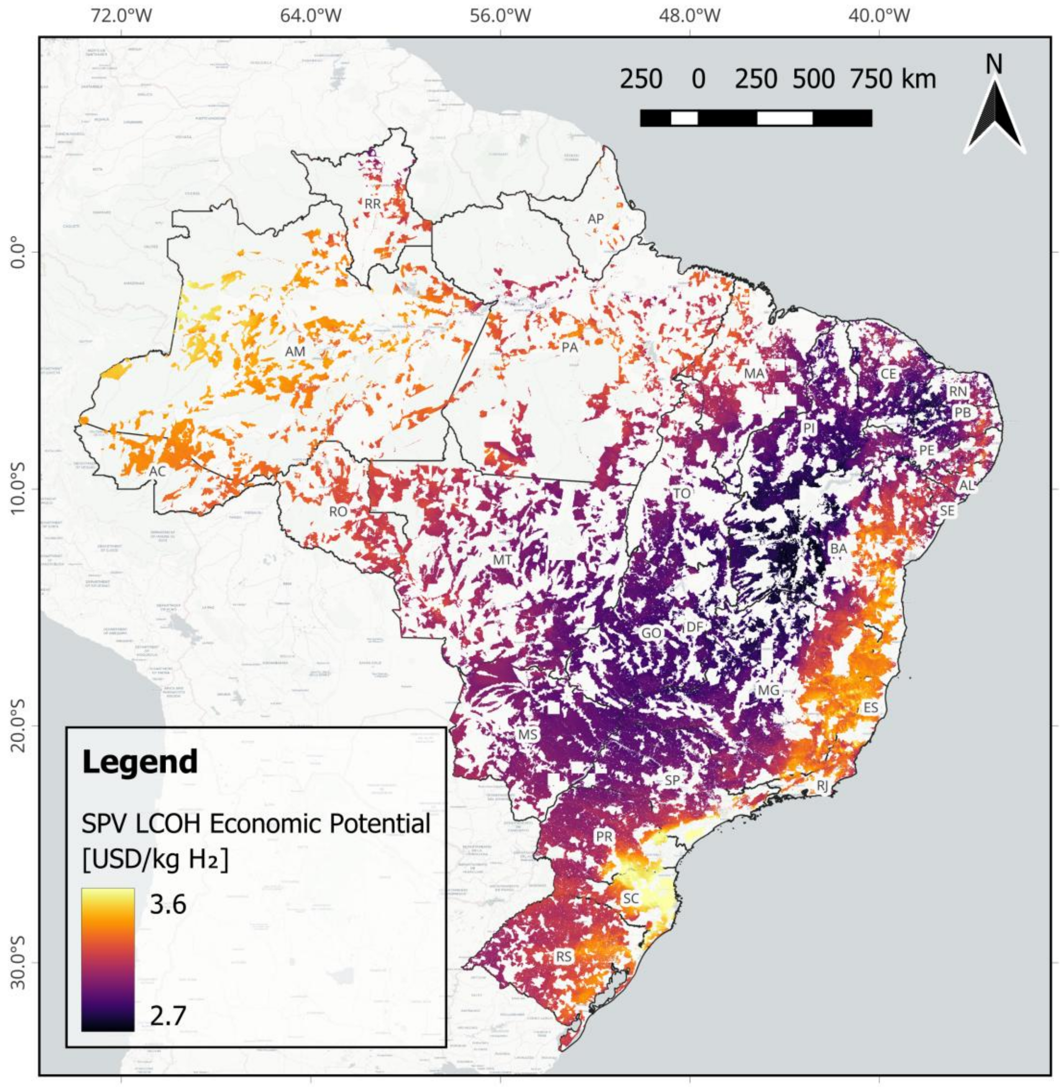

Figure 18 – Economic potential as relative LCOH from utility-scale SPV.
Source: Own elaboration.

4.1.2 Onshore wind (ONW)

Brazil's ONW resource exhibits considerable gross potential for producing hydrogen and its derivatives, yet spatial and operational constraints significantly diminish the final amount of exploitable land. As shown in Figure 19, the gross potential for ONW spans a wide portion of the country, implying high levels of power output and energy production.

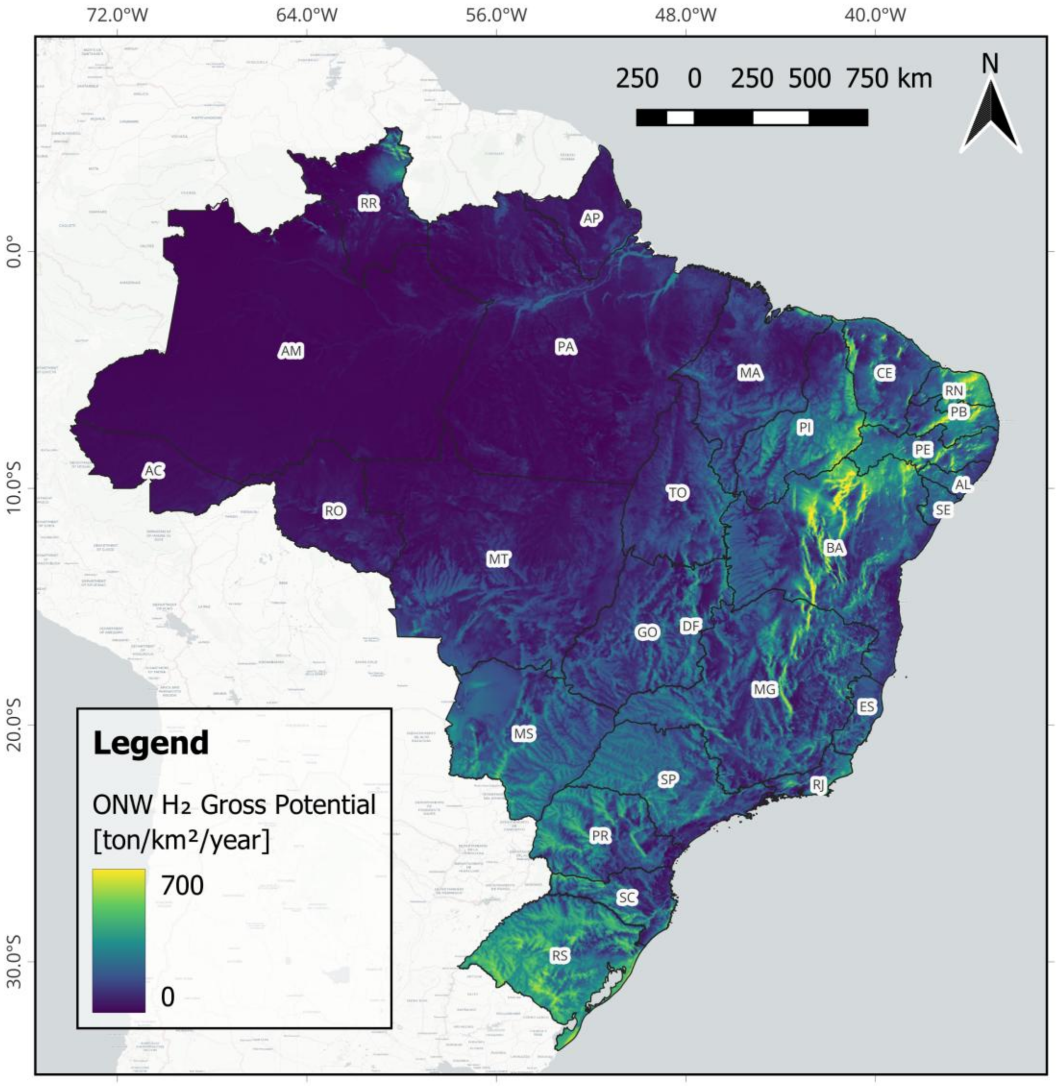

Figure 19 - Gross hydrogen production potential from ONW.
Source: Own elaboration.

In the context of the gross and technical potential for the production of hydrogen and derivatives form onshore wind in Brazil reveals a substantial decrease between the theoretical maximum (gross potential) and the more constrained technical potential. Table 16 shows the Brazilian gross and technical potential of energy, hydrogen and derivatives from ONW.

Table 16 - Brazil’s gross and technical potential of energy, hydrogen and derivatives from ONW.

Mask Name	Area (1000 km²)	Power (GW)	Energy (TWh/year)	H2 (Mton/year)	NH3 (Mton/year)	MeOH (Mton/year)
Gross Potential	**8.449**	**49.663**	**46.840**	**830**	**4.278**	**3.349**
Oil & Gas pipelines	8.443	49.626	46.787	829	4.274	3.345
Oil & Gas fields	8.366	49.177	46.262	820	4.226	3.308
Transport infrastructure	8.312	48.854	45.859	813	4.188	3.279
Conservation Units	6.924	40.698	41.216	731	3.765	2.947
Priority Areas for B.C.	5.930	34.853	31.913	566	2.915	2.282
Archaeological sites	8.449	49.659	46.831	830	4.278	3.349
Water bodies	8.297	48.771	45.867	813	4.190	3.280
Urbanized areas	8.400	49.373	46.428	823	4.241	3.320
Rural settlements	7.737	45.476	44.764	793	4.089	3.201
Quilombola areas	8.418	49.481	46.708	828	4.266	3.340
Indigenous lands	7.304	42.931	44.772	794	4.090	3.201
Slope	8.446	49.646	46.805	830	4.276	3.347
Capacity Factor	1.421	8.353	21.261	377	1.942	1.520
Power transmission	8.312	48.856	45.622	809	4.167	3.262
Technical Potential	**777**	**4.569**	**11.362**	**201**	**1.038**	**813**

Source: Own elaboration.

The gross potential for onshore wind energy encompasses an area of 8449 km², yielding 49,663 GW of power and corresponding energy yields of 5347 GWh/year. However, after accounting for various constraints, the technical potential drops remarkably to 777 km² with a corresponding power potential of just 4569 GW, marking a reduction of approximately 92%. This sharp decline in technical potential is seen throughout the hydrogen and derivative columns, with H_2 production dropping from 830 Mton/year in the gross potential to only 201 Mton/year in the technical potential—an approximately 75% decrease. Similar reductions are seen for ammonia (NH_3) and methanol (MeOH), which both experience declines of around 76%.

These reductions can be attributed to the overlaying of various spatial constraints. The most impactful constraints on Brazil's technical potential for onshore wind energy are the "Conservation Units," "Priority Areas for B.C.," and "Capacity Factor." Conservation Units alone reduce the available area from 8,449 (1000 km²) to 6,924 (1000 km²—an 18% decrease. Meanwhile, Priority Areas for Biodiversity Conservation decrease the area by 30% (from 8,449 to 5,930 km²). The "Capacity Factor" further reduces the technically exploitable area by 83%, with a drop from 8,449 to 1,421 km². Figure 20 illustrates the technical potential for the production of hydrogen from ONW.

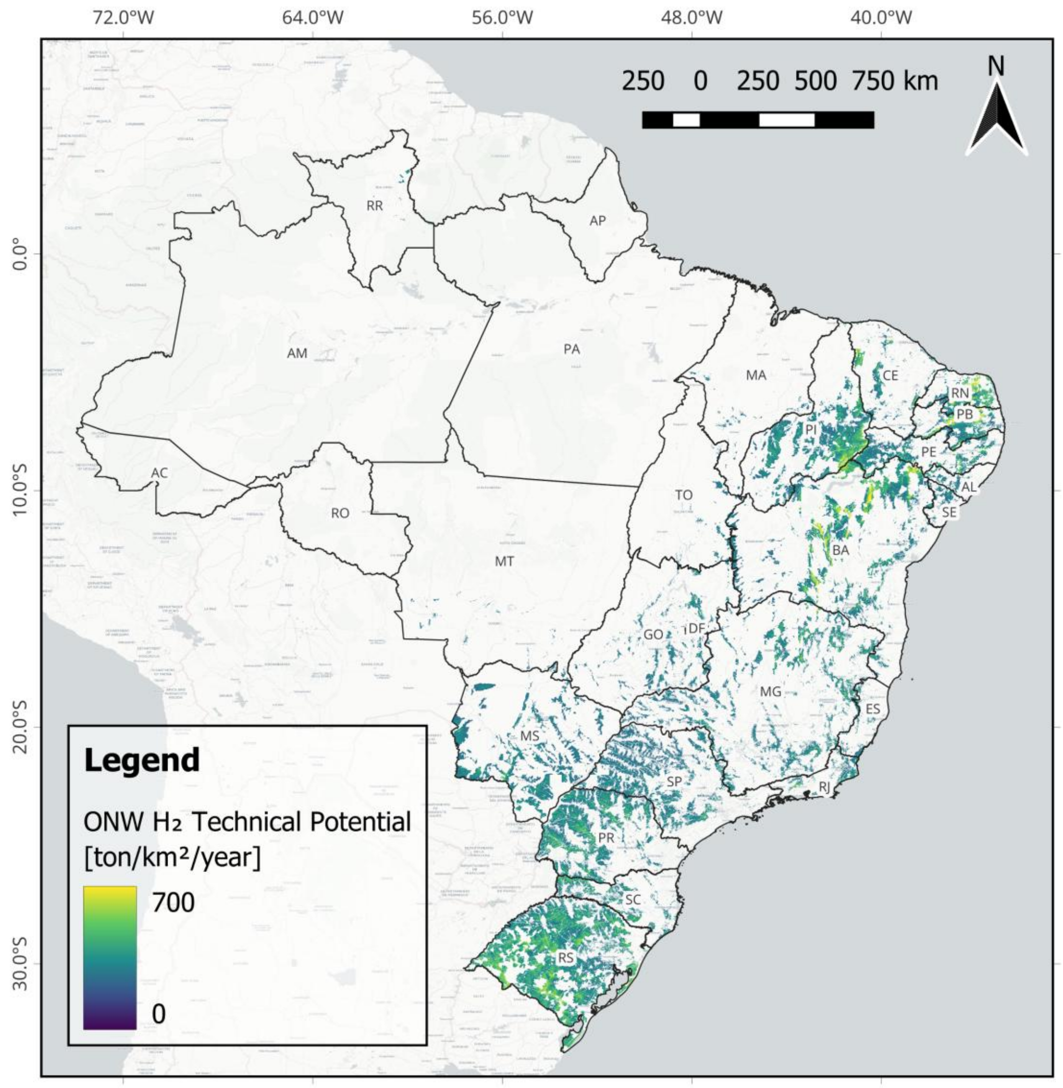

Figure 20 - Technical hydrogen production potential from ONW.
Source: Own elaboration.

However, as better explained in Section 4.1.1, overlapping areas arise because individual constraints often apply to the same geographic location. Table 17 show the overlapping matrix when assessing potential for the production of hydrogen from ONW in Brazil. This matrix illustrates the spatial overlap between various constraints and its impact on the technical potential for onshore wind-based hydrogen production. The upper triangle (green cells) shows the overlap as a percentage of the area covered by the column mask, while the lower triangle (blue cells) indicates the overlap concerning the row mask's area, highlighting the directional spatial relationship between each constraint. For example, the "Capacity Factor" constraint shows notable overlap with "Priority Areas for Biodiversity Conservation" (83%), further constraining potential land for development. Similarly, "Slope" overlaps significantly with "Conservation Units" (41%), emphasizing both environmental protections and topographical difficulties that together limit usable land. The diagonal (orange) and final column always show 100%, as each constraint fully overlaps with itself. These interactions between constraints compound the reduction in usable land, causing the “Unified Onshore

Wind Mask" to significantly reduce total available land and, consequently, the technical potential for hydrogen production from onshore wind resources.

Table 17 - Overlapping of constraints matrix when assessing technical potential of hydrogen production from ONW.

	Oil & Gas pipelines	Oil & Gas fields	Transport infrastructure	Conservation Units	Priority Areas for Biodiversity Conservation	Archaeological sites	Water bodies	Urbanized areas	Rural settlements	Quilombola areas	Indigenous lands	Slope	Capacity Factor	Power transmission cables	Unified Onshore Wind Mask
Oil & Gas pipelines	100%	6%	12%	8%	36%	0%	1%	15%	2%	0%	0%	0%	72%	9%	100%
Oil & Gas fields	0%	100%	2%	3%	25%	0%	2%	1%	6%	0%	0%	0%	79%	3%	100%
Transport infrastructure	1%	1%	100%	9%	36%	0%	12%	6%	4%	0%	3%	0%	76%	5%	100%
Conservation Units	0%	0%	1%	100%	9%	0%	2%	0%	20%	1%	7%	0%	91%	0%	100%
Priority Areas for Biodiversity Conservation	0%	1%	2%	5%	100%	0%	3%	1%	8%	0%	1%	0%	83%	2%	100%
Archaeological sites	1%	1%	5%	10%	40%	100%	3%	4%	4%	0%	5%	0%	63%	14%	100%
Water bodies	0%	1%	11%	19%	44%	0%	100%	0%	6%	0%	4%	0%	81%	1%	100%
Urbanized areas	2%	1%	16%	7%	33%	0%	0%	100%	1%	0%	0%	0%	70%	4%	100%
Rural settlements	0%	1%	1%	43%	28%	0%	1%	0%	100%	0%	1%	0%	95%	1%	100%
Quilombola areas	0%	1%	1%	45%	29%	0%	2%	0%	9%	100%	0%	0%	90%	1%	100%
Indigenous lands	0%	0%	0%	10%	1%	0%	0%	0%	1%	0%	100%	0%	98%	0%	100%
Slope	0%	0%	1%	41%	30%	0%	0%	0%	1%	1%	11%	100%	58%	1%	100%
Capacity Factor	0%	1%	1%	20%	30%	0%	2%	0%	10%	0%	16%	0%	100%	1%	100%
Power transmission cables	0%	2%	5%	6%	34%	0%	1%	1%	4%	0%	0%	0%	67%	100%	100%
Unified Onshore Wind Mask	0%	1%	2%	20%	33%	0%	2%	1%	9%	0%	15%	0%	92%	2%	100%

Legend:
Upper Triangle (green): Overlap as a percentage of the column mask's area.
Lower Triangle (blue): Overlap as a percentage of the row mask's area.
Diagonal and last column (orange): Always 100% because a mask fully overlaps with itself

Source: Own elaboration.

Some constraints can have a considerable impact when evaluating the potential of hydrogen production from ONW. In particular, applying a restriction of <20% on the capacity factor can substantially reduce the technical potential. ONW resources in Brazil have a relatively high theoretical capacity, but the capacity factor constraint identifies and excludes areas with lower efficiency, which can dramatically alter the outcomes. Figure 21 demonstrates the varying effects of different capacity factor restrictions on the technical and gross potential for hydrogen production from ONW.

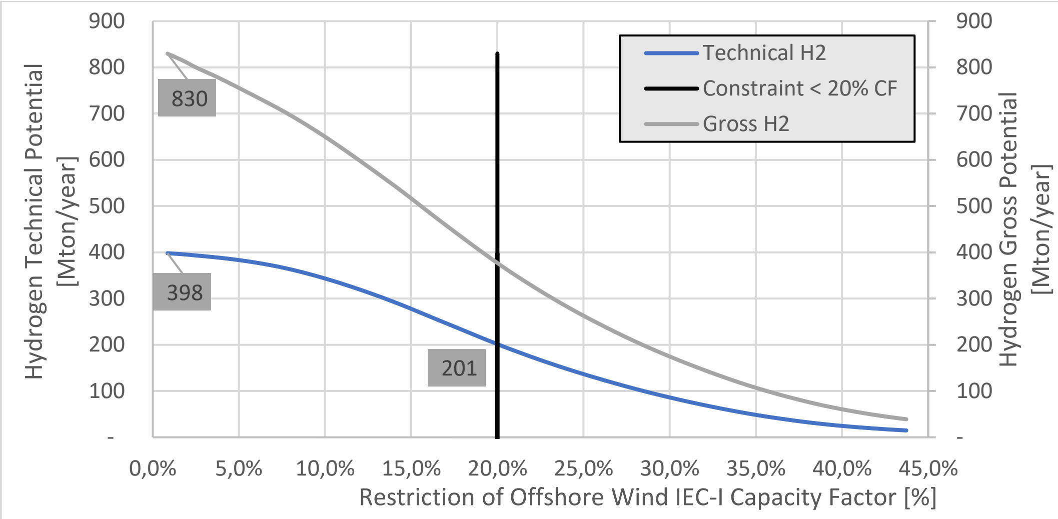

Figure 21 - Technical e gross potential of hydrogen production from ONW in function of restriction of capacity factor.
Source: Own elaboration.

In the assessment of hydrogen production potential from ONW across Brazilian states, it is evident that the interaction of spatial and environmental constraints substantially reduces the initially estimated (gross) potential. Figure 22 illustrates, for each state, the area constrained by each layer, the gross and technical potentials, and the degree of overlap among constraints. From results, it is clear that states such as Rio Grande do Sul (RS), Maranhão (MA), and Minas Gerais (MG) exemplify sizable discrepancies between gross and technical potentials. In RS, for instance, the gross potential of approximately 297.60 (1,000 km²) drops to around 157.14 (1,000 km²) once overlapping constraints are excluded, signifying a reduction of roughly 47%. MA displays an even more pronounced change, declining from 320.89 to just 3.67 (1,000 km²), which constitutes a decrease of nearly 99%. Similarly, MG's gross potential (598.87 1,000 km²) diminishes by about 86% upon accounting for constraints, leaving a technical potential of 81.12 (1,000 km²). These steep declines highlight the cumulative impact of factors including conservation units, priority biodiversity areas, and capacity-factor limitations. While certain constraints (e.g., oil and gas infrastructure or large urbanized areas) are more significant in some states than in others, the overlap matrix indicates that multiple, smaller exclusions can collectively remove large swaths of land from the initial (gross) estimate. When focusing on states like Acre (AC) and Amapá (AP)—which one might expect to have fewer transmission or pipeline conflicts—the effect of conservation- and biodiversity-related constraints emerges even more starkly. In AC, the gross potential of 160.64 (1,000 km²) is essentially reduced to near zero in the technical assessment (the table indicates no remaining area under strict technical feasibility), pointing to an approximate 98% contraction. AP's reduction is similarly severe, with effectively its entire gross potential of 137.41 (1,000 km²) is excluded once overlapping protected and priority areas are considered.

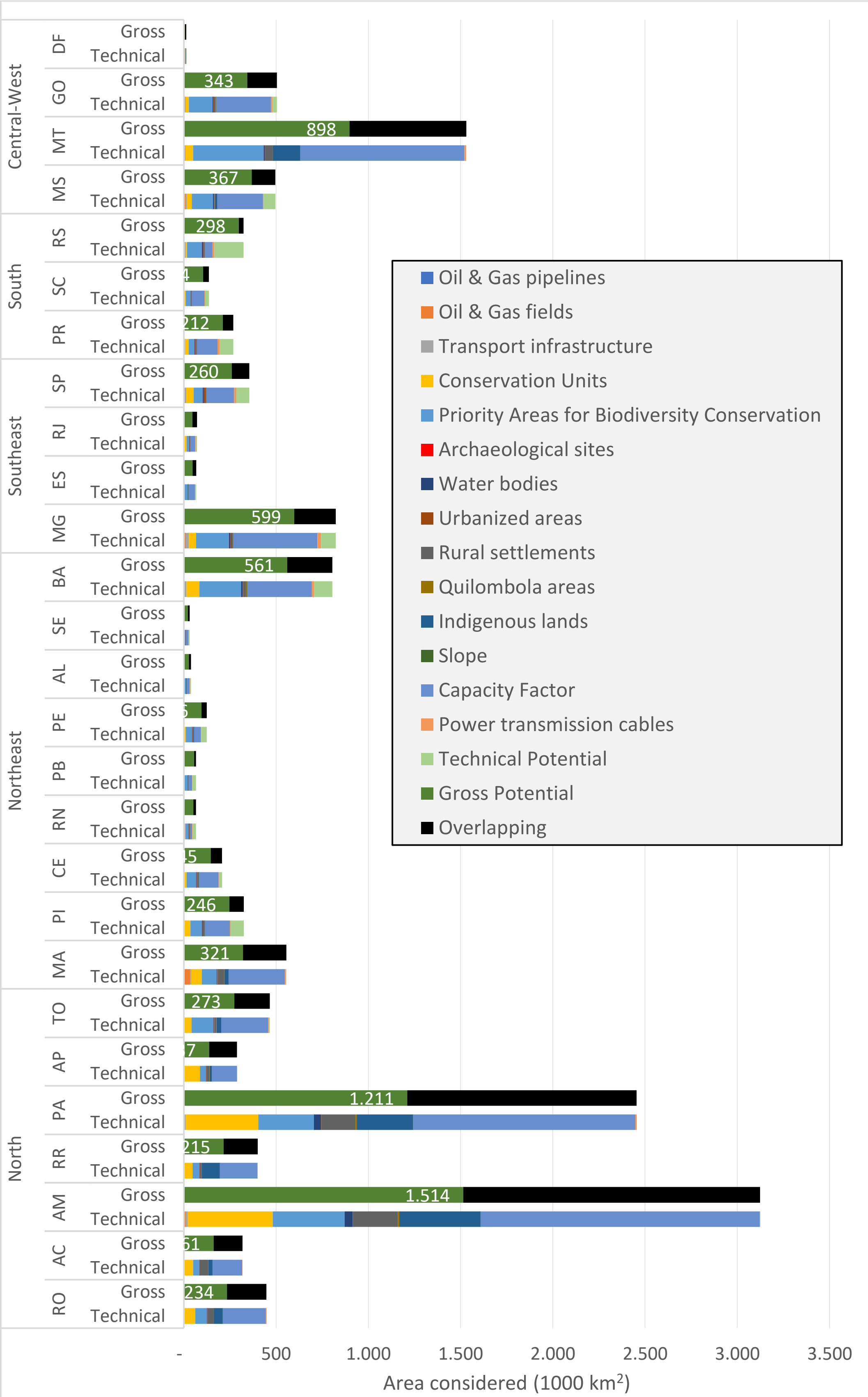

Figure 22 - Area constrained for each constraint layer, technical and gross potential and overlapping when assessing ONW for each state.
Source: Own elaboration.

The results in Table 18 underline significant regional disparities in the feasibility ONW-based hydrogen production across Brazil. In absolute terms, Rio Grande do Sul (RS) leads with a technical H_2 potential of 46 Mton/year, followed by Bahia (BA) at 27 Mton/year, and Piauí (PI) and Paraná (PR) each at 19 Mton/year. Despite these noteworthy figures, each state faces a large drop from its gross to technical potential. BA, for instance, retains roughly 26% of its original hydrogen capacity (104 Mton/year → 27 Mton/year), while Minas Gerais (MG) decreases by about 66% (85 → 19 Mton/year), and Mato Grosso (MT) plummets by 98% (58 → 1 Mton/year). In some cases, such as Acre (AC) and Amapá (AP), the technical potential effectively drops to zero, underscoring how overlapping constraints (e.g., conservation areas or low capacity factors) can fully negate initially promising resources.

Table 18 - Potential production of hydrogen and derivative from ONW for each state in Brazil.

	Technical Potential			Gross Potential		
State	H2 (Mton/year)	NH3 (Mton/year)	MeOH (Mton/year)	H2 (Mton/year)	NH3 (Mton/year)	MeOH (Mton/year)
RO	0	0	0	9	48	38
AC	-	-	-	4	22	18
AM	0	0	0	24	122	96
RR	0	1	1	11	57	45
PA	0	0	0	48	249	195
AP	-	-	-	7	37	29
TO	1	6	5	28	142	111
MA	1	4	3	31	160	125
PI	19	96	75	44	228	178
CE	4	20	16	23	117	91
RN	6	33	26	15	75	59
PB	6	31	24	13	69	54
PE	7	37	29	21	108	84
AL	1	6	5	5	24	19
SE	1	5	4	4	19	15
BA	27	140	109	104	535	418
MG	19	98	77	85	440	344
ES	1	6	5	7	38	30
RJ	2	10	8	8	39	31
SP	15	78	61	44	225	176
PR	19	99	77	39	199	156
SC	5	26	20	16	84	66
RS	46	236	185	81	416	326
MS	15	75	59	61	312	244
MT	1	3	2	58	298	233
GO	5	26	20	41	210	164
DF	0	0	0	1	4	3

Source: Own elaboration.

For the economic potential, the LCOE and LCOH were calculated for the constrained area. The economic viability of onshore wind resources in Brazil is captured through the Levelized Cost of Electricity (LCOE), which varies significantly across different regions. Figure 23 showcases these spatial disparities, highlighting areas where strong wind resources and supportive infrastructure contribute to lower LCOE values.

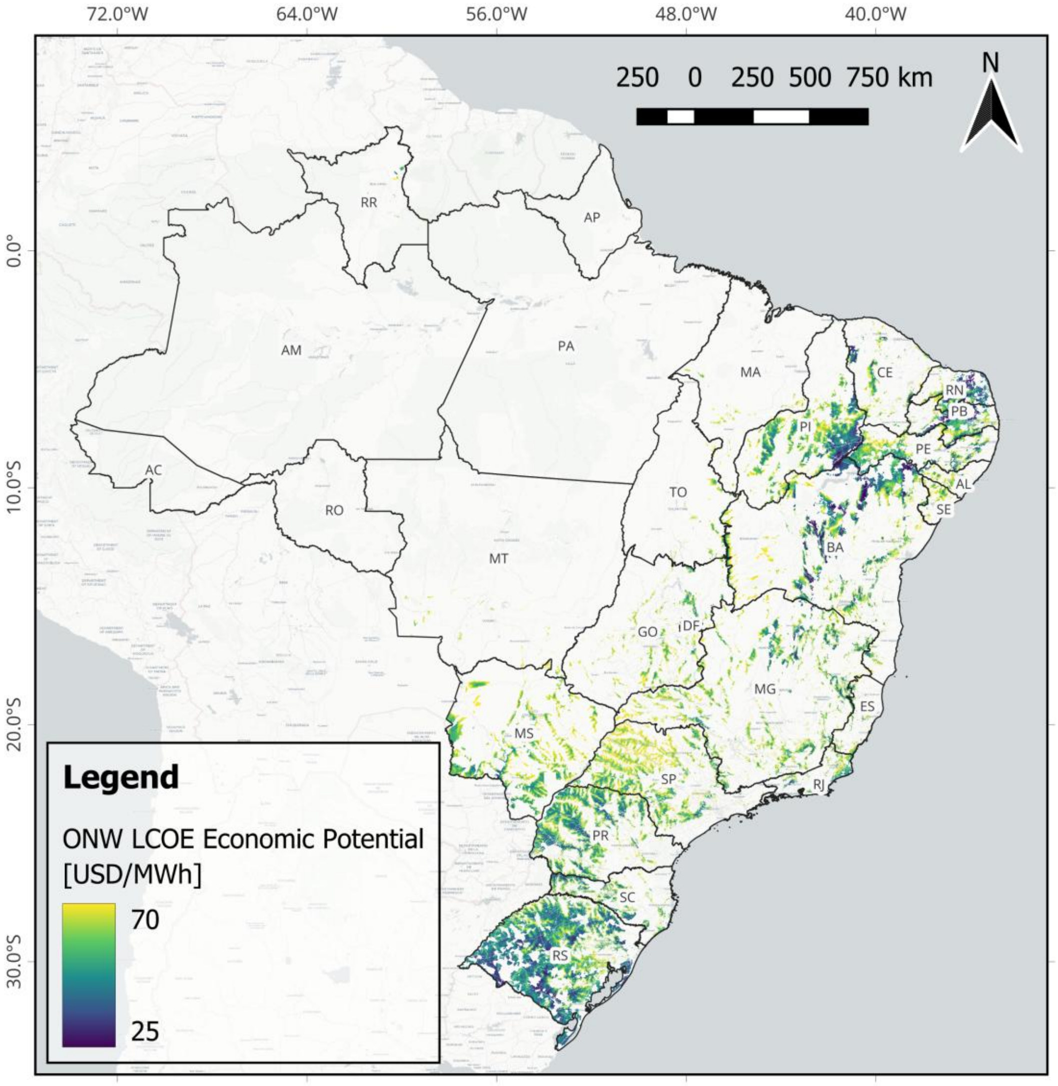

Figure 23 - Economic potential as LCOE of ONW.
Source: Own elaboration.

As depicted in Figure 24, the relative relative LCOH from ONW underlines regional contrasts in both wind resource quality. Areas with robust wind speeds exhibit notably lower hydrogen production costs, while regions hampered by marginal capacity factors face steeper LCOH values.

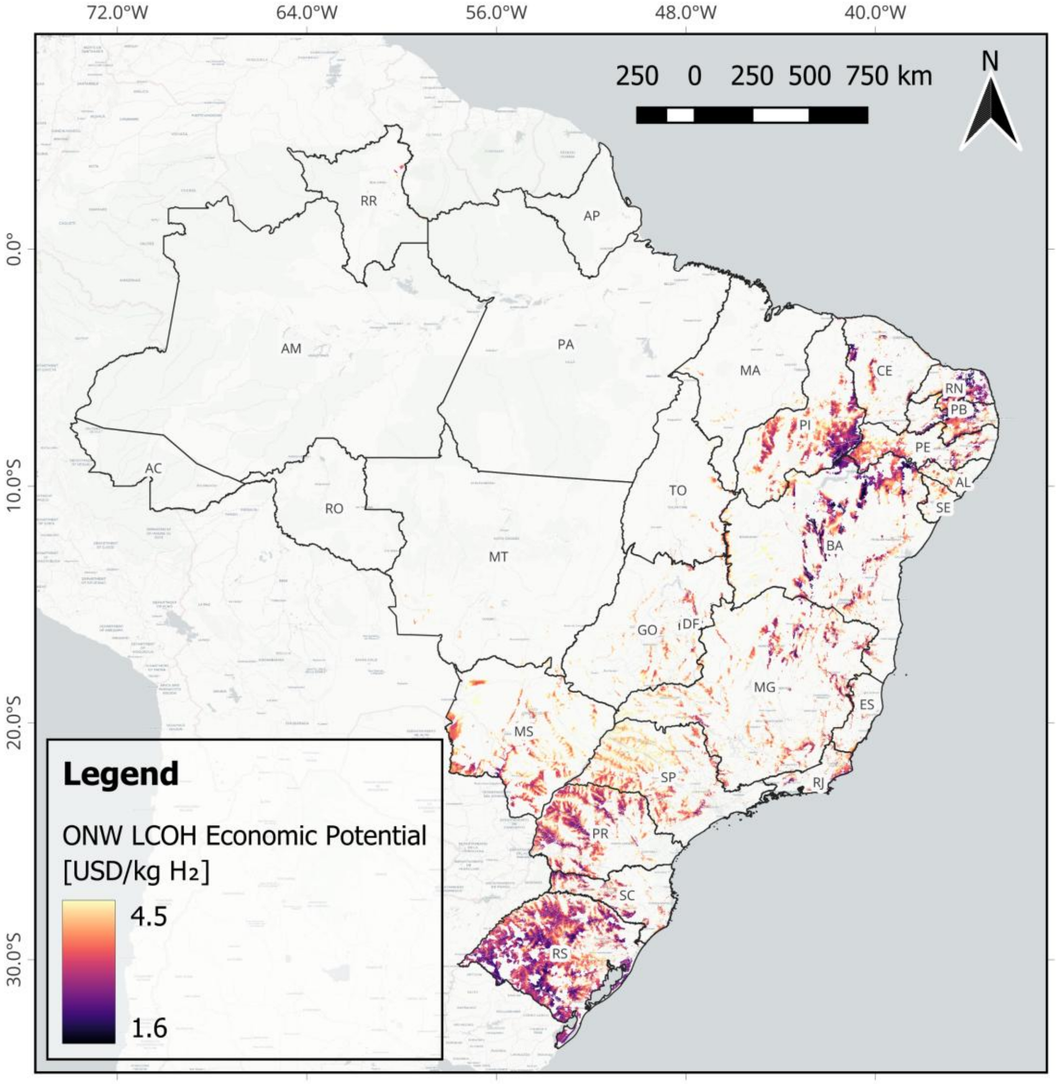

Figure 24 - Economic potential as relative LCOH from ONW.
Source: Own elaboration.

4.1.3 Offshore wind (OFW)

Brazil's extensive coastline and favorable maritime wind conditions confer a substantial theoretical potential for producing hydrogen and related derivatives from OFW. As seen in Figure 25, the gross estimate for OFW stretches across vast ocean areas, indicating the sheer scale of these resources if unconstrained by environmental, technical, social or environmental limitations.

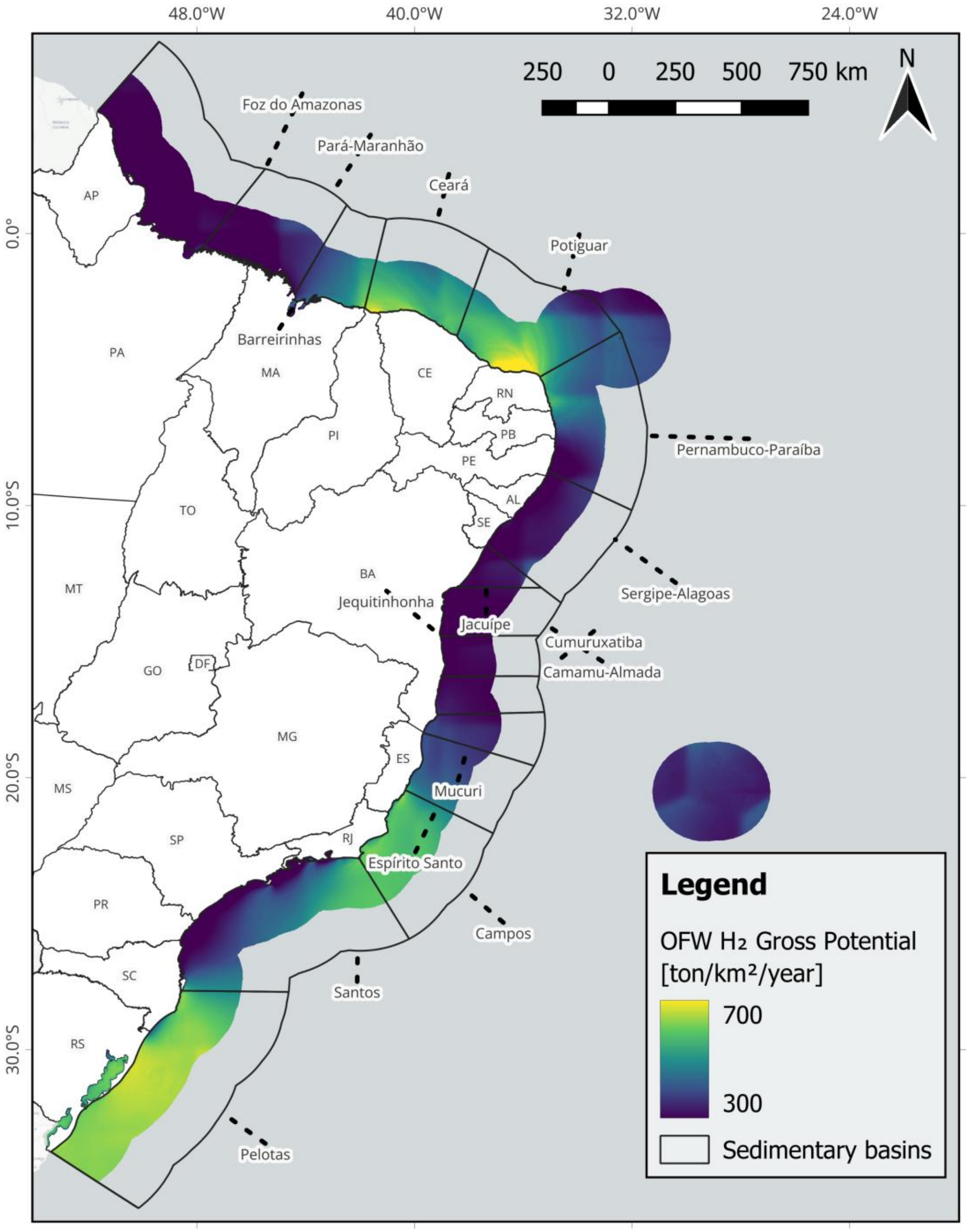

Figure 25 - Gross hydrogen production potential from OFW.
Source: Own elaboration.

However, translating this theoretical potential into a practical, "technical" figure involves systematically applying a range of exclusion layers—such as ocean-depth thresholds, biodiversity considerations, and capacity-factor cutoffs—that substantially reduce the final exploitable acreage. Table 19 outlines the results for gross, technical potential and partial potential considering each constraint layer. Brazil's offshore wind potential reflects large disparities between gross and technical estimates for energy and hydrogen production.

Table 19 - Brazil's gross and technical potential of energy, hydrogen and derivatives from OFW.

Mask Name	Area (1000 km²)	Power (GW)	Energy (GWh/year)	H2 (Mton/year)	NH3 (Mton/year)	MeOH (Mton/year)
Gross potential	1.692	13.295	40.225.920	713	3.674	2.876
Navigation routes	1.518	11.928	35.933.520	637	3.282	2.569
Oil & Gas pipelines	1.691	13.286	40.199.640	712	3.672	2.874
Oil & Gas fields	1.612	12.666	38.009.640	674	3.472	2.718
Coastal setbacks	1.500	11.784	35.854.680	636	3.275	2.564
Conservation Units	1.480	11.628	36.064.920	639	3.294	2.579
Priority Areas for B. C.	858	6.740	19.552.320	347	1.786	1.398
Depth	856	6.730	20.708.640	367	1.892	1.481
Capacity Factor	980	7.698	28.207.200	500	2.577	2.017
Technical potential	62	490	1.795.800	32	164	129

Source: Own elaboration.

The "Gross potential" values, which represent the theoretical maximum without considering spatial or operational constraints, indicate an expansive opportunity, with 1,692 x 10^3 km² of area and a hydrogen production capacity of 713 Mton/year. However, various spatial and environmental constraints reduce this potential significantly when factoring in real-world limitations. For example, "Navigation routes," as a constraint, reduces the area substantially (from 1,692 x 10^3 km² to 1,518 x 10^3 km²), yet the impact on hydrogen production is less severe, with only a reduction of 10% (from 713 Mton/year to 637 Mton/year). Similarly, restrictions such as "Oil & Gas pipelines" and "Conservation Units" produce modest reductions in both area and hydrogen outputs, while constraints such as "Priority Areas for Biodiversity Conservation" and "Depth" result in more significant decreases. Notably, "Depth" alone limits the area to 856 x 10^3 km² and further reduces hydrogen potential by nearly 50%. The most profound constraint is the "Capacity Factor," which alone cuts the area to 980 x 10^3 km², ultimately limiting hydrogen production to just 500 Mton/year. The final "Technical potential"—represented as the calculated, realistic estimate after all constraints are considered—is just 62 x 10^3 km², with a hydrogen production potential of 32 Mton/year, drastically lower than the gross potential. Figure 26 illustrates the technical potential for the production of hydrogen from ONW.

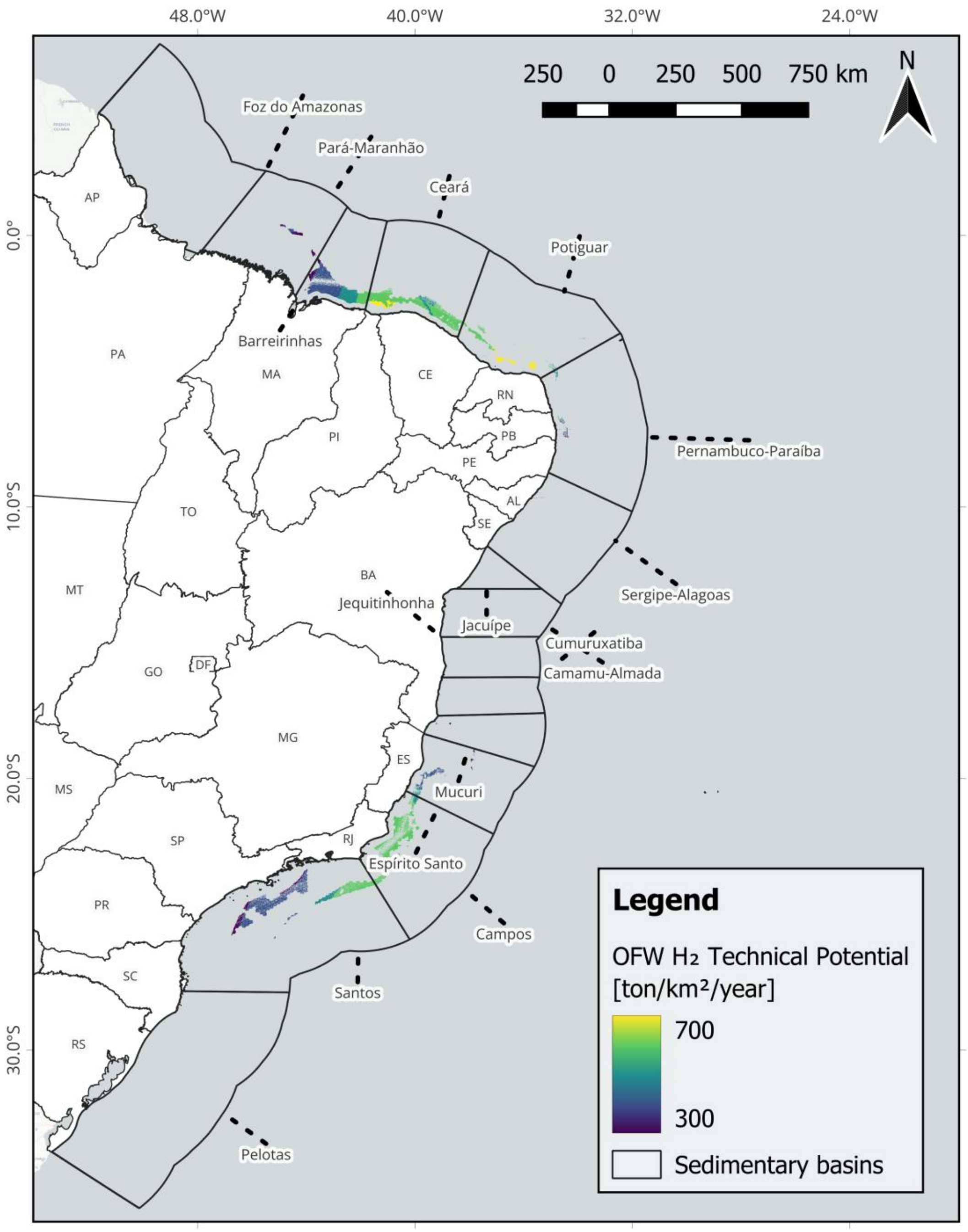

Figure 26 - Technical hydrogen production potential from OFW.
Source: Own elaboration.

Figure 27 offers a stepwise depiction of how various constraints sequentially diminish the gross offshore wind-to-hydrogen potential, ultimately revealing the much smaller technical potential. Starting at a relatively modest 32 Mton/year of hydrogen (the "Technical Potential"), each bar highlights an incremental smaller impact from factors such as "Navigation Routes," "Oil & Gas fields," and "Coastal Setbacks," which collectively push a total of 167 Mton/year against the original gross potential of 713 Mton/year. When analyzing the individual impact of each constraint on the technical potential from OFW, it is observed key reductions when large constraints—such as "Priority Areas for Biodiversity Conservation," "Depth," and “Capacity Factor”—are imposed. However, it is important noting that a substantial part of the constraints are overlapping.

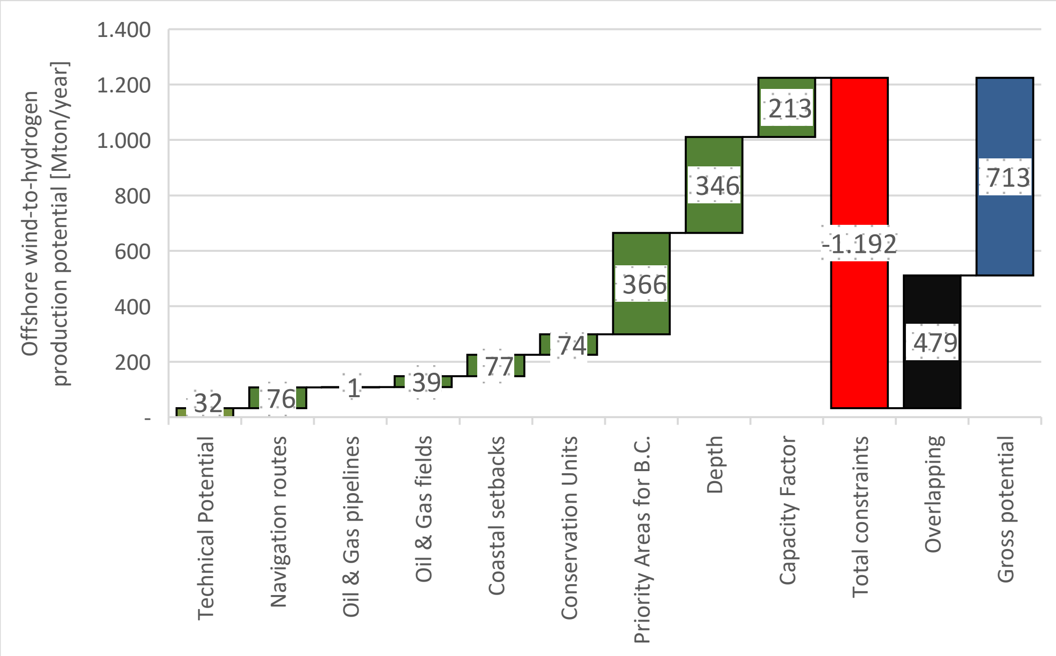

Figure 27 – Offshore wind-to-hydrogen production potential waterfall chart.

For better visualization of the overlapping impact of each constraint, the overlapping matrix of the considered area was calculated when assessing offshore wind-to-hydrogen potential. Table 20 shows the results of this matrix. The percentages in each cell represent the degree of overlap between the row and column constraints, offering a clear view of the cumulative restrictions on potential wind farm sites. For instance, "Navigation Routes" overlaps heavily with "Oil & Gas pipelines" (18.2%) and "Depth" (52.9%), highlighting the significant spatial competition between these elements in offshore areas. Similarly, "Conservation Units" and "Priority Areas for Biodiversity Conservation" show substantial overlap, indicating that these environmental protections occupy large swaths of overlapping areas, with as much as 71.7% of "Depth" limitations falling within "Conservation Units." The final row, "Unified Offshore Wind Mask," represents the total spatial footprint remaining after all constraints, consolidating the compounded effects found throughout the matrix.

Table 20 - Overlapping of constraints matrix when assessing technical potential of hydrogen production from OFW.

	Navigation routes	Oil & Gas pipelines	Oil & Gas fields	Coastal setbacks (viewshed setbacks)	Conservation Units	Priority Areas for Biodiversity Conservation	Depth	Capacity Factor	Unified Offshore Wind Mask
Navigation routes	100,0%	0,1%	6,7%	6,2%	1,9%	43,7%	52,9%	31,6%	100,0%
Oil & Gas pipelines	18,2%	100,0%	23,4%	22,1%	2,9%	43,4%	31,1%	18,7%	100,0%
Oil & Gas fields	14,5%	0,3%	100,0%	1,2%	0,0%	22,6%	69,8%	20,8%	100,0%
Coastal setbacks (viewshed setbacks)	5,6%	0,1%	0,5%	100,0%	25,9%	63,6%	2,9%	51,4%	100,0%
Conservation Units	1,6%	0,0%	0,0%	23,5%	100,0%	2,0%	71,7%	68,9%	100,0%
Priority Areas for Biodiversity	9,1%	0,1%	2,2%	14,7%	0,5%	100,0%	20,0%	37,6%	100,0%
Depth	11,0%	0,0%	6,7%	0,7%	18,2%	20,0%	100,0%	41,8%	100,0%
Capacity Factor	7,7%	0,0%	2,3%	13,9%	20,5%	44,1%	49,1%	100,0%	100,0%
Unified Offshore Wind Mask	10,7%	0,1%	4,9%	11,8%	13,0%	51,2%	51,3%	43,7%	100,0%

Source: Own elaboration.

Some constraints can have a considerable impact when evaluating the potential of hydrogen production from OSW. In particular, it was identified that “Capacity Factor”, “Depth” and “Priority Areas for Biodiversity Conservation” constraints leads to the most significant impact when assessing Brazil’s OFW potential. Fo instance, the Capacity Factor for OFW was restricted <30% in this work simulations. While Brazil’s OFW resources exhibit a high theoretical capacity due to generally favorable wind conditions over open waters, the capacity factor constraint effectively filters out locations with lower performance, ensuring that only the most efficient sites are considered viable for development. This targeted exclusion can alter the overall potential. It led to a 16% decrease in technical potential and around 42% decrease in gross. However, as shown in Figure 28, assuming higher capacity factor threshold can lead to drastically effect of potential assessment.

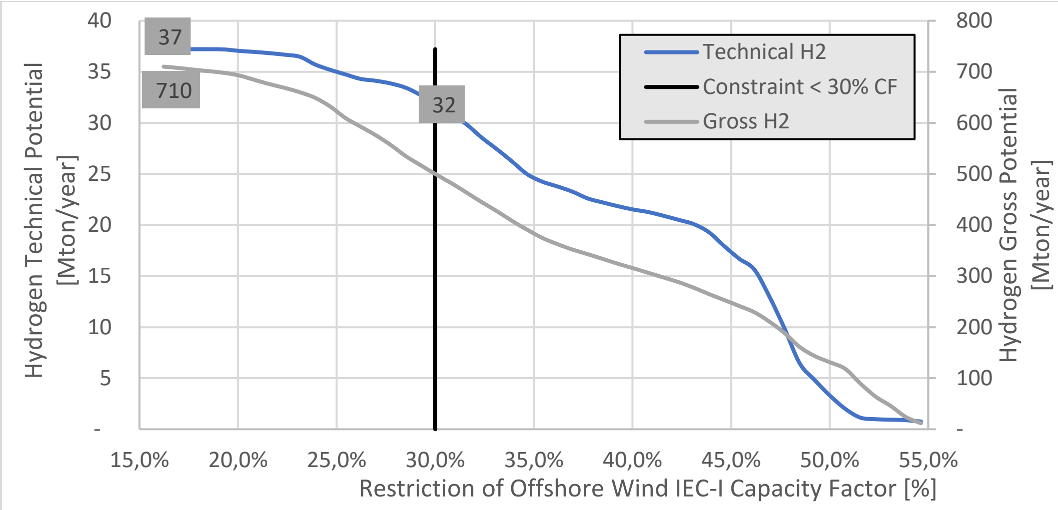

Figure 28 - Technical e gross potential of hydrogen production from SPV in function restriction of capacity factor.
Source: Own elaboration.

As already mentioned, the constrained layer of ocean depth led to a major impact on potential assessment of OFW in Brazil. This work assumed a <1300 depth restriction due to technology barriers for floating platforms. However, with technological improvements, this threshold could be relaxed, and higher ocean depths could be considered on potential assessment. As shown in Figure 29, considering higher depths as threshold could lead to a significant change of potential assessment of hydrogen production from OFW.

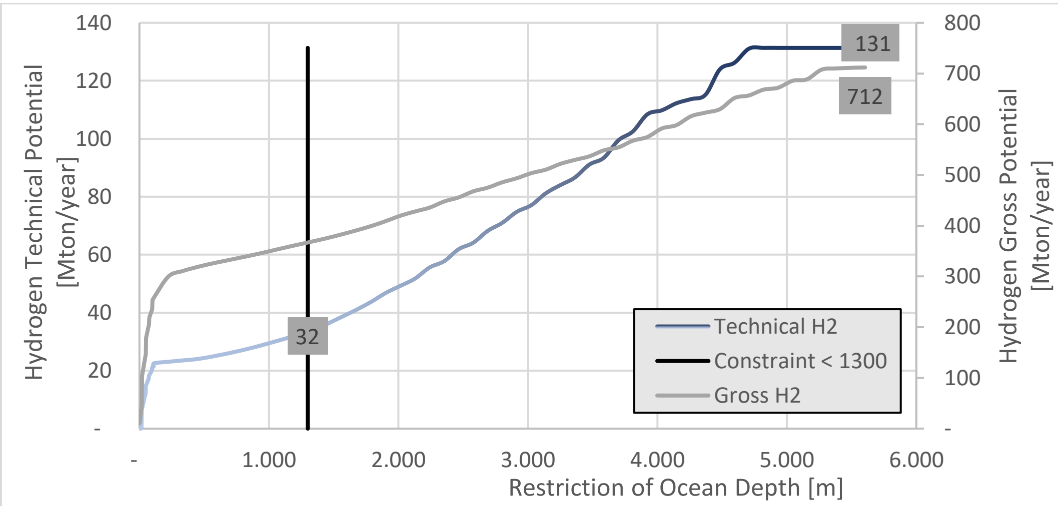

Figure 29 - Technical e gross potential of hydrogen production from SPV in function of restriction of ocean depth.
Source: Own elaboration.

A simulation was conducted to understand the potential assessment for each sedimentary basin along the Brazilian coast. Sedimentary basins—geologically defined regions characterized by extensive accumulations of sedimentary deposits and often associated with hydrocarbon reserves—serve as important regions for OFW potential assessments. Among the sedimentary basins analyzed, as shown in

Figure 30, the Santos basin exhibits the highest gross potential, reaching approximately 204.84 (in units of 1000 km^2), and it also delivers the highest technical potential at about 16.34. In Santos, the Priority Areas for Biodiversity Conservation—which registers a value of 138.49—emerges as the dominant constraint, substantially reducing the theoretically available area despite the region's favorable overall resource endowment. Ceará and Barreirinhas also offer a high technical feasible area for OFW projects. In stark contrast, several basins (including Cumuruxatiba, Foz do Amazonas, Jequitinhonha, Jacuípe, Camamu-Almada, and Sergipe-Alagoas) display a technical potential of zero, indicating that the cumulative impact of exclusion layers completely negates any feasible area for development. Notably, the Campos basin, with a gross potential of 87.58, is particularly affected by extremely high ocean depths, which serves as the most significant limiting constraint and results in a technical potential feasible area of only 9.78. Basins with inherently low gross potentials—such as Jacuípe (25.85) and Jequitinhonha (33.87)—naturally yield negligible technical potentials. Pelotas basis has the most significant impact from Priority Areas for Biodiversity Conservation, and this challenge must be surpassed for OFW projects in the region.

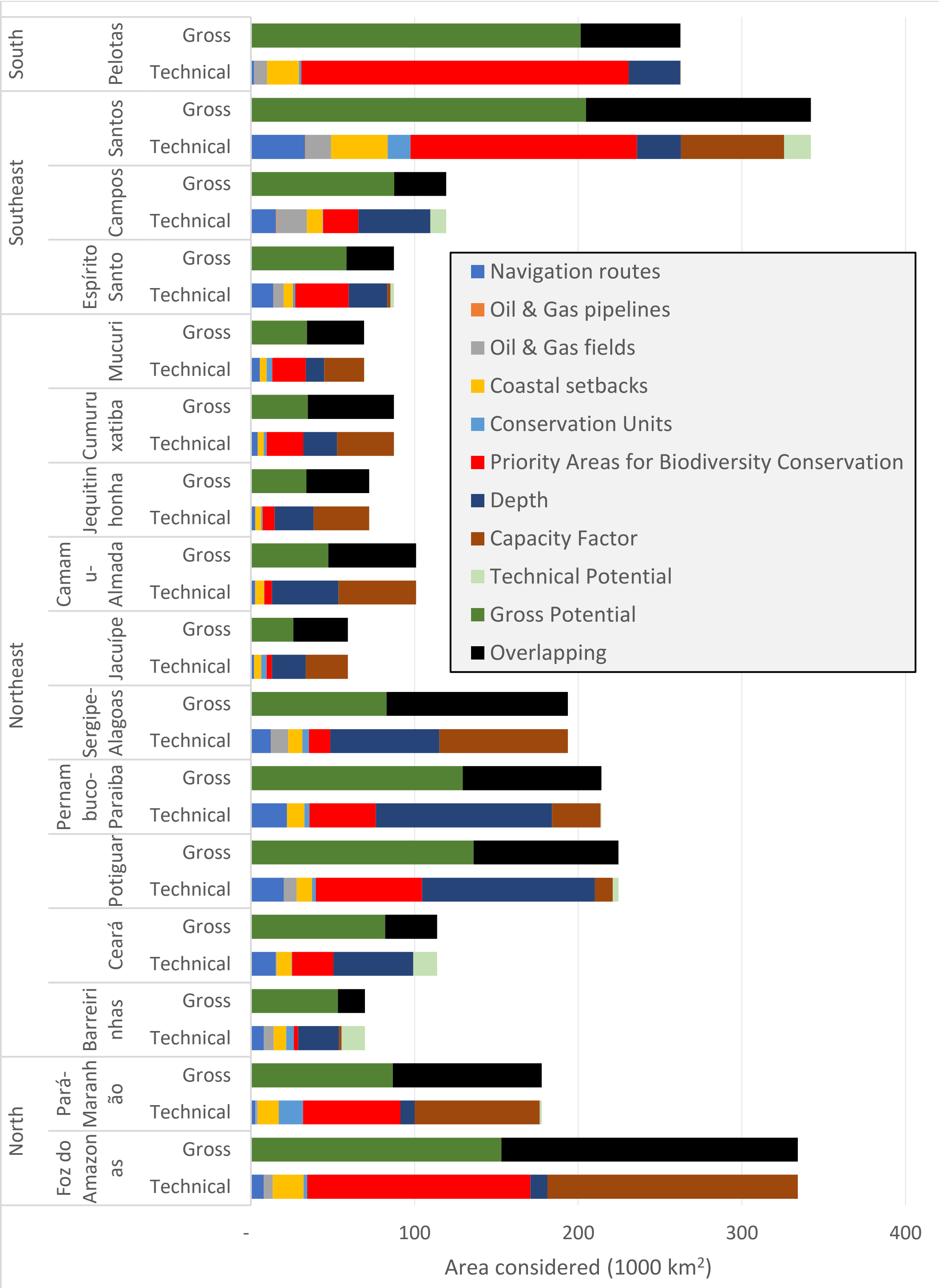

Figure 30 - Area constrained for each constraint layer, technical and gross potential and overlapping when assessing ONW for each sedimentary basin.
Source: Own elaboration.

As shown in Table 21, when comparing technical and gross production potential of hydrogen and derivatives form offshore wind, Pará–Maranhão's gross hydrogen potential of 20 Mton/year collapses to zero technical potential, while Potiguar retains only ~3.8% (2 vs. 53 Mton/year). Santos, with the highest gross figures—63 Mton/year for H_2, 325 Mton/year for NH_3, and 255 Mton/year for MeOH—drops to 6, 28, and 22 Mton/year respectively, representing retention ratios of roughly 9.5% for hydrogen and 8.6–8.7% for derivatives. In contrast, Barreirinhas shows relatively higher retention, with 5 Mton/year of H_2 from a gross of 18 Mton/year (~27.8%). Basins such as Cumuruxatiba, Foz do Amazonas, Jequitinhonha, Jacuípe, Mucuri, Camamu–Almada, and Sergipe–Alagoas exhibit no technical potential despite nonzero gross values, indicating complete exclusion by applied constraints. Ceará retains about 18.2% of its gross hydrogen potential (6 vs. 33 Mton/year), whereas Pelotas, despite a gross hydrogen potential of 94 Mton/year, is entirely excluded at the technical level, mainly because of Priority Areas for Biodiversity Conservation constraint.

Table 21 - Potential production of hydrogen and derivative from OFW for each state in Brazil.

	Technical Potential			Gross Potential		
Basin	H2 (Mton/year)	NH3 (Mton/year)	MeOH (Mton/year)	H2 (Mton/year)	NH3 (Mton/year)	MeOH (Mton/year)
Pará-Maranhão	0	2	1	20	102	80
Potiguar	2	8	7	53	274	215
Cumuruxatiba	-	-	-	8	42	33
Foz do Amazonas	-	-	-	29	150	117
Pernambuco-Paraiba	0	1	1	40	204	159
Santos	6	28	22	63	325	255
Campos	4	22	17	38	194	152
Espírito Santo	1	3	3	18	93	73
Barreirinhas	5	25	20	18	93	73
Jequitinhonha	-	-	-	8	39	30
Jacuípe	-	-	-	6	31	25
Mucuri	0	0	0	9	47	37
Camamu-Almada	-	-	-	10	50	39
Sergipe-Alagoas	-	-	-	20	101	79
Ceará	6	33	26	33	172	135
Pelotas	0	0	0	94	486	380

Source: Own elaboration.

For the economic potential, the LCOE and LCOH were calculated for the constrained area. As depicted in Figure 31, OFW development along Brazil's coastline exhibits notable spatial variation in LCOE.

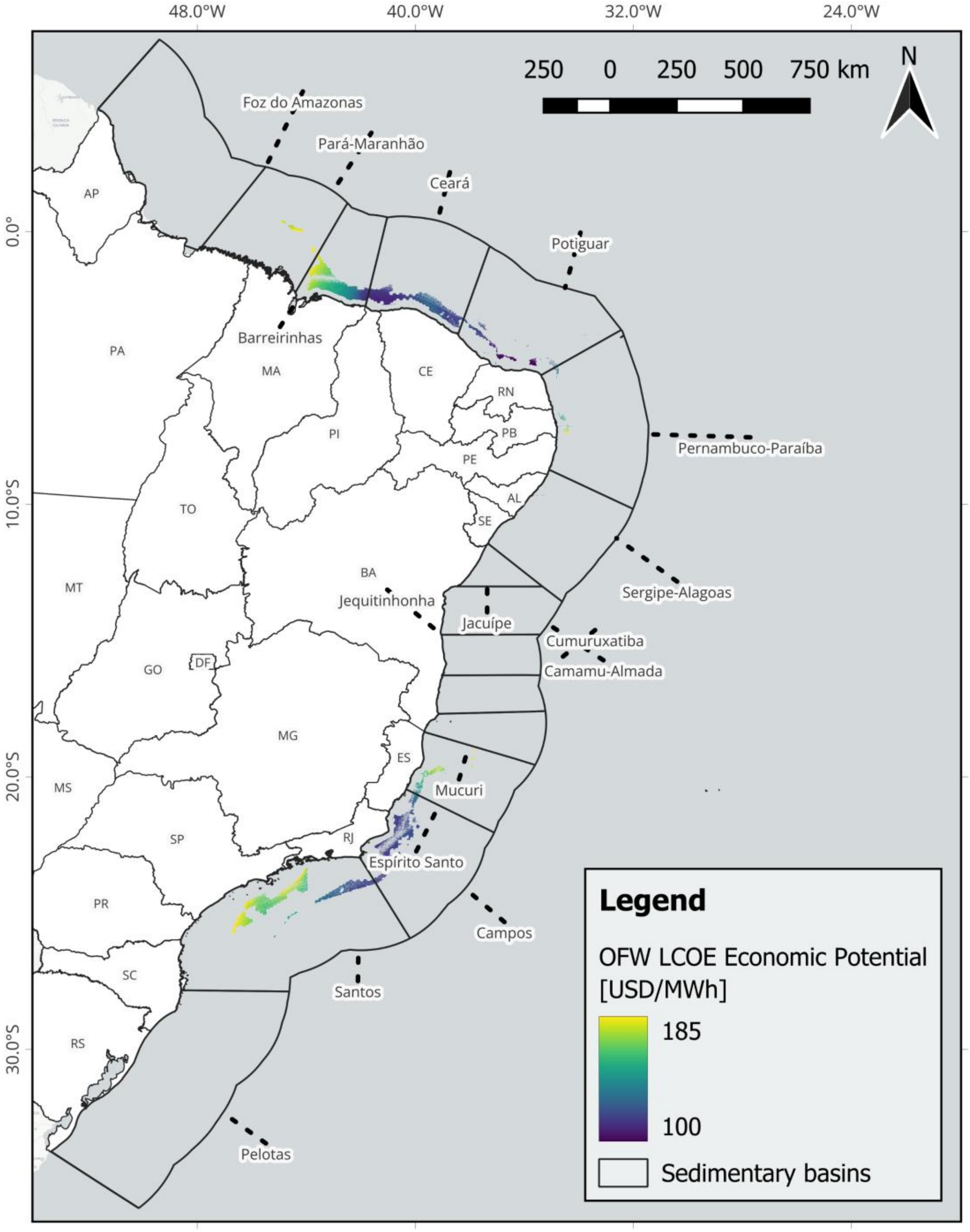

Figure 31 - Economic potential as LCOE of Offshore Wind (OFW).
Source: Own elaboration.

Much like the electricity cost map, Figure 32 illustrates significant regional differences in the LCOH for Brazil's offshore wind resources. Areas with high wind speeds, exhibit comparatively lower hydrogen production costs, making them prime candidates for early OFW-to-hydrogen development.

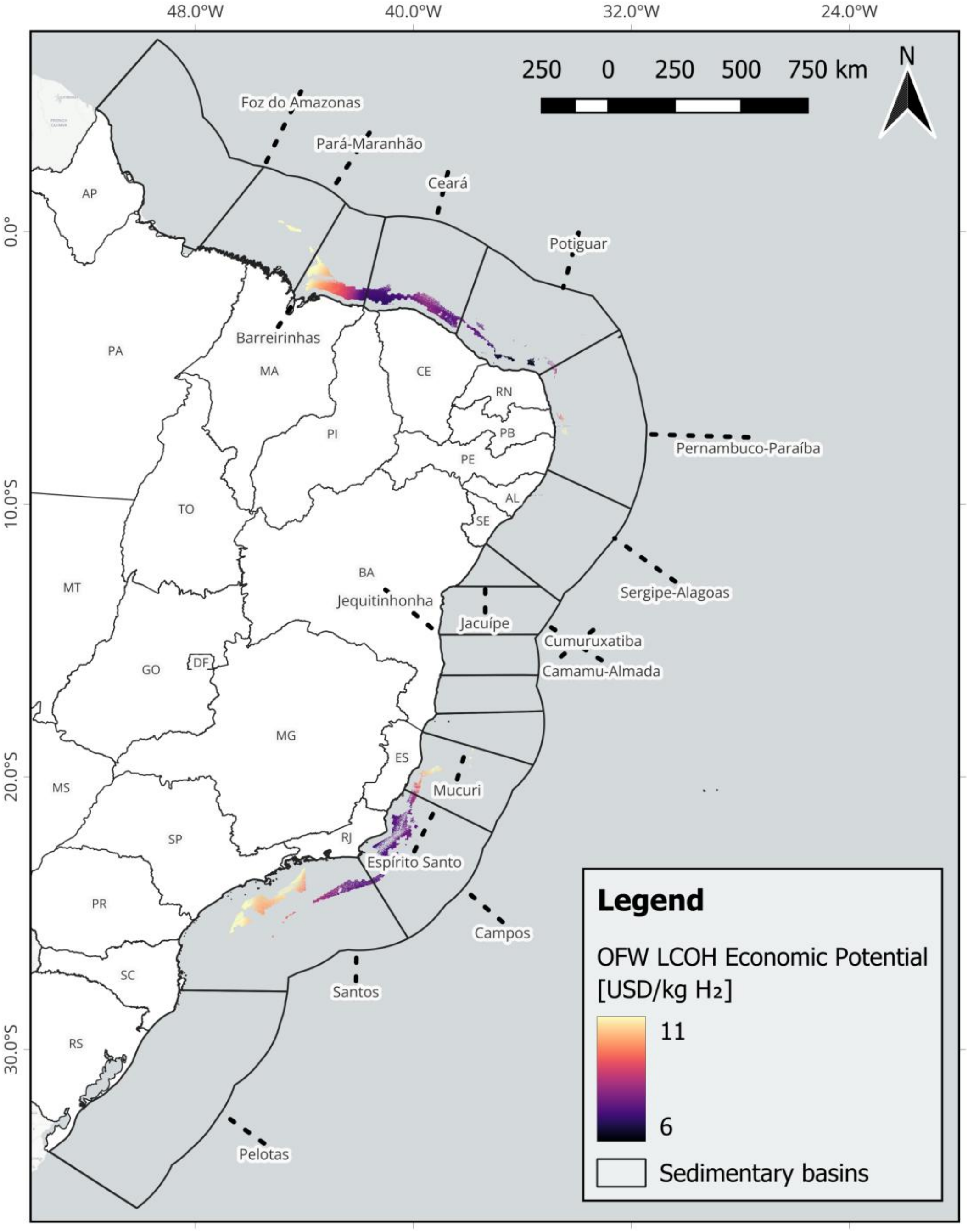

Figure 32 - Economic potential as relative LCOH from Offshore Wind (OFW).
Source: Own elaboration.

4.2 Feasibility analysis tool (FAT) case studies

To demonstrate the capabilities of the developed GeoH$_2$-FAT described in Section 3.2, this section presents a set of results in the form of a case study supported by sensitivity analysis. The selected case proposes the installation of a hydrogen plant in São Gonçalo do Amarante, Ceará, at the Port of Pecém. Hydrogen is produced via water electrolysis using PEM technology, and the plant's electricity supply is hybrid: on-site solar PV, on-site wind, and grid electricity purchased under an ACL contract. The hydrogen produced is stored as compressed gas in pressurized tanks. Downstream transport is not considered in this case, because an on-site use assumption is adopted. Table 22 shows the base-case configuration for the proposed case scenarios.

Table 22 – Base-case assumptions for the studied case scenarios.

	BASE-CASE CONFIGURATION	
	Energy	
SOLAR PV	*Location of generating plant*	São Gonçalo do Amarante - CE
SOLAR PV	*Latitude*	-5.7852
SOLAR PV	*Longitude*	-35.3305
SOLAR PV	*Installation type*	Central plant (fixed tilt)
SOLAR PV	*PV module model*	DAH DHM-72X10-530 W
SOLAR PV	*Degradation rate*	0.5 % yr^{-1}
WIND	*Latitude*	-5.9255
WIND	*Longitude*	-35.0197
WIND	*Capacity factor*	44.61 %
WIND	*Turbine model*	Vestas V80-1.8
WIND	*IEC class*	IEC I
ACL	*Sub-market*	Northeast
ACL	*ACL contract price*	BRL 231.01 MWh^{-1}
ACL	*Total i-REC cost*	BRL 0.63 MWh^{-1}
	Hydrogen Production	
	Location	São Gonçalo do Amarante
	Latitude	-5.7852
	Longitude	-35.3305
	Electrolyser technology	Silyzer 200
	Plant electrical capacity	100 MW
	Capacity factor	60 %
	Water tariff	CAGECE
	O&M cost (production block)	3 % yr^{-1}
	Transport	
	Point of sale	São Gonçalo do Amarante
	Distance	0 km
	Latitude	-5.7852
	Longitude	-35.3305
	Transport mode	None
	Storage	
	Physical state	Gaseous
	Storage technology	Pressurised tanks

Source: Own elaboration.

On the basis of these assumptions, the following subsections present results and sensitivity analyses for three different case scenarios: 100 % on-site solar PV, 100 % on-site wind, and a one-third mix of on-site solar, on-site wind, and ACL electricity with i-RECs. The impact on the tool's key indicators—LCOE, LCOH, IRR, and avoided-emissions revenue—is assessed against changes in the main technical and economic input variables.

4.2.1 Case 1: 100% on-site solar PV

The first case assumes the base-case hydrogen plant is powered entirely by self-generated solar PV. Table 23 summarizes the simulation outputs.

Table 23 - Key results of case 1 with 100 % solar self-generation.

Category	***Indicator***	***Value (BRL)***	***≈ Value (USD*)***	***Unit***
Energy	Rated capacity of the power plant	R$ 248,298 kW	-	kW (AC)
	Annual electricity generation	R$ 533,603 MWh	USD 106,721 MWh	MWh yr^{-1}
	Number of PV modules	609,032	—	—
	Number of wind turbines	0	—	—
Production	Electricity consumption	R$ 485,093,059 kWh	USD 97,018,612 kWh	kWh yr^{-1}
	Hydrogen production	7,824,082	—	kg H_2 yr^{-1}
	Water consumption	94,608	—	m^3 yr^{-1}
Transport	Mode of transport	None	—	—
	Distance	0	—	km
	Volume	21.43	—	t day^{-1}
	Specific cost	R$ 0.00 kg^{-1} H_2	USD 0.00 kg^{-1}	—
Storage	Levelised cost of storage (LCOS)	R$ 15 kg^{-1} H_2	USD 3 kg^{-1}	—
Economic & Financial	CAPEX – Hydrogen production plant	R$ 245,003,004	USD 49,000,601	—
	CAPEX – Power-generation plant	R$ 993,190,226	USD 198,638,045	—
	OPEX – O&M (production)	R$ 7,350,090 yr^{-1}	USD 1,470,018 yr^{-1}	—
	OPEX – O&M (energy)	R$ 19,367,209 yr^{-1}	USD 3,873,442 yr^{-1}	—
	Storage cost	R$ 7,432,878 yr^{-1}	USD 1,486,576 yr^{-1}	—
	Water cost	R$ 1,748,356 yr^{-1}	USD 349,671 yr^{-1}	—
	Transport cost	—	—	—
	Total CAPEX	**R$ 1,238,193,230**	**USD 247,638,646**	—
	Total OPEX	**R$ 35,898,533 yr^{-1}**	**USD 7,179,707 yr^{-1}**	—
Cost Metrics	LCOH – Production cost	R$ 1.90 kg^{-1} H_2	USD 0.38 kg^{-1}	—

	LCOH – Energy cost	R$ 6.35 kg⁻¹ H_2	USD 1.27 kg⁻¹	—
	LCOH – O&M (production)	R$ 0.94 kg⁻¹ H_2	USD 0.19 kg⁻¹	—
	LCOH – O&M (energy)	R$ 2.48 kg⁻¹ H_2	USD 0.50 kg⁻¹	—
	LCOH – Storage cost	R$ 0.95 kg⁻¹ H_2	USD 0.19 kg⁻¹	—
	LCOH – Water cost	R$ 0.22 kg⁻¹ H_2	USD 0.04 kg⁻¹	—
	LCOH – Transport cost	—	—	—
	Total LCOH	**R$ 16.39 kg⁻¹ H_2**	**USD 3.28 kg⁻¹**	—
Financial Indicators	Internal rate of return (IRR)	0.62 % month⁻¹	—	—
	Minimum DSCR	1.17	—	—
	Payback period	113	—	months
	Levelised cost of electricity (LCOE)	R$ 190.29 MWh⁻¹	USD 38.06 MWh⁻¹	—

*Conversion factor: 1 USD = 5 BRL.
Source: Own elaboration.

In the base case, both the LCOE (R$ 190.29 MWh⁻¹ ≈ USD 38.06 MWh⁻¹) and the LCOH (R$ 16.39 kg⁻¹ H_2 ≈ USD 3.28 kg⁻¹ H_2) align with the ranges reported in the literature. Specifically, photovoltaic LCOE values between R$ 100 – 210 MWh⁻¹ (≈ USD 20 – 42 MWh⁻¹) and green-hydrogen LCOH values between R$ 10 – 19 kg⁻¹ H_2 (≈ USD 2 – 3.8 kg⁻¹ H_2) are expected under current conditions [111,139].

A sensitivity analysis was conducted by varying the hydrogen-plant capacity factor between 10 % and 100 %. The PV-plant CAPEX ranged from the minimum R$ 2,800 kWp⁻¹ (≈ USD 560 kWp⁻¹) to the maximum R$ 5,800 kWp⁻¹ (≈ USD 1,160 kWp⁻¹) reported in the 2021 Generation Cost Compendium [111]. For the solar self-generation facility, an average OPEX of R$ 60 kWp⁻¹ month⁻¹ (≈ USD 12 kWp⁻¹ month⁻¹) was assumed. As illustrade in Figure 33, the LCOH varied from R$ 15 – 36 kg⁻¹ H_2 (≈ USD 3 – 7.2 kg⁻¹ H_2), governed by the two parameters. The lowest LCOH values (R$ 15 – 20 kg⁻¹ H_2, ≈ USD 3 – 4 kg⁻¹ H_2) were obtained for hydrogen capacity factors between 27 % and 100 %, depending on the generation-plant CAPEX. These figures lie at the upper end of the range reported for green hydrogen in 2019 [140].

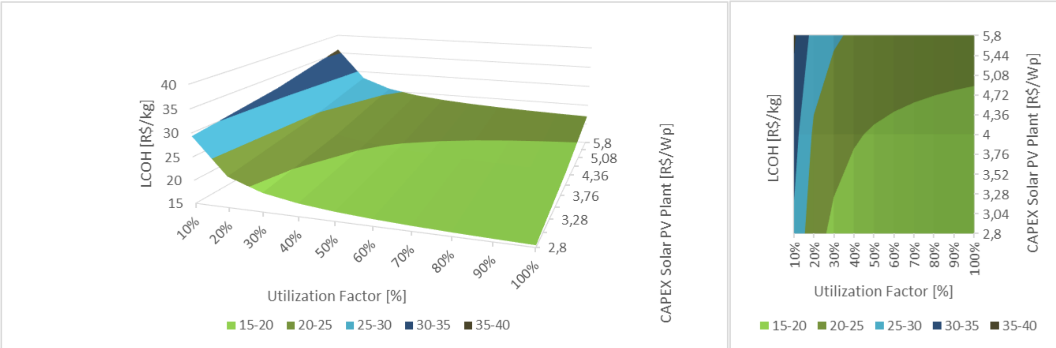

Figure 33 - LCOH as a function of the solar PV plant's CAPEX and H2 utilization factor.
Source: Own elaboration.

In a second analysis, the PV-plant OPEX was varied from R$ 20 kWp^{-1} $month^{-1}$ to R$ 82 kWp^{-1} $month^{-1}$ (≈ USD 4 – 16.4 kWp^{-1} $month^{-1}$), while the CAPEX remained fixed at R$ 4,000 kWp^{-1} (≈ USD 800 kWp^{-1}) and the hydrogen utilization factor ranged from 10 % to 100 %. As observed in Figure 34, the resulting mean LCOH spanned R$ 15 – 35 kg^{-1} H_2 (≈ USD 3 – 7 kg^{-1} H_2). The most competitive values (< R$ 20 kg^{-1} H_2, ≈ < USD 4 kg^{-1} H_2) corresponded to capacity factors between 30 % and 40 % with OPEX of R$ 20 – 28 kWp^{-1} $month^{-1}$ (≈ USD 4 – 5.6 kWp^{-1} $month^{-1}$), remaining below the R$ 19 kg^{-1} H_2 (≈ USD 3.8 kg^{-1} H_2) upper bound cited for green hydrogen (EPE, 2021b). Conversely, capacity factors below 20 % yielded LCOH values of R$ 25 – 35 kg^{-1} H_2 (≈ USD 5 – 7 kg^{-1} H_2) for OPEX exceeding R$ 60 kWp^{-1} $month^{-1}$ (≈ USD 12 kWp^{-1} $month^{-1}$), significantly above the aforementioned benchmark.

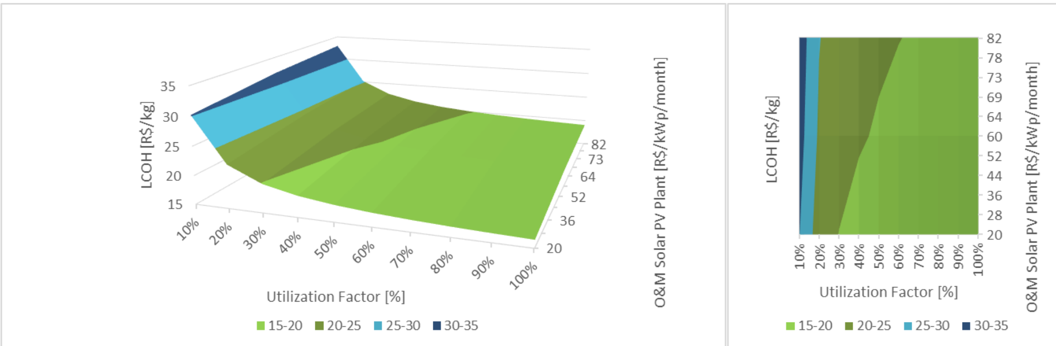

Figure 34 - LCOH as a function of the solar PV plant's OPEX and H_2 utilization factor.
Source: Own elaboration.

These findings show that the LCOH obtained herein attains lower values over a broader range of utilization factors, indicating that operating expenditures (OPEX) exert less influence than capital expenditures (CAPEX). Capital costs therefore dominate the economics of the power plant relative to post-commissioning operational costs. Consequently, the expenses required to maintain plant operation throughout its service life have a comparatively minor impact on the final hydrogen cost.

4.2.2 Case 2: 100% on-site wind

The second scenario uses the reference case with electricity produced entirely by an on-site wind farm. The simulation outcomes are consolidated in Table 24.

Table 24 - Key results of case 2 with 100% wind self-generation.

Category	***Indicator***	***Value (BRL)***	***≈ Value (USD*)***	***Unit***
Energy	Rated capacity of the power plant	R$ 136,407 kW	USD 27,281 kW	kW (AC)
	Annual electricity generation	R$ 533,069 MWh	USD 106,614 MWh	MWh yr^{-1}
	Number of PV modules	0	—	—
	Number of wind turbines	76	—	—
Production	Electricity consumption	R$ 485,093,059 kWh	USD 97,018,612 kWh	kWh yr^{-1}
	Hydrogen production	7,824,082	—	kg H_2 yr^{-1}
	Water consumption	94,608	—	m^3 yr^{-1}
Transport	Mode of transport	None	—	—
	Distance	0	—	km
	Volume	21.436	—	t day^{-1}
	Specific cost	R$ 0.00 kg^{-1} H_2	USD 0.00 kg^{-1}	—
Storage	Levelised cost of storage (LCOS)	R$ 15 kg^{-1} H_2	USD 3 kg^{-1}	—
Economic & Financial	CAPEX – Hydrogen production plant	R$ 245,003,004	USD 49,000,601	—
	CAPEX – Power-generation plant	R$ 647,933,305	USD 129,586,661	—
	OPEX – O&M (production)	R$ 7,350,090 yr^{-1}	USD 1,470,018 yr^{-1}	—
	OPEX – O&M (energy)	—	—	—
	Storage cost	R$ 7,432,878 yr^{-1}	USD 1,486,576 yr^{-1}	—
	Water cost	R$ 1,748,356 yr^{-1}	USD 349,671 yr^{-1}	—
	Transport cost	—	—	—
	Total CAPEX	**R$ 892,936,309**	**USD 178,587,262**	—
	Total OPEX	**R$ 16,531,323 yr^{-1}**	**USD 3,306,265 yr^{-1}**	—
Cost Metrics	LCOH – Production cost	R$ 1.90 kg^{-1} H_2	USD 0.38 kg^{-1}	—
	LCOH – Energy cost	R$ 4.14 kg^{-1} H_2	USD 0.83 kg^{-1}	—
	LCOH – O&M (production)	R$ 0.94 kg^{-1} H_2	USD 0.19 kg^{-1}	—
	LCOH – O&M (energy)	R$ 1.13 kg^{-1} H_2	USD 0.23 kg^{-1}	—
	LCOH – Storage cost	R$ 0.95 kg^{-1} H_2	USD 0.19 kg^{-1}	—

	LCOH – Water cost	R$ 0.22 kg⁻¹ H_2	USD 0.04 kg⁻¹	—
	LCOH – Transport cost	—	—	—
	Total LCOH	**R$ 11.24 kg⁻¹ H_2**	**USD 2.25 kg⁻¹**	—
Financial Indicators	Internal rate of return (IRR)	1.16 % month⁻¹	—	—
	Minimum DSCR	1.99	—	—
	Payback period	99	—	months
	Levelised cost of electricity (LCOE)	R$ 111.23 MWh⁻¹	USD 22.25 MWh⁻¹	—

*Conversion factor: 1 USD = 5 BRL.
Source: Own elaboration.

In the base case, both the LCOE (R$ 111.23 MWh⁻¹ ≈ USD 22.25 MWh⁻¹) and the LCOH (R$ 11.24 kg⁻¹ H_2 ≈ USD 2.25 kg⁻¹ H_2) are consistent with the ranges reported in the literature. Current expectations point to LCOE intervals of R$ 100 – 170 MWh⁻¹ (≈ USD 20 – 34 MWh⁻¹) and LCOH intervals of R$ 10 – 19 kg⁻¹ H_2 (≈ USD 2 – 3.8 kg⁻¹ H_2) for green hydrogen [111,139]. Moreover, the Ten-Year Energy Expansion Plan 2031 cites an LCOE of R$ 161.2 MWh⁻¹ (≈ USD 32.24 MWh⁻¹) for the interior of Ceará [70].

A sensitivity analysis assessed the impact of three variables—wind-plant CAPEX, wind-plant OPEX, and the hydrogen-plant capacity factor—on the LCOH. Figure 35 illustrates the LCOH as a function of CAPEX: values range from R$ 15 – 30 kg⁻¹ H_2 (≈ USD 3 – 6 kg⁻¹ H_2), with the most competitive figures (R$ 15 – 18 kg⁻¹ H_2, ≈ USD 3 – 3.6 kg⁻¹ H_2) achieved at capacity factors between 30 % and 100 %, depending on capital costs. These results fall within the favorable benchmark of R$ 10 – 19 kg⁻¹ H_2 [139].

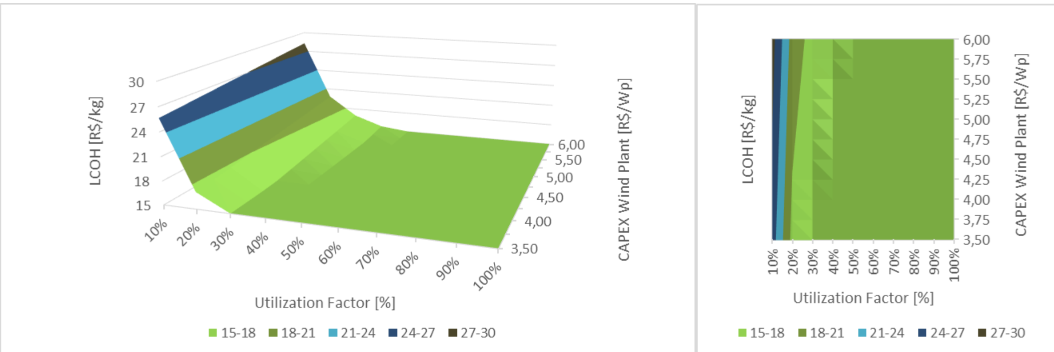

Figure 35 - LCOH as a function of the wind plant’s CAPEX and H2 utilization factor.
Source: Own elaboration.

In Figure 36, the CAPEX is fixed at R$ 4,750 kW⁻¹ (≈ USD 950 kW⁻¹), while the capacity factor (10 % – 100 %) and wind-plant OPEX (R$ 50 – 80 kWp⁻¹ month⁻¹ ≈ USD 10 – 16 kWp⁻¹ month⁻¹) vary. Under these conditions, the mean LCOH spans R$ 15 – 30 kg⁻¹ H_2 (≈ USD 3 – 6 kg⁻¹ H_2). The lowest values, below R$ 18 kg⁻¹ H_2 (≈ USD 3.6 kg⁻¹ H_2), correspond to capacity factors of 30 % – 40 % and OPEX of R$ 20 – 28 kWp⁻¹ month⁻¹ (≈ USD 4 – 5.6 kWp⁻¹ month⁻¹). Conversely, capacity factors below 20 % yield

LCOH values of R$ 21 – 30 kg^{-1} H_2 (≈ USD 4.2 – 6 kg^{-1} H_2), reinforcing the dominant influence of the utilization rate on hydrogen costs.

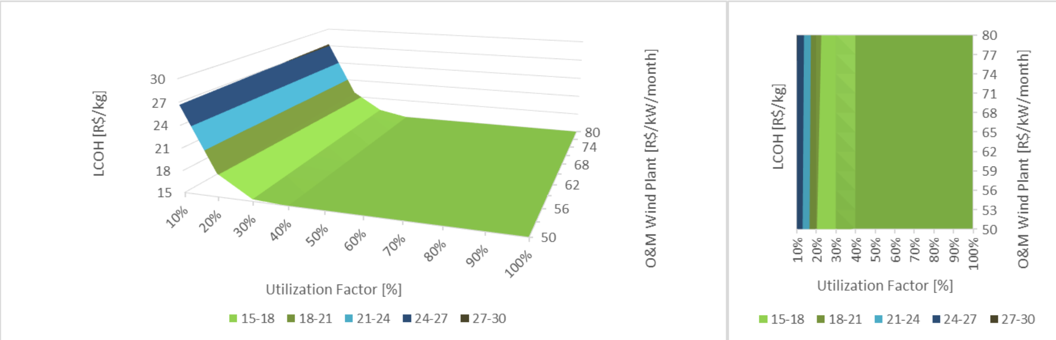

Figure 36 - LCOH as a function of the wind plant's OPEX and H2 utilization factor. Source: Own elaboration.

Taken together, these scenarios confirm that the hydrogen-plant capacity factor remains the principal driver of the LCOH, while capital expenditure exerts a more pronounced effect than operational expenditure on the cost of wind-generated electricity.

4.2.3 Case 3: Mix of 33 % solar, 33 % wind, 33 % ACL

In this case study the hydrogen plant is supplied by a balanced mix of electricity: 33 % on-site photovoltaic (PV) generation, 33 % on-site wind generation, and 33 % renewable electricity purchased on the ACL and backed by I-REC certificates. The shares were sized to match the plant's electricity demand during its first year of operation. Table 25 shows the key results for Case 3.

Table 25 - Key results of Case 3 with a hybrid energy mix.

Category	***Indicator***	***Value (BRL)***	***≈ Value (USD*)***	***Unit***
Energy	Rated capacity of the power plant	R$ 115,962 kW	USD 23,192 kW	kW (AC)
	Annual electricity generation	R$ 320,442 MWh	USD 64,088 MWh	MWh yr^{-1}
	PV modules installed	185,095	—	—
	Wind turbines installed	23	—	—
Production	Electricity consumption	R$ 485,093,059 kWh	USD 97,018,612 kWh	kWh yr^{-1}
	Hydrogen production	7,824,082	—	kg H_2 yr^{-1}
	Water consumption	94,608	—	m^3 yr^{-1}
Transport	Mode of transport	None	—	—
	Distance	0	—	km

	Volume	21.436	—	t day^{-1}
	Specific cost	R$ 0.00 kg^{-1} H_2	USD 0.00 kg^{-1}	—
Storage	Levelised cost of storage (LCOS)	R$ 15 kg^{-1} H_2	USD 3 kg^{-1}	—
Economic & Financial	CAPEX – Hydrogen production plant	R$ 245,003,004	USD 49,000,601	—
	CAPEX – Power-generation plant	R$ 494,221,154	USD 98,844,231	—
	OPEX – O&M (production)	R$ 7,350,090 yr^{-1}	USD 1,470,018 yr^{-1}	—
	OPEX – O&M (energy)	R$ 5,886,000 yr^{-1}	USD 1,177,200 yr^{-1}	—
	Storage cost	R$ 7,432,878 yr^{-1}	USD 1,486,576 yr^{-1}	—
	Water cost	R$ 1,748,356 yr^{-1}	USD 349,671 yr^{-1}	—
	Transport cost	—	—	—
	Total CAPEX	**R$ 739,224,158**	**USD 147,844,832**	—
	Total OPEX	**R$ 22,417,323 yr^{-1}**	**USD 4,483,465 yr^{-1}**	—
Cost Metrics	LCOH – Production cost	R$ 1.90 kg^{-1} H_2	USD 0.38 kg^{-1}	—
	LCOH – Energy cost	R$ 3.16 kg^{-1} H_2	USD 0.63 kg^{-1}	—
	LCOH – O&M (production)	R$ 0.94 kg^{-1} H_2	USD 0.19 kg^{-1}	—
	LCOH – O&M (energy)	R$ 1.09 kg^{-1} H_2	USD 0.22 kg^{-1}	—
	LCOH – Storage cost	R$ 0.95 kg^{-1} H_2	USD 0.19 kg^{-1}	—
	LCOH – Water cost	R$ 0.22 kg^{-1} H_2	USD 0.04 kg^{-1}	—
	LCOH – Transport cost	—	—	—
	Total LCOH	**R$ 15.04 kg^{-1} H_2**	**USD 3.01 kg^{-1}**	—
Financial Indicators	Internal rate of return (IRR)	1.21 % $month^{-1}$	—	—
	Minimum DSCR	1.72	—	—
	Pay-back period	98	—	months
	LCOE	R$ 177.87 MWh^{-1}	USD 35.57 MWh^{-1}	—

*Conversion factor: 1 USD = 5 BRL.

Source: Own elaboration.

The calculation may assume average electricity prices under several circumstances, in which power can originate from dedicated renewable generation (self-production), from the non-renewable grid, from the renewable grid (considering fiscal benefits), or from a situation in which self-generated renewable electricity could be complemented by grid power [141]. For cases in which the grid is used, the values adopted are the annual national average of the *Preço da Liquidação das Diferenças* (PLD) which is electricity spot maket price traded in the ACL since 2018. Assuming the purchased electricity is renewable and acquired through long-term power-purchase agreements (PPAs), the prices range from R$ 182 MWh^{-1} (≈ USD 36.4 MWh^{-1}) to R$ 282 MWh^{-1} (≈ USD 56.4 MWh^{-1}).

To illustrate the tool’s full capability in measuring environmental parameters in different considered boundaries, the final consumer is assumed to be located in Fortaleza, capital of the state of Ceará, and transport along the 552 km route is carried out by pipeline in the form of compressed hydrogen.

As shown in Table 26, one can observe the environmental impact, in terms of carbon-dioxide-equivalent emissions, of the electricity-generation stage, hydrogen-production stage and transport stage.

Table 26 - Detailed environmental impacts calculated by the tool for the cradle-to-gate (plant) and cradle-to-gate (consumer) boundaries.

Block	Type	Unit	Value
Energy	Solar energy	t CO_2 eq	303.200
	Wind energy	t CO_2 eq	45.292
	Grid electricity	t CO_2 eq	0
Production	PEM electrolysis	t CO_2 eq	1.282
	Compression	t CO_2 eq	22.795
Transport	Compressed H_2 + Pipeline	t CO_2 eq	43.518
Total cradle-to-gate	—	t CO_2 eq	372.570
(plant gate)	—	t CO_2 eq kg^{-1} H_2	2.615
Total cradle-to-user’s gate	—	t CO_2 eq	416.088
(consumer gate)	—	t CO_2 eq kg^{-1} H_2	2.921

Source: Own elaboration.

Electric-power generation accounts for 94 % of cradle-to-gate emissions, while transport adds a 12 % increase relative to emissions at the plant gate. Assuming that ACL electricity purchases do not entail additional emissions (i.e. their own footprints are already accounted for), 87 % of production-stage emissions are linked to photovoltaic generation. Within hydrogen production, compression inside the plant boundary represents 95 % of the total.

In Table 27 and Table 28, the potential equivalent emission reduction of fossil fuel substitution or emerging fuels such as ammonia are presented for maritime passenger and cargo transport applications.

Table 27 - Cradle-to-grave environmental-impact assessment for substituting conventional fuels with hydrogen-based technology in passenger maritime transport.

Fuel replaced ↓	***Substitution fuel – Energy***	***Δ Impact***
Natural gas – ICE	Hydrogen – PEMFC	-48 %
Marine gasoline – ICE	Hydrogen – PEMFC	-49 %

Source: Own elaboration.

Table 28 - Cradle to grave environmental impact assessment for substituting conventional fuels with hydrogen based technology in freight maritime transport.

Fuel replaced ↓	***Green ammonia (wind)***	***Green ammonia (hydro)***	***H_2 (wind) – PEMFC***	***H_2 (wind) + marine diesel (50:50 energy basis)***	***H_2 (hydro) – PEMFC***	***H_2 (hydro) + marine diesel (50:50 energy basis)***
Green ammonia (wind)	–	-7 %	-54 %	+21 %	-63 %	+16 %

Green ammonia (hydro)	+8 %	–	-50 %	+30 %	-60 %	+25 %
Heavy marine diesel	-51 %	-54 %	-77 %	-41 %	-82 %	-43 %

Maritime application (cargo transport; 51 500 t payload)

Fuel replaced ↓	Green ammonia (wind)	Green ammonia (hydro)	H_2 (wind) – PEMFC	H_2 (wind) + marine diesel (50:50 energy basis)	H_2 (hydro) – PEMFC	H_2 (hydro) + marine diesel (50:50 energy basis)
Green ammonia (wind)	–	-9 %	-39 %	+66 %	-47 %	+63 %
Green ammonia (hydro)	+10 %	–	-32 %	+83 %	-41 %	+80 %
Heavy marine diesel	-64 %	-67 %	-78 %	-40 %	-81 %	-41 %

Maritime application (cargo transport; tanker – 100 000 t payload)
Source: Own elaboration.

Replacing fossil fuels (natural gas, marine gasoline and heavy marine diesel) with green hydrogen and green ammonia yields emission reductions of 48–82 % and 32–63 %, respectively. For partial substitution, the reduction reaches up to 43 %.

Table 29 illustrates the analysis of road mobility applications.

Table 29 - Cradle to grave environmental impact assessment for substituting conventional fuels with hydrogen based technology in road transport.

Fuel replaced ↓	H_2 – PEMFC	H_2 – hybrid ICE	H_2 – ICE	H_2 + natural gas – ICE*	H_2 + gasoline† – dual-fuel ICE
Diesel – hybrid ICE	-52 %	-71 %	-67 %	-55 %	-43 %
Diesel – ICE	-59 %	-75 %	-71 %	-62 %	-51 %
Gasoline – hybrid ICE	-58 %	-75 %	-71 %	-61 %	-51 %
Gasoline – ICE	-65 %	-79 %	-76 %	-68 %	-59 %
Natural gas – hybrid ICE	+4 %	-37 %	-28 %	-4 %	+23 %
Natural gas – ICE	-38 %	-74 %	-72 %	-44 %	-32 %
Sugar-cane ethanol – ICE	-4 %	-42 %	-34 %	-11 %	+13 %
Sugar-cane ethanol – SOFC	-36 %	-62 %	-56 %	-41 %	-25 %
Corn ethanol – SOFC	-41 %	-65 %	-60 %	-46 %	-31 %
Electricity (wind) – BEV	+496 %	+258 %	+312 %	+449 %	+601 %
Electricity (hydro) – BEV	+527 %	+277 %	+333 %	+477 %	+637 %
Electricity (solar) – BEV	+82 %	+10 %	+26 %	+68 %	+114 %

* Hydrogen blended with natural gas at 20 % vol (≈ 7.3 % on an energy basis).
† Hydrogen blended with gasoline at 7.3 % on an energy basis (dual-fuel ICE).
Source: Own elaboration.

The figure shows that replacing thermal-engine technology—regardless of fuel—with hydrogen-fuelled internal-combustion engines (ICE) or hybrids consistently reduces emissions by 28–79 %. With PEM-fuel-cell technology, the reduction is lower or may yield no environmental benefit for natural-gas hybrids.

In all simulated scenarios hydrogen technologies do not outperform battery-electric vehicles, which show emission increases of 26–527 % in comparison.

Changing the type of application, Table 30presents the potential for reducing emissions in electricity generation using fuel cells. When fossil resources are replaced, the reduction is always substantial, ranging from 83–97 % of original emissions. Substituting photovoltaic or biomass technologies may also be advantageous, albeit to a lesser extent (24–68 %), and scenarios exist in which environmental impacts increase. Conversely, the hydrogen-production route is not competitive in environmental terms (specifically CO_2-equivalent emissions) with wind-based electricity, which exhibits the lowest impact.

Table 30 - Cradle to grave environmental impact assessment for substituting conventional power generation with hydrogen and fuel cell technology.

Fuel replaced ↓	*PEMFC – constant production*	*SOFC – constant production*	*PEMFC – constant energy*	*SOFC – constant energy*
Coal	-99 %	-94 %	-89 %	-86 %
Lignite	-97 %	-95 %	-91 %	-89 %
Natural gas	-95 %	-92 %	-86 %	-83 %
Petroleum	-95 %	-93 %	-86 %	-84 %
Biomass	-52 %	-24 %	+41 %	+70 %
Solar	-68 %	-48 %	-4 %	+16 %
Wind	+50 %	+141 %	+344 %	+435 %

Source: Own elaboration.

For the sensitivity analysis in this case, tornado diagrams were generated for the main economic and environmental indicators. Beginning with the principal energy-block indicator, the LCOE is sensitive to the cost of the renewable-energy plant that supplies the self-generated fraction and, additionally, to the cost of the energy acquired via PPA. In this scenario, one may infer that policies aimed at reducing energy costs—such as tax exemptions for the hydrogen-supply chain—are important.

The results presented in the tornado chart of Figure 37 reinforce the observation that the relative cost of electricity in the electrolysis plant depends on the source employed, as all variables considered show an LCOE impact of 0.8–11 % from the nominal value of R$ 140.77 MWh^{-1} (≈ USD 28.15 MWh^{-1}). For comparison, the LCOE values for electricity from wind, solar and the ACL are R$ 111.23, 190.29 and 232.00 MWh^{-1} (≈ USD 22.25, 38.06 and 46.40 MWh^{-1}), respectively. Hence, with the energy mix considered, the LCOE tends toward the lower range, rendering electricity more competitive than in the case of exclusively photovoltaic generation.

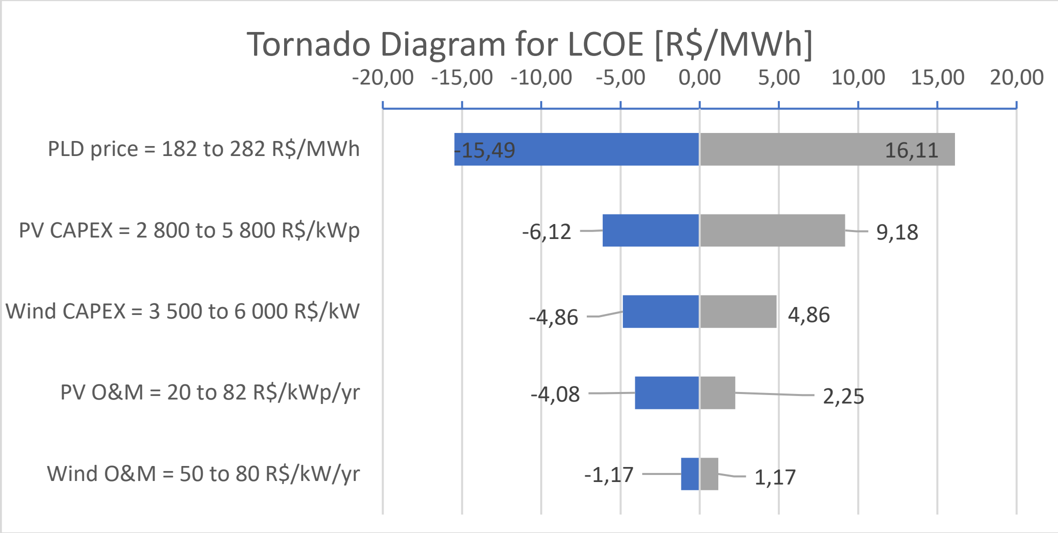

Figure 37 - Tornado diagram for the relative variation of LCOE, departing from a base value of R$ 140.77 MWh^{-1}.
Source: Own elaboration.

In the present case, in which each source supplies one-third of total energy demand, the impact of the ACL-contracted-energy price variation is greater than that of solar energy, which in turn is much greater than that of wind energy. In renewable-energy projects the cost of electricity is more capital-intensive than in conventional technologies, and OPEX costs have a smaller impact. For solar power, technology cost represents a significant share of the investment and thus exerts a greater influence on the LCOE.

For the production block the key indicator is the LCOH. Given that many factors can affect the LCOH, sensitivity analysis was applied to identify the key drivers of the unit hydrogen-production cost and understand their correlation. In this study, the effects of all factors (energy CAPEX, ACL electricity-contract price, OPEX and electrolyser CAPEX) are presented in Figure 38. The capacity factor was not included because the model assumes a constant utilization factor of 60 %. The hydrogen-production cost was studied by varying the factors between their maximum and minimum values.

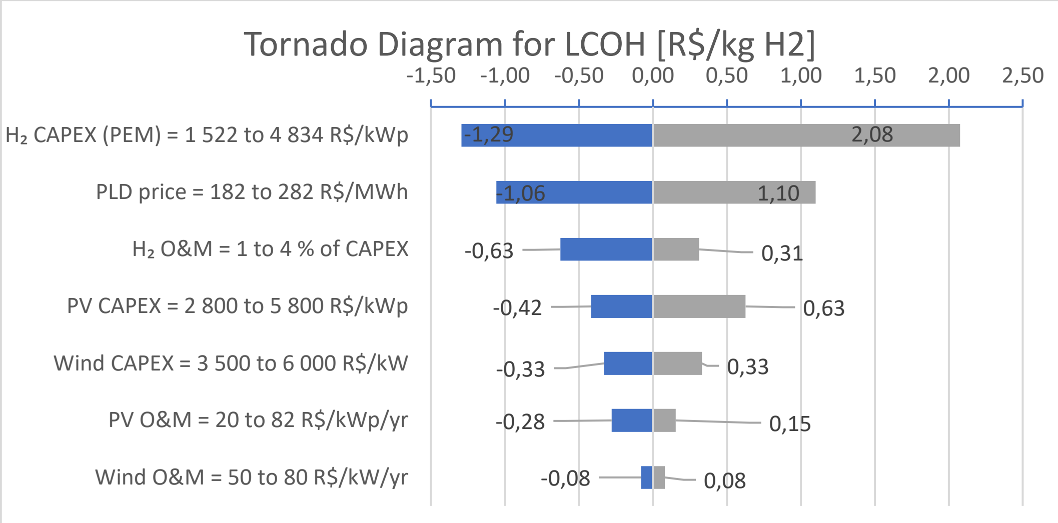

Figure 38 - Tornado diagram for the relative variation of LCOH, departing from a base value of R$ 13.62 kg^{-1} H_2 (≈ USD 2.72 kg^{-1} H_2).
Source: Own elaboration.

In this 33 % PV / 33 % wind / 33 % ACL blend, relative to the base value of 13.62 R$/kg, varying PEM-electrolyser CAPEX produces a –9 % to +15 % swing in the LCOH, making it the dominant driver. The ACL electricity price then contributes a –8 % to +8 % variation. Photovoltaic CAPEX yields a –3 % to +5 % impact, and wind CAPEX a –2 % to +2 % impact. Accordingly, reducing hydrogen costs in this mixed-supply scenario depends primarily on lowering electrolyser CAPEX and securing cheaper ACL or photovoltaic electricity; wind-generation costs play a secondary role.

Continuing the analysis of economic parameters, the project's internal rate of return (IRR) was calculated. As seen in Figure 39, for a given capacity factor and LCOH, the IRR is heavily dependent on the hydrogen selling price and on the availability of low-cost financing. Specifically, the percentage participation of zero-cost financing (grants) in the project's funding sources has a relatively more significant impact than low-interest repayable financing.

In general, a project can rely on various funding sources that may or may not share the same conditions (interest rates, terms, shares, etc.). For simplicity only two debt sources were considered, in addition to equity: one repayable (Financing 1) and one non-repayable (grants). Figure 39 shows that a 25 % share of the former adds virtually the same IRR as a 60 % share of the latter.

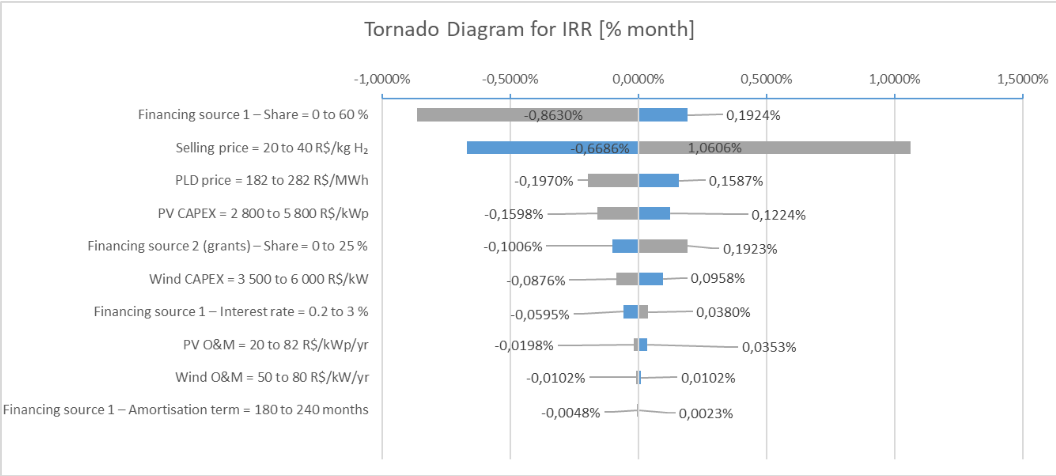

Figure 39 - Tornado diagram for the relative variation of IRR, departing from a base value of 0.28 % month⁻¹.
Source: Own elaboration.

Because the IRR values are centered on 0.28 % month⁻¹, the project will exhibit a negative IRR (be unviable) only for parameters whose negative variation exceeds 0.28 in absolute magnitude. This situation arises only for the variables "Financing 1 share" and "selling price." Thus, the project tolerates individual variations at the lower limits for all other variables.

The final parameter to assess project profitability is the quantity of CBIOs the hydrogen production will generate, i.e. a remuneration (economic value) obtained by substituting natural gas with hydrogen. Table 31 depicts the calculated values for substituting coal, lignite, natural gas and petroleum derivatives with hydrogen.

Table 31 - Evaluation of avoided emission remuneration for substituting fossil sources with hydrogen

Fuel replaced by H_2	***Average annual value (R$/year)***	***Value per unit mass (R$/kg)***	***Average annual value (USD/year)***	***Value per unit mass (USD/kg)***
Coal	R$ 5.095.758	R$ 0,651	USD 1.019.151,60	USD 0,1302
Lignite	R$ 4.127.693	R$ 0,528	USD 825.538,60	USD 0,1056
Natural gas	R$ 890.258	R$ 0,114	USD 178.051,60	USD 0,0228
Petroleum products	− R$ 1.271.850	− R$ 0,163	− USD 254.370,00	− USD 0,0326

Source: Own elaboration.

According to the adopted methodology, avoided-emission remuneration is generated except when petroleum derivatives are replaced. Therefore, when normalised per unit mass of hydrogen produced, the value remains marginal—no more than 4 %—when compared with the LCOH of R$ 15.04 kg⁻¹ H_2 (≈ USD 3.01 kg⁻¹ H_2).

Regarding sensitivity analysis, the methodology evaluated the influence of key variables on the decarbonisation credit. The tornado diagram in Figure

40indicates the best- and worst-case results for decarbonisation credits for each variable (emission factor of PV and wind generation, emission factor of PEM hydrogen production, compression factor for local storage, and CBIO price). Consequently, the decarbonisation credit is highly dependent on, and related to, the environmental impact of solar energy. Indeed, within the price range R$ 45.45–119.55 (≈ USD 9.09–23.91) found in the literature [142], the variation is ± 120 % of the nominal value for the simulated case, producing a pessimistic scenario (high PV generation emissions) in which no decarbonisation credits are generated, because the case yields negative remuneration. The next most impactful factor was the CBIO price itself, influencing remuneration potential by up to 34 %. The environmental impact of wind energy used in the electricity blend accounts for only 10 % of the calculated result. Both the hydrogen compression factor after production and the PEM production-emission factor have little influence (1 % and 0.1 % of the calculated value, respectively).

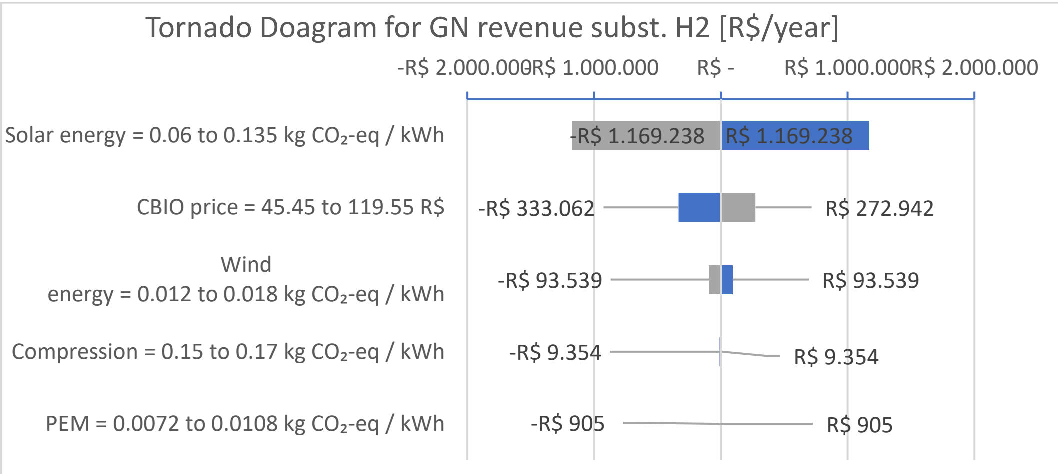

Figure 40 - Tornado diagram for the variation of remuneration via substitution of natural gas with hydrogen (R$/yr).
Variations depart from a base value of R$ 641 752 yr^{-1} (≈ USD 128 350 yr^{-1}); blue bars show the maximum value variation, and grey bars the minimum value variation).
Source: Own elaboration.

The results obtained in this section demonstrate the model’s sensitivity to the complexity of the technical and economic-financial scenario. The variations observed in the sensitivity analysis corroborate current practices in the hydrogen economy—namely, incentives for R&D investment in electrolysis and solar-generation technologies to raise efficiency, reduce costs and minimize environmental impacts. Furthermore, the use of low-cost or zero-cost financing lines (grants) is recommended to improve plant economics.

5 Conclusions and future work

This thesis has introduced and demonstrated two interconnected geospatial tools—GeoH$_2$-PAM and GeoH$_2$-FAT—that together provide a comprehensive pathway from resource assessment to project-level feasibility analysis for green hydrogen and its derivatives in Brazil. GeoH$_2$-PAM leverages high-resolution solar photovoltaic (SPV), onshore wind (ONW), and offshore wind (OFW) datasets, integrating eighteen layers of environmental, technical, social, and economic constraints to generate detailed maps of gross, technical, and economic potentials. In parallel, GeoH$_2$-FAT translates these regional insights into plant-scale techno-economic and environmental performance metrics, enabling developers and policymakers to evaluate the implications of alternative power-supply configurations, capital and operating cost assumptions, and emission-reduction targets.

The results produced by GeoH$_2$-PAM clearly highlight the divergence between theoretical resource abundance and realistic deployment opportunities. For SPV, Brazil's gross hydrogen potential of over 17 Mton H$_2$/year is curtailed by more than sixty percent when sensitive areas—such as biodiversity conservation units, rural settlements, and Indigenous lands—are excluded, yielding a technical potential of approximately 6.5 Mton H$_2$/year. The constraint-overlap analysis reveals that multiple exclusion criteria frequently coincide in the same geographic areas, compounding their individual impacts and underscoring the necessity of a multi-layered approach. Similarly, GeoH$_2$-PAM's assessment of onshore wind resource demonstrates that although the nation's gross ONW potential exceeds 830 Mton H$_2$/year, the imposition of capacity-factor thresholds, slope restrictions, and environmental protections reduces technical potential by roughly seventy-five percent to just over 200 Mton H$_2$/year. Offshore wind, despite its expansive Exclusive Economic Zone, follows the same pattern: an initial gross potential of 713 Mton H$_2$/year is brought down to 32 Mton H$_2$/year after applying navigational, ecological, depth, and performance constraints. Across all three technologies, economic-potential mapping—presented in terms of LCOE and LCOH—identifies inland SPV sites and high-capacity-factor wind regions as the most cost-effective location for hydrogen production, while revealing that many areas with theoretical promise remain financially marginal once real-world limitations are factored in.

GeoH$_2$-FAT extends these regional findings into project-level insights. Through three illustrative case studies at São Gonçalo do Amarante (Port of Pecém), the tool assesses hydrogen plants powered exclusively by solar PV, exclusively by onshore wind, and by a balanced mix of photovoltaics, wind, and grid-sourced renewable power. These simulations reveal that a wind-powered configuration achieves the lowest LCOH (around R\$ 11/kg H$_2$) and highest internal rate of return (approximately 1.16% per month), while a mixed energy supply can further optimize financial performance by smoothing generation profiles and reducing reliance on high-cost grid contracts. The life-cycle emissions analysis embedded in GeoH$_2$-FAT demonstrates that cradle-to-gate carbon footprints range from 2.6 to 2.9 kg CO$_2$e/kg H$_2$, with photovoltaic generation and electrolysis compression representing the bulk of emissions. Substitution assessments confirm that replacing maritime and road transport fuels with green hydrogen or ammonia can yield emission reductions of up to 80%, although battery-electric alternatives often deliver even greater gains in passenger mobility applications.

Collectively, $GeoH_2$-PAM and $GeoH_2$-FAT represent a significant advance over prevailing resource assessments. By moving beyond simplistic, unconstrained estimates of gross potential, $GeoH_2$-PAM incorporates site suitability, land-use conflicts, and socio-environmental priorities into a unified modelling framework. Meanwhile, $GeoH_2$-FAT translates these spatial outputs into actionable project metrics—capital and operating costs, cost of hydrogen, financial indicators, and environmental impacts—thereby bridging the gap between territory-wide planning and individual investment decisions. This integration of high-resolution geospatial analysis with techno-economic simulation not only enhances the realism of hydrogen-potential estimates but also provides stakeholders with the decision-support tools needed to prioritize investment, inform policy, and de-risk project development.

In sum, this thesis has delivered a pair of complementary geospatial tools that together chart a clear route from Brazil's vast renewable endowment to practicable green hydrogen projects. By quantifying both the geographical constraints on technical potential and the economic bearings on project feasibility, $GeoH_2$-PAM and $GeoH_2$-FAT equip researchers, planners, and investors with the insights required to navigate the complex terrain of hydrogen deployment. As Brazil and the world pursue aggressive decarbonization targets, these methodologies will prove essential in identifying where, at what scale, and under which conditions green hydrogen can most effectively contribute to a sustainable energy future. Looking ahead, the $GeoH_2$-PAM can be strengthened by making its key assumptions more flexible and data-driven. For example, instead of using a single, fixed capacity-density for all sites, future work could derive capacity-density values from actual farm layouts or optimization studies, better reflecting how turbine spacing or panel tilt changes with terrain and land use. Similarly, the hydrogen-production model could include dynamic electrolyser performance curves and explore alternative plant setups—such as small hybrid PV-wind microgrids, battery storage, or co-located desalination units—to see how these affect both yields and costs. Expanding the resource base to cover hydropower, CSP, biomass, geothermal, and ocean energy would also help capture the full range of Brazil's renewable potential. Moreover, using finer-scale terrain and land-cover maps (for example, LiDAR or local weather station data) and testing different global resource datasets would show how sensitive the results are to the choice of inputs—and help pinpoint areas where small features or local measurements make a big difference.

On the constraints side, adding new exclusion layers and real-world policy rules will make both $GeoH_2$-PAM and $GeoH_2$-FAT more useful for decision-makers. Future studies could bring in maps of cultural heritage sites, water availability zones, grid interconnection points, or social vulnerability indices to paint a fuller picture of where projects really can go ahead. Linking the models directly to national and international certification schemes—such as Guarantees of Origin or hydrogen export rules—and embedding standard GHG accounting methods will let users estimate not only technical potential and costs but also the true emissions savings and possible revenue from carbon credits.

6 References

[1] IEA. Net Zero by 2050 - A Roadmap for the Global Energy Sector. 2021.
[2] Calvin K, Dasgupta D, Krinner G, Mukherji A, Thorne PW, Trisos C, et al. IPCC, 2023: Climate Change 2023: Synthesis Report. Contribution of Working Groups I, II and III to the Sixth Assessment Report of the Intergovernmental Panel on Climate Change [Core Writing Team, H. Lee and J. Romero (eds.)]. IPCC, Geneva, Switzerland. First. Intergovernmental Panel on Climate Change (IPCC); 2023. https://doi.org/10.59327/IPCC/AR6-9789291691647.
[3] IEA IEA. Global Hydrogen Review 2024. 2024.
[4] BloomberNEF. Hydrogen Economy Outlook. 2020.
[5] EPE E de PE, MME M de M e E. Potencial dos Recursos Energéticos no Horizonte 2050 2018:186.
[6] Snow J. On the Mode of Communication of Cholera 1855:76.
[7] Foresman TW. The History of Geographic Information Systems: Perspectives from the Pioneers 1998:383.
[8] Sørensen B, Meibom P. GIS tools for renewable energy modelling. Renew Energy 1999;16:1262–7. https://doi.org/10.1016/S0960-1481(98)00514-X.
[9] Šúri M, Huld TA, Dunlop ED. PV-GIS: a web-based solar radiation database for the calculation of PV potential in Europe. Int J Sustain Energy 2005;24:55–67. https://doi.org/10.1080/14786450512331329556.
[10] Aydin NY, Kentel E, Duzgun S. GIS-based environmental assessment of wind energy systems for spatial planning: A case study from Western Turkey. Renew Sustain Energy Rev 2010;14:364–73. https://doi.org/10.1016/j.rser.2009.07.023.
[11] Brown A, Beiter P, Heimiller D, Davidson C, Denholm P, Melius J, et al. Estimating Renewable Energy Economic Potential in the United States: Methodology and Initial Results. Renew Energy 2016.
[12] Lopez A, Zuckerman G, Pinchuk P, Gleason M, Rivers M, Roberts O, et al. Renewable Energy Technical Potential and Supply Curves for the Contiguous United States: 2024 Edition. 2025. https://doi.org/10.2172/2500362.
[13] Connelly E, Penev M, Milbrandt A, Roberts B, Gilroy N, Melaina M. Resource Assessment for Hydrogen Production. 2020. https://doi.org/10.2172/1660128.
[14] Sigal A, Leiva EPM, Rodríguez CR. Assessment of the potential for hydrogen production from renewable resources in Argentina. Int J Hydrog Energy 2014;39:8204–14. https://doi.org/10.1016/j.ijhydene.2014.03.157.
[15] Asare-Addo M. Green hydrogen potential assessment in Ghana: application of PEM electrolysis process and geospatial-multi-criteria approach. Int J Sustain Energy 2023;42:1202–25. https://doi.org/10.1080/14786451.2023.2256892.
[16] Dinh VN, Leahy P, McKeogh E, Murphy J, Cummins V. Development of a viability assessment model for hydrogen production from dedicated offshore wind farms. Int J Hydrog Energy 2021;46:24620–31. https://doi.org/10.1016/j.ijhydene.2020.04.232.
[17] Yapa LS. Is GIS appropriate technology. Int J Geogr Inf Syst 1991;5:41–58. https://doi.org/10.1080/02693799108927830.

[18] Florin M, Gabriel E. Integrated resource management: The answer to a socio-economic problem. GeoJournal 1991;25. https://doi.org/10.1007/BF00179777.
[19] Graham RL, Liu W, Downing M, Noons CE, Daly M, Moore A. THE EFFECT OF LOCATION AND FACILITY DEMAND ON THE MARGINAL COST OF DELIVERED WOOD CHIPS FROM ENERGY CROPS: A CASE STUDY OF THE STATE OF TENNESSEE n.d.
[20] Noon CE, Daly MJ. GIS-BASED BIOMASS RESOURCE ASSESSMENT WITH n.d.
[21] Simmons D HJ. Farming the winds: mapping renewable energy resources with GIS 1995;GIS Eur 4:30–32.
[22] Biljecki F. A scientometric analysis of selected GIScience journals. Int J Geogr Inf Sci 2016;30:1302–35. https://doi.org/10.1080/13658816.2015.1130831.
[23] Kinoshita T, Inoue K, Iwao K, Kagemoto H, Yamagata Y. A spatial evaluation of forest biomass usage using GIS. Appl Energy 2009;86:1–8. https://doi.org/10.1016/j.apenergy.2008.03.017.
[24] Masera O, Ghilardi A, Drigo R, Angel Trossero M. WISDOM: A GIS-based supply demand mapping tool for woodfuel management. Biomass Bioenergy 2006;30:618–37. https://doi.org/10.1016/j.biombioe.2006.01.006.
[25] Freppaz D, Minciardi R, Robba M, Rovatti M, Sacile R, Taramasso A. Optimizing forest biomass exploitation for energy supply at a regional level. Biomass Bioenergy 2004;26:15–25. https://doi.org/10.1016/S0961-9534(03)00079-5.
[26] Schmidt J, Leduc S, Dotzauer E, Kindermann G, Schmid E. Potential of biomass-fired combined heat and power plants considering the spatial distribution of biomass supply and heat demand. Int J Energy Res 2010;34:970–85. https://doi.org/10.1002/er.1623.
[27] Inman RH, Pedro HTC, Coimbra CFM. Solar forecasting methods for renewable energy integration. Prog Energy Combust Sci 2013;39:535–76. https://doi.org/10.1016/j.pecs.2013.06.002.
[28] Bergamasco L, Asinari P. Scalable methodology for the photovoltaic solar energy potential assessment based on available roof surface area: Further improvements by ortho-image analysis and application to Turin (Italy). Sol Energy 2011;85:2741–56. https://doi.org/10.1016/j.solener.2011.08.010.
[29] Huld T, Amillo A. Estimating PV Module Performance over Large Geographical Regions: The Role of Irradiance, Air Temperature, Wind Speed and Solar Spectrum. Energies 2015;8:5159–81. https://doi.org/10.3390/en8065159.
[30] Huang Y, Chen Z, Wu B, Chen L, Mao W, Zhao F, et al. Estimating Roof Solar Energy Potential in the Downtown Area Using a GPU-Accelerated Solar Radiation Model and Airborne LiDAR Data. Remote Sens 2015;7:17212–33. https://doi.org/10.3390/rs71215877.
[31] Hoogwijk M, De Vries B, Turkenburg W. Assessment of the global and regional geographical, technical and economic potential of onshore wind energy. Energy Econ 2004;26:889–919. https://doi.org/10.1016/j.eneco.2004.04.016.
[32] Janjai S, Masiri I, Promsen W, Pattarapanitchai S, Pankaew P, Laksanaboonsong J, et al. Evaluation of wind energy potential over Thailand

by using an atmospheric mesoscale model and a GIS approach. J Wind Eng Ind Aerodyn 2014;129:1–10. https://doi.org/10.1016/j.jweia.2014.03.010.
[33] Tsoutsos T, Tsitoura I, Kokologos D, Kalaitzakis K. Sustainable siting process in large wind farms case study in Crete. Renew Energy 2015;75:474–80. https://doi.org/10.1016/j.renene.2014.10.020.
[34] Voivontas D, Assimacopoulos D, Mourelatos A, Corominas J. Evaluation of Renewable Energy potential using a GIS decision support system. Renew Energy 1998;13:333–44. https://doi.org/10.1016/S0960-1481(98)00006-8.
[35] Dagdougui H. Decision support systems for sustainable renewable energy systems and hydrogen logistics: modelling, control and risk analysis. École Nationale Supérieure des Mines de Paris; Università degli studi di Genova, 2012.
[36] Esteves NB, Sigal A, Leiva EPM, Rodríguez CR, Cavalcante FSA, De Lima LC. Wind and solar hydrogen for the potential production of ammonia in the state of Ceará – Brazil. Int J Hydrog Energy 2015;40:9917–23. https://doi.org/10.1016/j.ijhydene.2015.06.044.
[37] Rahmouni S, Settou N, Negrou B, Gouareh A. GIS-based method for future prospect of hydrogen demand in the Algerian road transport sector. Int J Hydrog Energy 2016;41:2128–43. https://doi.org/10.1016/j.ijhydene.2015.11.156.
[38] Ashrafi ZN, Ghasemian M, Shahrestani MI, Khodabandeh E, Sedaghat A. Evaluation of hydrogen production from harvesting wind energy at high altitudes in Iran by three extrapolating Weibull methods. Int J Hydrog Energy 2018;43:3110–32. https://doi.org/10.1016/j.ijhydene.2017.12.154.
[39] Touili S, Alami Merrouni A, Azouzoute A, El Hassouani Y, Amrani A. A technical and economical assessment of hydrogen production potential from solar energy in Morocco. Int J Hydrog Energy 2018;43:22777–96. https://doi.org/10.1016/j.ijhydene.2018.10.136.
[40] Nielsen S, Skov IR. Investment screening model for spatial deployment of power-to-gas plants on a national scale – A Danish case. Int J Hydrog Energy 2019;44:9544–57. https://doi.org/10.1016/j.ijhydene.2018.09.129.
[41] Nematollahi O, Alamdari P, Jahangiri M, Sedaghat A, Alemrajabi AA. A techno-economical assessment of solar/wind resources and hydrogen production: A case study with GIS maps. Energy 2019;175:914–30. https://doi.org/10.1016/j.energy.2019.03.125.
[42] Feitz A, Tenthorey E, Coghlan R. Prospective hydrogen production regions of Australia. Geoscience Australia; 2019. https://doi.org/10.11636/Record.2019.015.
[43] Messaoudi D, Settou N, Negrou B, Settou B. GIS based multi-criteria decision making for solar hydrogen production sites selection in Algeria. Int J Hydrog Energy 2019;44:31808–31. https://doi.org/10.1016/j.ijhydene.2019.10.099.
[44] Almutairi K, Hosseini Dehshiri SS, Hosseini Dehshiri SJ, Mostafaeipour A, Jahangiri M, Techato K. Technical, economic, carbon footprint assessment, and prioritizing stations for hydrogen production using wind energy: A case study. Energy Strategy Rev 2021;36:100684. https://doi.org/10.1016/j.esr.2021.100684.
[45] Herwartz S, Pagenkopf J, Streuling C. Sector coupling potential of wind-based hydrogen production and fuel cell train operation in regional rail transport in Berlin and Brandenburg. Int J Hydrog Energy 2021;46:29597–615. https://doi.org/10.1016/j.ijhydene.2020.11.242.

[46] Dinh QV, Dinh VN, Mosadeghi H, Todesco Pereira PH, Leahy PG. A geospatial method for estimating the levelised cost of hydrogen production from offshore wind. Int J Hydrog Energy 2023;48:15000–13. https://doi.org/10.1016/j.ijhydene.2023.01.016.
[47] Hosseini Dehshiri SS, Hosseini Dehshiri SJ. Locating wind farm for power and hydrogen production based on Geographic information system and multi-criteria decision making method: An application. Int J Hydrog Energy 2022;47:24569–83. https://doi.org/10.1016/j.ijhydene.2022.03.083.
[48] Messaoudi D, Settou N, Allouhi A. Geographical, technical, economic, and environmental potential for wind to hydrogen production in Algeria: GIS-based approach. Int J Hydrog Energy 2024;50:142–60. https://doi.org/10.1016/j.ijhydene.2023.07.263.
[49] Müller LA, Leonard A, Trotter PA, Hirmer S. Green hydrogen production and use in low- and middle-income countries: A least-cost geospatial modelling approach applied to Kenya. Appl Energy 2023;343:121219. https://doi.org/10.1016/j.apenergy.2023.121219.
[50] Agora Energiewende. Brazil map of hydrogen production costs – documentation. 2024.
[51] Agora Industry, Agora Energiewende. EU map of hydrogen production costs – documentation 2024.
[52] Agora Industry, Agora Energiewende. Southeast Asia map of hydrogen production costs – documentation 2024.
[53] Rosa L, Mazzotti M. Potential for hydrogen production from sustainable biomass with carbon capture and storage. Renew Sustain Energy Rev 2022;157:112123. https://doi.org/10.1016/j.rser.2022.112123.
[54] Raillani B, Mezrhab A, Amraqui S, Moussaoui MA, Mezrhab A. Regression-based spatial GIS analysis for an accurate assessment of renewable energy potential. Energy Sustain Dev 2022;69:118–33. https://doi.org/10.1016/j.esd.2022.06.003.
[55] Okunlola A, Davis M, Kumar A. The development of an assessment framework to determine the technical hydrogen production potential from wind and solar energy. Renew Sustain Energy Rev 2022;166:112610. https://doi.org/10.1016/j.rser.2022.112610.
[56] Caravantes D, Carbajal J, Marcelo-Aldana D. Estimation of Green Hydrogen production potential in the Piura region from water electrolysis. 2022 IEEE Int. Conf. Autom. Congr. Chil. Assoc. Autom. Control ICA-ACCA, Curicó, Chile: IEEE; 2022, p. 1–6. https://doi.org/10.1109/ICA-ACCA56767.2022.10006002.
[57] Juárez-Casildo V, Cervantes I, González-Huerta RDG. Solar hydrogen production in urban areas of Mexico: towards hydrogen cities. Int J Hydrog Energy 2022;47:30012–26. https://doi.org/10.1016/j.ijhydene.2022.06.137.
[58] Irfan M, Razzaq A, Chupradit S, Javid M, Rauf A, Aini Farooqi TJ. Hydrogen production potential from agricultural biomass in Punjab province of Pakistan. Int J Hydrog Energy 2022;47:2846–61. https://doi.org/10.1016/j.ijhydene.2021.10.257.
[59] Ali F, Bennui A, Chowdhury S, Techato K. Suitable Site Selection for Solar-Based Green Hydrogen in Southern Thailand Using GIS-MCDM Approach. Sustainability 2022;14:6597. https://doi.org/10.3390/su14116597.
[60] Hosseini Dehshiri SS, Firoozabadi B. A novel four-stage integrated GIS based fuzzy SWARA approach for solar site suitability with hydrogen storage

system. Energy 2023;278:127927. https://doi.org/10.1016/j.energy.2023.127927.
[61] Hoogwijk M, Graus W. GLOBAL POTENTIAL OF RENEWABLE ENERGY SOURCES: A LITERATURE ASSESSMENT n.d.
[62] Krewitt W, Simon S, Pregger T. Renewable energy deployment potentials in large economies n.d.
[63] Resch G, Held A, Faber T, Panzer C, Toro F, Haas R. Potentials and prospects for renewable energies at global scale. Energy Policy 2008;36:4048–56. https://doi.org/10.1016/j.enpol.2008.06.029.
[64] Stangeland DA. The Potential and Barriers for Renewable Energy n.d.
[65] Cox SL, Lopez AJ, Watson AC, Grue NW, Leisch JE. Renewable Energy Data, Analysis, and Decisions: A Guide for Practitioners. 2018. https://doi.org/10.2172/1427970.
[66] Lopez A, Mai T, Lantz E, Harrison-Atlas D, Williams T, Maclaurin G. Land use and turbine technology influences on wind potential in the United States. Energy 2021;223:120044. https://doi.org/10.1016/j.energy.2021.120044.
[67] Lopez A, Roberts B, Heimiller D, Blair N, Porro G. U.S. Renewable Energy Technical Potentials: A GIS-Based Analysis. Renew Energy 2012.
[68] U.S. Department of Energy (DOE). Enabling Wind Power Nationwide 2015.
[69] MME M de M e E, EPE E de PE. Plano Nacional de Energia 2050 2020:243.
[70] MME M de M e E, EPE E de PE. Plano Decenal de Expansão de Energia 2031 2022:411.
[71] Perez R, Ineichen P, Seals R, Michalsky J, Stewart R. Modeling daylight availability and irradiance components from direct and global irradiance. Sol Energy 1990;44:271–89. https://doi.org/10.1016/0038-092X(90)90055-H.
[72] Duffie (Deceased) JA, Beckman WA, Blair N. Solar Engineering of Thermal Processes, Photovoltaics and Wind. 1st ed. Wiley; 2020. https://doi.org/10.1002/9781119540328.
[73] David King, Boyson W, Kratochvil J. Photovoltaic array performance model. 2004. https://doi.org/10.2172/919131.
[74] Henrique Paulino De Azevedo J. AVALIAÇÃO TÉCNICA, ECONÔMICA E AMBIENTAL GEORREFERENCIADA DE SISTEMAS FOTOVOLTAICOS. MESTRE EM ENGENHARIA MECÂNICA. PONTIFÍCIA UNIVERSIDADE CATÓLICA DO RIO DE JANEIRO, 2020. https://doi.org/10.17771/PUCRio.acad.50329.
[75] Pereira E, Martins F, Gonçalves A, Costa R, Lima F, Rüther R, et al. Atlas brasileiro de energia solar. 2nd ed. Universidade Federal de São Paulo; 2017. https://doi.org/10.34024/978851700089.
[76] ESMAP. Global Solar Atlas 2.0 Technical Report. Washington, DC: World Bank; 2019.
[77] Bolinger M, Bolinger G. Land Requirements for Utility-Scale PV: An Empirical Update on Power and Energy Density. IEEE J Photovolt 2022;12:589–94. https://doi.org/10.1109/JPHOTOV.2021.3136805.
[78] CEPEL. Atlas do Potencial Eólico Brasileiro: Simulações 2013 2017.
[79] GWA 3.1. Global Wind Atlas v3.1 2020.
[80] Davis NN, Badger J, Hahmann AN, Hansen BO, Mortensen NG, Kelly M, et al. The Global Wind Atlas: A High-Resolution Dataset of Climatologies and Associated Web-Based Application. Bull Am Meteorol Soc 2023;104:E1507–25. https://doi.org/10.1175/BAMS-D-21-0075.1.

[81] IEC. IEC 61400-1 - Wind turbines – Part 1: Design requirements. 3.1 Edition 2014.
[82] Draxl C, Clifton A, Hodge B-M, McCaa J. The Wind Integration National Dataset (WIND) Toolkit. Appl Energy 2015;151:355–66. https://doi.org/10.1016/j.apenergy.2015.03.121.
[83] Burton T, Jenkins N, Bossanyi E, Sharpe D, Graham M. Wind Energy Handbook 3e. 1st ed. Wiley; 2021. https://doi.org/10.1002/9781119451143.
[84] DTU. Global Wind Atlas v3 2019.
[85] Marinha do Brasil. Limites Marítimos 2020.
[86] IRENA. IRENA Global Atlas Spatial planning techniques 2-day seminar. Session 2b: Wind power spatial planning techniques. 2014.
[87] Vestas. Vesta V112-3.45 MW™ IEC IA Datasheet 2022.
[88] Enevoldsen P, Jacobson MZ. Data investigation of installed and output power densities of onshore and offshore wind turbines worldwide. Energy Sustain Dev 2021;60:40–51. https://doi.org/10.1016/j.esd.2020.11.004.
[89] Borrmann R. Capacity Densities of European Offshore Wind Farms 2018.
[90] Brooks A. Renewable Energy Resource Assessment Information for the United States. 2022. https://doi.org/10.2172/1855910.
[91] Musial W, Heimiller D, Beiter P, Scott G, Draxl C. 2016 Offshore Wind Energy Resource Assessment for the United States. 2016. https://doi.org/10.2172/1324533.
[92] Harrison-Atlas D, Maclaurin G, Lantz E. Spatially-Explicit Prediction of Capacity Density Advances Geographic Characterization of Wind Power Technical Potential. Energies 2021;14:3609. https://doi.org/10.3390/en14123609.
[93] EPE, editor. Roadmap eólica offshore brasil 2020.
[94] Pfaffel S, Faulstich S, Rohrig K. Performance and Reliability of Wind Turbines: A Review. Energies 2017;10:1904. https://doi.org/10.3390/en10111904.
[95] Bosch J, Staffell I, Hawkes AD. Temporally explicit and spatially resolved global offshore wind energy potentials. Energy 2018;163:766–81. https://doi.org/10.1016/j.energy.2018.08.153.
[96] Eurek K, Sullivan P, Gleason M, Hettinger D, Heimiller D, Lopez A. An improved global wind resource estimate for integrated assessment models. Energy Econ 2017;64:552–67. https://doi.org/10.1016/j.eneco.2016.11.015.
[97] Rezaei M, Akimov A, Gray EMA. Techno-economics of offshore wind-based dynamic hydrogen production. Appl Energy 2024;374:124030. https://doi.org/10.1016/j.apenergy.2024.124030.
[98] Rezaei M, Akimov A, Gray EMacA. Economics of renewable hydrogen production using wind and solar energy: A case study for Queensland, Australia. J Clean Prod 2024;435:140476. https://doi.org/10.1016/j.jclepro.2023.140476.
[99] Saygin D, Blanco H, Boshell F, Cordonnier J, Rouwenhorst K, Lathwal P, et al. Ammonia Production from Clean Hydrogen and the Implications for Global Natural Gas Demand. Sustainability 2023;15:1623. https://doi.org/10.3390/su15021623.
[100] Cesaro Z, Ives M, Nayak-Luke R, Mason M, Bañares-Alcántara R. Ammonia to power: Forecasting the levelized cost of electricity from green ammonia in large-scale power plants. Appl Energy 2021;282:116009. https://doi.org/10.1016/j.apenergy.2020.116009.

[101] McKenna R, Pfenninger S, Heinrichs H, Schmidt J, Staffell I, Bauer C, et al. High-resolution large-scale onshore wind energy assessments: A review of potential definitions, methodologies and future research needs. Renew Energy 2022;182:659–84. https://doi.org/10.1016/j.renene.2021.10.027.
[102] World Bank. Scenarios for Offshore Wind Development in Brazil 2024.
[103] Matute G. Techno-economic modelling of water electrolysers in the range of several MW to provide grid services while generating hydrogen for different applications: A case study in Spain applied to mobility with FCEVs. N T E R N T O N J O U R N O F H R O G E N E N E R G n.d.
[104] IRENA. Hydrogen from renewable power: technology outlook for the energy transition. Abu Dhabi: International Renewable Energy Agency; 2018.
[105] Wang L. Power-to-fuels via solid-oxide electrolyzer_ Operating window and techno-economics. Renew Sustain Energy Rev 2019.
[106] Proost J. State-of-the art CAPEX data for water electrolysers, and their impact on renewable hydrogen price settings. N T E R N T O N J O U R N O F H R O G E N E N E R G n.d.
[107] Nguyen T. Grid-connected hydrogen production via large-scale water electrolysis. Energy Convers Manag 2019.
[108] Grigoriev SA. Current status, research trends, and challenges in water electrolysis science and technology. N T E R N T O N J O U R N O F H R O G E N E N E R G n.d.
[109] Bristowe G, Smallbone A. The Key Techno-Economic and Manufacturing Drivers for Reducing the Cost of Power-to-Gas and a Hydrogen-Enabled Energy System 2021.
[110] Jang D, Kim K, Kim K-H, Kang S. Techno-economic analysis and Monte Carlo simulation for green hydrogen production using offshore wind power plant. Energy Convers Manag 2022;263:115695. https://doi.org/10.1016/j.enconman.2022.115695.
[111] EPE. Caderno de Preços de Geração 2021 2021.
[112] Matute G, Yusta JM, Correas LC. Techno-economic modelling of water electrolysers in the range of several MW to provide grid services while generating hydrogen for different applications: A case study in Spain applied to mobility with FCEVs. Int J Hydrog Energy 2019;44:17431–42. https://doi.org/10.1016/j.ijhydene.2019.05.092.
[113] Yang C, Ogden J. Determining the lowest-cost hydrogen delivery mode. Int J Hydrog Energy 2007;32:268–86. https://doi.org/10.1016/j.ijhydene.2006.05.009.
[114] Bartels JR. A feasibility study of implementing an Ammonia Economy. Master of Science. Iowa State University, Digital Repository, 2008. https://doi.org/10.31274/etd-180810-1374.
[115] IRENA. Hydrogen: A renewable energy perspective 2019.
[116] Short W, Packey DJ, Holt T. A manual for the economic evaluation of energy efficiency and renewable energy technologies. 1995. https://doi.org/10.2172/35391.
[117] Minister of Natural Resources Canada. Clean Energy Project Analysis: RETScreen Engineering & Cases Textbook 2005.
[118] E.R. Yescombe. Principles of Project Finance. vol. Second edition. Elsevier Inc; 2014.

[119] BNDES Finem - Geração de energia. BNDES n.d. http://www.bndes.gov.br/wps/portal/site/home/financiamento/produto/bndes-finem-energia (accessed April 21, 2025).
[120] ISO 14040:2006 - Environmental management — Life cycle assessment — Principles and framework n.d. https://www.iso.org/standard/37456.html (accessed April 21, 2025).
[121] Mann M, Spath P. Life Cycle Assessment of Renewable Hydrogen Production via Wind/Electrolysis: Milestone Completion Report. 2004. https://doi.org/10.2172/15006927.
[122] Bauer C, Hofer J, Althaus H-J, Del Duce A, Simons A. The environmental performance of current and future passenger vehicles: Life cycle assessment based on a novel scenario analysis framework. Appl Energy 2015;157:871–83. https://doi.org/10.1016/j.apenergy.2015.01.019.
[123] Reiter G, Lindorfer J. Global warming potential of hydrogen and methane production from renewable electricity via power-to-gas technology. Int J Life Cycle Assess 2015;20:477–89. https://doi.org/10.1007/s11367-015-0848-0.
[124] Simons A, Bauer C. A life-cycle perspective on automotive fuel cells. Appl Energy 2015;157:884–96. https://doi.org/10.1016/j.apenergy.2015.02.049.
[125] Ahmadi P, Kjeang E. Realistic simulation of fuel economy and life cycle metrics for hydrogen fuel cell vehicles: Realistic simulation of fuel economy and life cycle metrics for FCVs. Int J Energy Res 2017;41:714–27. https://doi.org/10.1002/er.3672.
[126] Ghandehariun S, Kumar A. Life cycle assessment of wind-based hydrogen production in Western Canada. Int J Hydrog Energy 2016;41:9696–704. https://doi.org/10.1016/j.ijhydene.2016.04.077.
[127] Bicer Y, Dincer I. Clean fuel options with hydrogen for sea transportation: A life cycle approach. Int J Hydrog Energy 2018;43:1179–93. https://doi.org/10.1016/j.ijhydene.2017.10.157.
[128] Mehmeti A, Angelis-Dimakis A, Arampatzis G, McPhail S, Ulgiati S. Life Cycle Assessment and Water Footprint of Hydrogen Production Methods: From Conventional to Emerging Technologies. Environments 2018;5:24. https://doi.org/10.3390/environments5020024.
[129] De Souza LLP, Lora EES, Palacio JCE, Rocha MH, Renó MLG, Venturini OJ. Comparative environmental life cycle assessment of conventional vehicles with different fuel options, plug-in hybrid and electric vehicles for a sustainable transportation system in Brazil. J Clean Prod 2018;203:444–68. https://doi.org/10.1016/j.jclepro.2018.08.236.
[130] Wulf C, Reuß M, Grube T, Zapp P, Robinius M, Hake J-F, et al. Life Cycle Assessment of hydrogen transport and distribution options. J Clean Prod 2018;199:431–43. https://doi.org/10.1016/j.jclepro.2018.07.180.
[131] Wulf C, Zapp P. Assessment of system variations for hydrogen transport by liquid organic hydrogen carriers. Int J Hydrog Energy 2018;43:11884–95. https://doi.org/10.1016/j.ijhydene.2018.01.198.
[132] Hwang SS, Gil SJ, Lee GN, Lee JW, Park H, Jung KH, et al. Life Cycle Assessment of Alternative Ship Fuels for Coastal Ferry Operating in Republic of Korea. J Mar Sci Eng 2020;8:660. https://doi.org/10.3390/jmse8090660.
[133] Sadeghi S, Ghandehariun S, Rosen MA. Comparative economic and life cycle assessment of solar-based hydrogen production for oil and gas industries. Energy 2020;208:118347. https://doi.org/10.1016/j.energy.2020.118347.

[134] Candelaresi D, Valente A, Iribarren D, Dufour J, Spazzafumo G. Comparative life cycle assessment of hydrogen-fuelled passenger cars. Int J Hydrog Energy 2021;46:35961–73. https://doi.org/10.1016/j.ijhydene.2021.01.034.
[135] Velandia Vargas JE, Seabra JEA. Fuel-cell technologies for private vehicles in Brazil: Environmental mirage or prospective romance? A comparative life cycle assessment of PEMFC and SOFC light-duty vehicles. Sci Total Environ 2021;798:149265. https://doi.org/10.1016/j.scitotenv.2021.149265.
[136] Turconi R, Boldrin A, Astrup T. Life cycle assessment (LCA) of electricity generation technologies: Overview, comparability and limitations. Renew Sustain Energy Rev 2013;28:555–65. https://doi.org/10.1016/j.rser.2013.08.013.
[137] De Oliveira Gabriel R. ANÁLISES ENERGÉTICA, ECONÔMICA E AMBIENTAL DE UM MICRO-CHP COM CÉLULA A COMBUSTÍVEL USANDO GÁS NATURAL E PAINÉIS FOTOVOLTAICOS PARA APLICAÇÕES RESIDENCIAIS E INDUSTRIAIS. MESTRE EM ENGENHARIA MECÂNICA. PONTIFÍCIA UNIVERSIDADE CATÓLICA DO RIO DE JANEIRO, 2020. https://doi.org/10.17771/PUCRio.acad.50338.
[138] Bicer Y, Khalid F. Life cycle environmental impact comparison of solid oxide fuel cells fueled by natural gas, hydrogen, ammonia and methanol for combined heat and power generation. Int J Hydrog Energy 2020;45:3670–85. https://doi.org/10.1016/j.ijhydene.2018.11.122.
[139] EPE. Balanço Energético Nacional 2021: Ano base 2020. Rio de Janeiro, RJ: 2021.
[140] EPE. Bases para a Consolidação da Estratégia Brasileira do Hidrogênio. Rio de Janeiro, RJ: 2021.
[141] Fan J-L, Yu P, Li K, Xu M, Zhang X. A levelized cost of hydrogen (LCOH) comparison of coal-to-hydrogen with CCS and water electrolysis powered by renewable energy in China. Energy 2022;242:123003. https://doi.org/10.1016/j.energy.2021.123003.
[142] B3. Índice de Crédito de Descarbonização B3 (ICBIO B3) | B3 n.d. https://www.b3.com.br/pt_br/market-data-e-indices/indices/indices-de-segmentos-e-setoriais/indice-de-credito-de-descarbonizacao-b3-icbio-b3.htm (accessed April 28, 2025).
[143] Staffell I, Green R. How does wind farm performance decline with age? Renew Energy 2014;66:775–86. https://doi.org/10.1016/j.renene.2013.10.041.
[144] Jordan DC, Kurtz SR. Photovoltaic Degradation Rates—an Analytical Review. Prog Photovolt Res Appl 2013;21:12–29. https://doi.org/10.1002/pip.1182.
[145] Rosso AP, Kroth G, Rampinelli GA, Schaeffer L. INFLUÊNCIA DO FATOR DE DIMENSIONAMENTO DE INVERSOR NO DESEMPENHO DE SISTEMAS FOTOVOLTAICOS CONECTADOS À REDE EM OPERAÇÃO NO SUL DO BRASIL, 2022. https://doi.org/10.59627/cbens.2022.1118.
[146] Hyypiä J, Karjunen H, Hosseinpour N, Inkeri E, Tynjälä T. Optimizing E-Methanol Production: Effect of Electricity Price and Renewable Energy Volatility on Optimum Dimensioning and Operation. In: Droege P, Quint L, editors. Proc. Int. Renew. Energy Storage Syst. Conf. IRES 2023, vol. 32,

Dordrecht: Atlantis Press International BV; 2024, p. 99–110. https://doi.org/10.2991/978-94-6463-455-6_11.
[147] Collodi G, Azzaro G, Ferrari N, Santos S. Demonstrating Large Scale Industrial CCS through CCU – A Case Study for Methanol Production. Energy Procedia 2017;114:122–38. https://doi.org/10.1016/j.egypro.2017.03.1155.
[148] World Bank. Global Shipping Traffic Density | Data Catalog 2021. https://datacatalog.worldbank.org/search/dataset/0037580/Global-Shipping-Traffic-Density (accessed April 21, 2025).
[149] ANP. GeoMapsANP n.d. https://geomaps.anp.gov.br/geoanp/ (accessed April 21, 2025).
[150] Ministério dos Transportes. GeoTransportes. Minist Transp n.d. https://www.gov.br/transportes/pt-br/assuntos/dados-de-transportes/bit/bit-mapas (accessed April 21, 2025).
[151] Instituto do Patrimônio Histórico e Artístico Nacional - IPHAN. Bancos de Dados - Patrimônio Arqueológico n.d. http://portal.iphan.gov.br/pagina/detalhes/1701/ (accessed April 21, 2025).
[152] Ministério do Meio Ambiente e Mudança do Clima. 2ª Atualização das Áreas Prioritárias para Conservação da Biodiversidade 2018. Minist Meio Ambiente E Mudança Clima n.d. https://www.gov.br/mma/pt-br/assuntos/biodiversidade-e-biomas/biomas-e-ecossistemas/conservacao-1/areas-prioritarias/2a-atualizacao-das-areas-prioritarias-para-conservacao-da-biodiversidade-2018 (accessed April 21, 2025).
[153] Ministério do Meio Ambiente e Mudança do Clima. Plataforma oficial de dados do Sistema Nacional de Unidades de Conservação da Natureza n.d. https://cnuc.mma.gov.br/ (accessed April 21, 2025).
[154] Agência Nacional de Águas - ANA. Massas d'Água. Catálogo Metadados ANA n.d. https://metadados.snirh.gov.br/geonetwork/srv/api/records/7d054e5a-8cc9-403c-9f1a-085fd933610c (accessed April 21, 2025).
[155] Instituto Brasileiro de Geografia e Estatística - IBGE. Áreas Urbanizadas 2019 n.d. https://www.ibge.gov.br/geociencias/cartas-e-mapas/redes-geograficas/15789-areas-urbanizadas.html?=&t=downloads (accessed April 21, 2025).
[156] Instituto Nacional de Colonização e Reforma Agrária - INCRA. Acervo Fundiário n.d. https://acervofundiario.incra.gov.br/acervo/acv.php (accessed April 21, 2025).
[157] Fundação Nacional dos Povos Indígenas - FUNAI. Terras Indígenas: Dados Geoespaciais e Mapas. Fundação Nac Povos Indígenas n.d. https://www.gov.br/funai/pt-br/atuacao/terras-indigenas/geoprocessamento-e-mapas (accessed April 21, 2025).
[158] Serviço Geológico do Brasil - SGB. Mapa de Declividade em Percentual do Relevo Brasileiro. SGB n.d. https://www.sgb.gov.br/mapa-de-declividade-em-percentual-do-relevo-brasileiro (accessed April 21, 2025).
[159] Serviço Geológico do Brasil - SGB. GeoSGB - Batimetria do Brasil n.d. https://geosgb.sgb.gov.br/geosgb/downloads.html (accessed April 21, 2025).
[160] Operador Nacional do Sistema - ONS. SINMAPS - Linhas de Transmissão n.d. https://sig.ons.org.br/app/sinmaps/ (accessed April 21, 2025).

[161] Instituto Brasileiro de Geografia e Estatística - IBGE. Malha Municipal n.d. https://www.ibge.gov.br/geociencias/organizacao-do-territorio/malhas-territoriais/15774-malhas.html (accessed April 21, 2025).

Appendix

A – Techno and economic modelling assumptions for $GeoH_2$-PAM

Table 32 - Global financial assumptions.

Parameter	*Value*	*Unit*	*Reference*
Analysis period	20	Years	-
Nominal discount rate	8	% a.a.	-
Inflation rate	5	% a.a.	-

Source: Own elaboration.

Table 33 - Hydrogen production assumptions.

Parameter	*Value*	*Unit*	*Reference*
Analysis period	20	Years	-
Nominal discount rate	8	% a.a.	-
Inflation rate	5	% a.a.	-
CAPEX electrolysis plant PEM	Figure 8	USD/kW	[104–109]
OPEX electrolysis plant PEM	3	% CAPEX/year	[112]
Overhaul value	60	% CAPEX	[110]
Time to overhaul	10	Years	[110]
Electrolyser degradation rate	1	%/year	[110]
Hydrogen leakage rate	0,1	%/year	[110]

Source: Own elaboration through references indicated in the table.

Table 34 -Onshore wind assumptions.

Parameter	*Value*	*Unit*	*Reference*
Onshore wind power plant	100	MW	-
CAPEX onshore wind plant	924	USD/kW	[111]
OPEX onshore wind plant	13	USD/kW/year	[111]
Wind turbine degradation rate	1,6	%/year	[143]

Source: Own elaboration through references indicated in the table.

Table 35 – Offshore wind assumptions.

Parameter	*Value*	*Unit*	*Reference*
Offshore wind power plant	100	MW	-
CAPEX offshore wind plant	2763	USD/kW	[111]
OPEX offshore wind plant	95	USD/kW/year	[111]
Wind turbine degradation rate	1,6	%/year	[143]

Source: Own elaboration through references indicated in the table.

Table 36 – Solar PV assumptions.

Parameter	*Value*	*Unit*	*Reference*
Solar PV power plant	100	MWp	-
Analysis period	20	Years	-
Nominal discount rate	8	% a.a.	-
Inflation rate	5	% a.a.	-
CAPEX solar PV plant	827	USD/kW	[111]
OPEX solar PV plant	10	USD/kW/year	[111]
PV module degradation rate	0,5	%/year	[144]
Inverter sizing factor	1,4	AC/DC	[145]

Source: Own elaboration through references indicated in the table.

Table 37 – Ammonia production assumptions.

Parameter	*Value*	*Unit*	*Reference*
CAPEX ammonia synthesis	3300	USD/kg NH3/ hr	[100]
OPEX ammonia synthesis	2	% CAPEX	[99]
Electricity for synthsis	0.65	kWh / kg NH3	[99]
CAPEX air separation unit	1450	USD/kg N2/ hr	[100]
OPEX air separation unit	2	% CAPEX/year	[99]
Electricity for air separation	0.265	kWh / kg N2	[99]
N2 consumption	0.9	kg/kg NH3	-
H2 consumption	0.177	kg/kg NH3	-

Source: Own elaboration through references indicated in the table.

Table 38 – Methanol production assumptions.

Parameter	*Value*	*Unit*	*Reference*
CAPEX methanol synthesis	800	EUR/kW MeOH	[146]
H2 consumption	0,208	kg/kg MeOH	[146]
CO2 consumption	1,45	kg/kg MeOH	[146]
CO2 supply cost	100	EUR/ton CO2	[146]
Methanol storage cost	100	EUR/ton MeOH	[146]
OPEX methanol synthesis	23	EUR/kW MEoH/year	[147]
CAPEX CO2 capture	93,379	EUR/kW MEoH	[147]
CO2 capture power consumption	1,5	kWh/kg MeOH	[147]
Methanol synthesis power consumption	0,75	kWh/kg MeOH	[147]

Source: Own elaboration through references indicated in the table.

B – Economic, environmental, social and technical constraints for GeoH$_2$-PAM

Economic Constraints

Navigation Routes: For solar PV and onshore wind, navigation routes are not applicable, as these technologies are predominantly installed on land where maritime traffic does not influence siting decisions. In contrast, for offshore wind, the dataset—developed using AIS data from a collaboration between the IMF and World Bank [148]—captures ship traffic density in raster cells approximately 500 m by 500 m. A high-density threshold of 1,400 ships/km²/year is used to exclude areas with intensive shipping activity. This exclusion is critical to avoid potential conflicts with maritime navigation, minimize risks to turbine installations, and ensure compliance with safety regulations in busy sea lanes. Figure 41illustrates the above mentioned data.

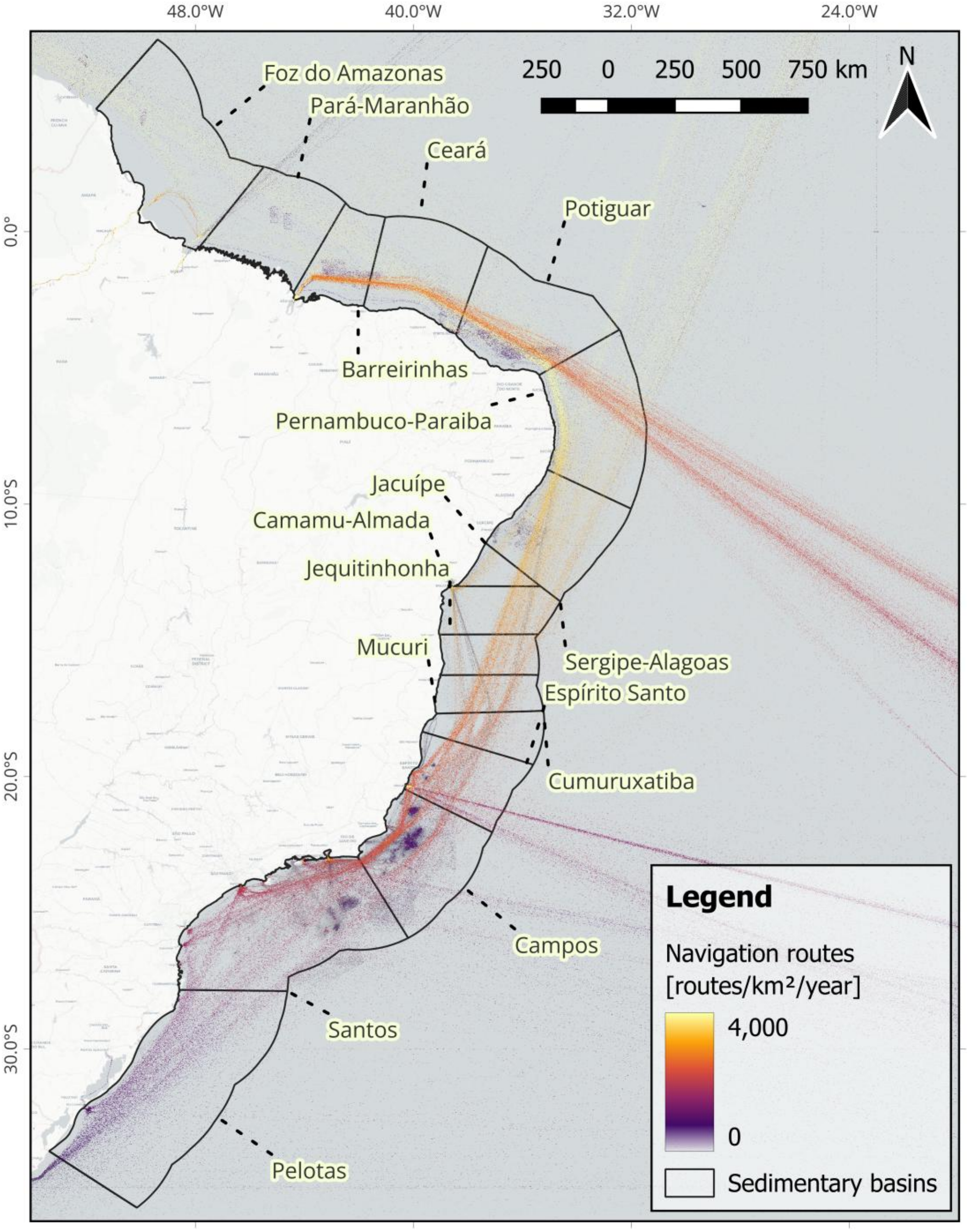

Figure 41 – Navigation routes layer dataset.
Source: Own elaboration with data from [148].

Oil & Gas Pipelines: The oil and gas pipelines dataset, maintained by EPE and ANP, includes details on various types of pipelines. A uniform setback exclusion of 100 meters is applied across all three RES. This restriction is imposed to ensure safe distances between energy infrastructure and pipeline corridors, thereby reducing the risk of accidental interference, damage, or safety hazards during construction and operation.

Oil & Gas Fields: Similarly, the dataset on oil and gas fields—sourced from ANP's *Superintendência de Dados Técnicos*—covers exploratory blocks and production fields. A setback of 250 meters is uniformly applied for SPV, ONW, and OFW. This exclusion zone is established to prevent conflicts with existing hydrocarbon operations, minimize interference with extraction activities, and adhere to regulatory guidelines governing resource exploitation areas. Oil & Gas Fields and Pipelines are illustrated in Figure 42.

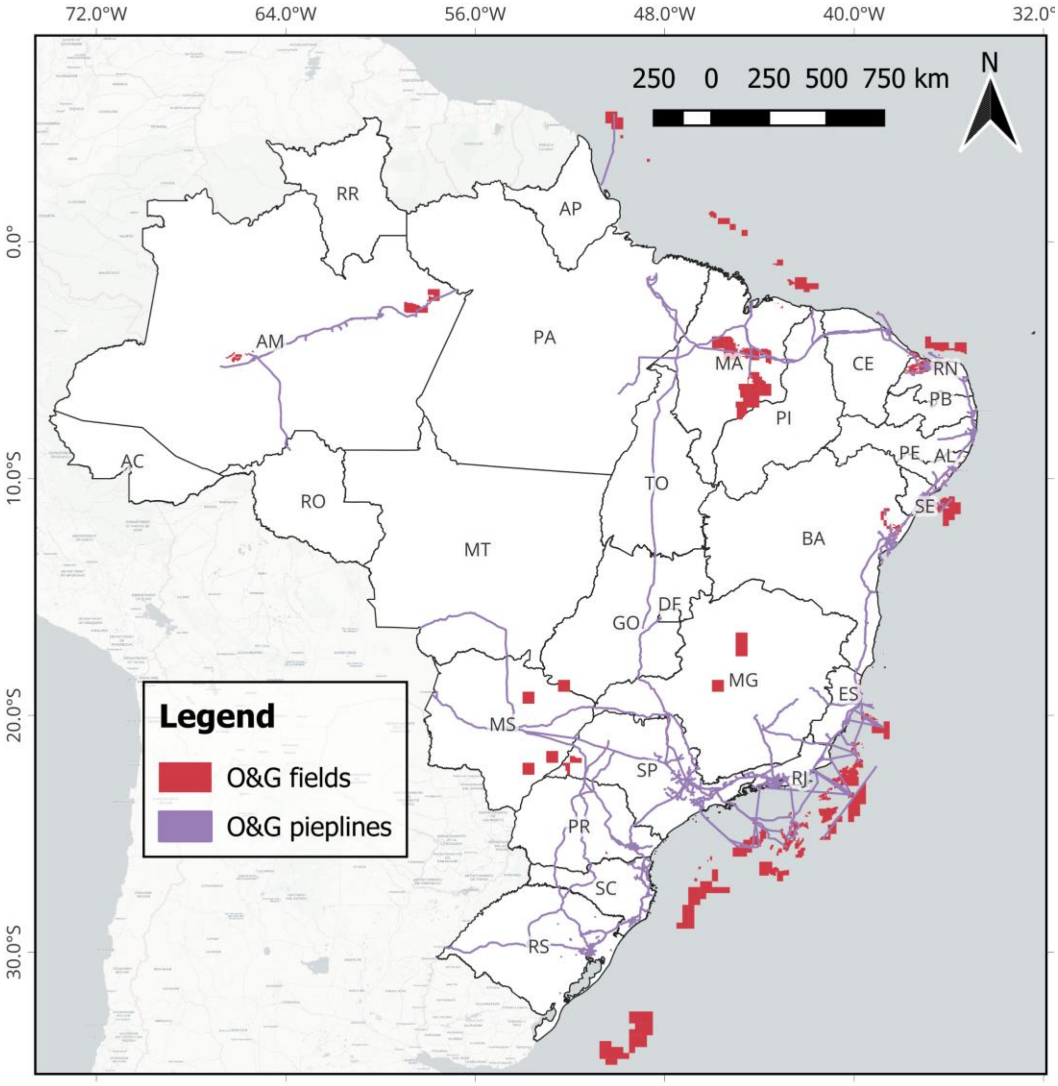

Figure 42 – Oil & Gas fields and pipelines layers dataset.
Source: Own elaboration with data from [149].

Transport Infrastructure: Transport infrastructure data encompass waterways, railways, and highways, sourced from agencies such as ANTAQ, DNIT, and related bodies. For solar PV installations, a conservative setback exclusion of 50 meters is applied, reflecting the relatively lower interference risk on built-up urban or peri-urban sites. In contrast, for both onshore and offshore wind, a more substantial setback of 300 meters is imposed. This larger buffer accounts for the higher physical footprint and potential visual or operational conflicts with major transport corridors, thereby ensuring that wind installations do not adversely affect transportation networks or vice versa. Figure 43 illustrates the transport infrastructure constraint.

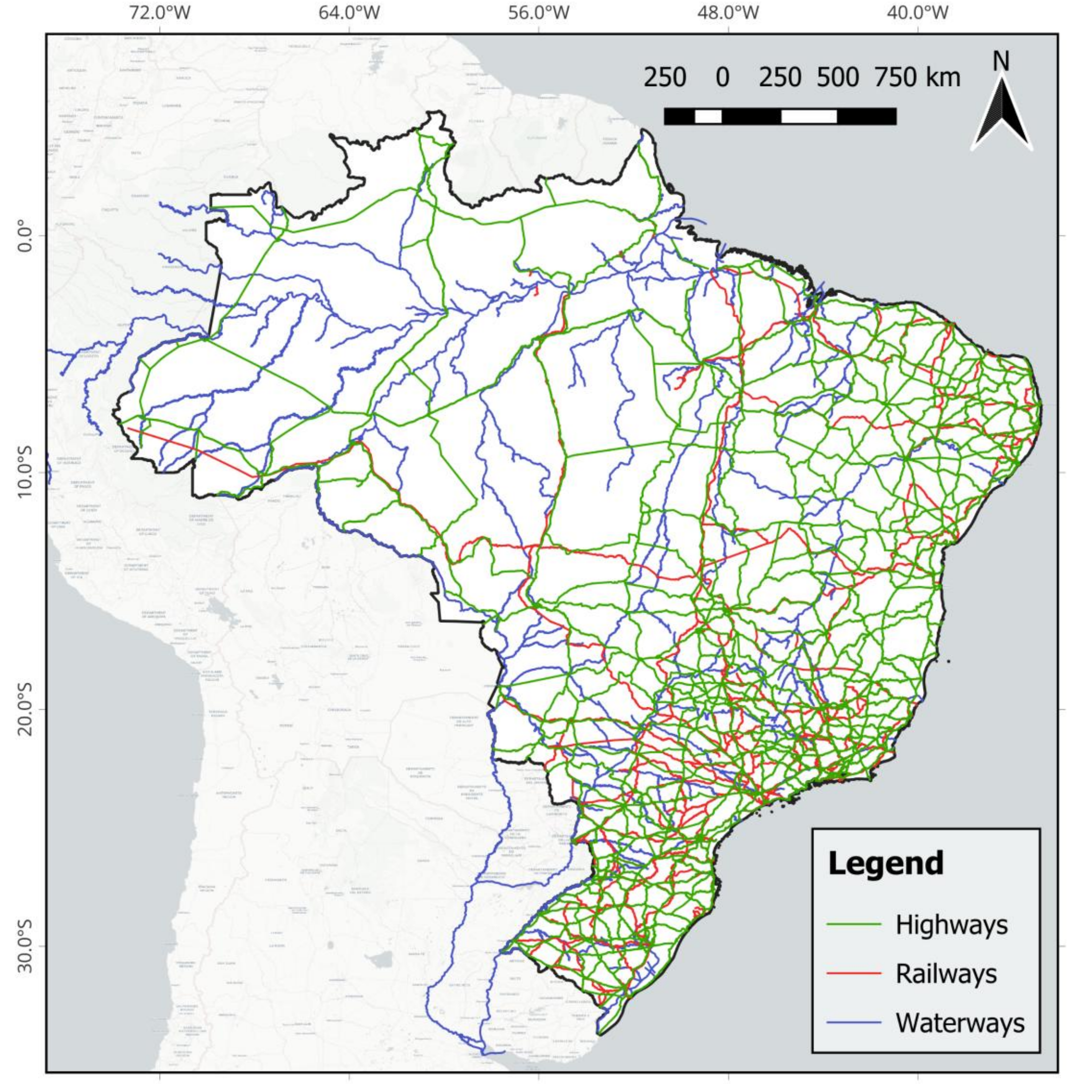

Figure 43 – Transport infrastructure layer dataset.
Source: Own elaboration with data from [150].

Environmental Constraints

Coastal Setbacks (Viewshed Setbacks): Coastal setbacks are not applicable for solar PV or onshore wind, as these installations are typically inland or in non-coastal regions. For offshore wind, however, a coastal setback is critical. Derived from IBGE (2023) data, a buffer of 12 nautical miles (approximately 22 km) is excluded from the coastline to protect coastal viewsheds, preserve maritime ecosystems, and adhere to coastal zone management policies.

Conservation Units: This dataset, provided by the Ministry of the Environment (MMA) and maintained in the National Register of Conservation Units (CNUC), is applied uniformly as an exclusion criterion across SPV, ONW, and OFW. The complete exclusion of conservation units is mandated to preserve legally protected areas and maintain ecological integrity, ensuring that renewable energy development does not encroach upon vital biodiversity reserves.

Priority Areas for Biodiversity Conservation: Although the dataset from the Brazilian Ministry of the Environment (MMA, 2018) identifies areas of high biodiversity importance and assigns priority levels, the authors have opted not to enforce an automatic exclusion for this layer. Instead, it is flagged as a "very sensible layer" that warrants a broader discussion (see Section XX) in order to balance conservation objectives with renewable energy deployment. This approach allows for case-by-case consideration, recognizing that while these areas are environmentally sensitive, there may be opportunities for sustainable development under stringent management regimes.

Archaeological Sites: Managed by IPHAN [151], the archaeological sites dataset represents culturally and historically significant locations. For solar PV and onshore wind, a full exclusion is applied to prevent any disturbance to cultural heritage sites and comply with legal protections. For offshore wind, this constraint is not applicable, given that such sites are predominantly terrestrial. Figure 44 illustrates Conservation Units, Priority Areas for Biodiversity Conservation and Archaeological Sites layers.

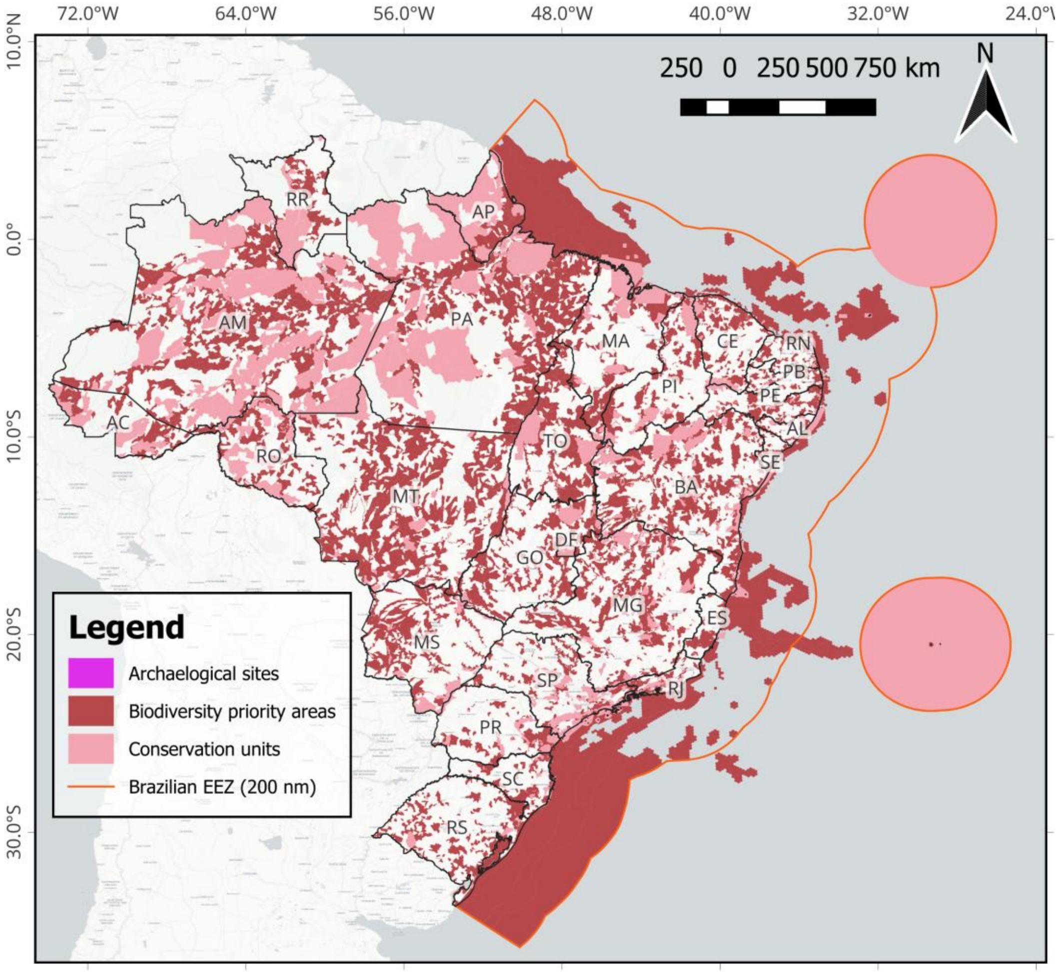

Figure 44 - Conservation Units, Priority Areas for Biodiversity Conservation and Archaeological Sites layers dataset.
Source: Own elaboration with data from [151–153].

Water Bodies: The ANA Water Bodies Dataset [154] maps both natural and artificial water bodies. For SPV and onshore wind installations, exclusion of these areas is essential to avoid conflicts with water resource management and to protect aquatic ecosystems. In the case of offshore wind, water bodies are inherently part of the marine environment; therefore, this constraint is not separately applied. Figure 45 illustrates the water bodies.

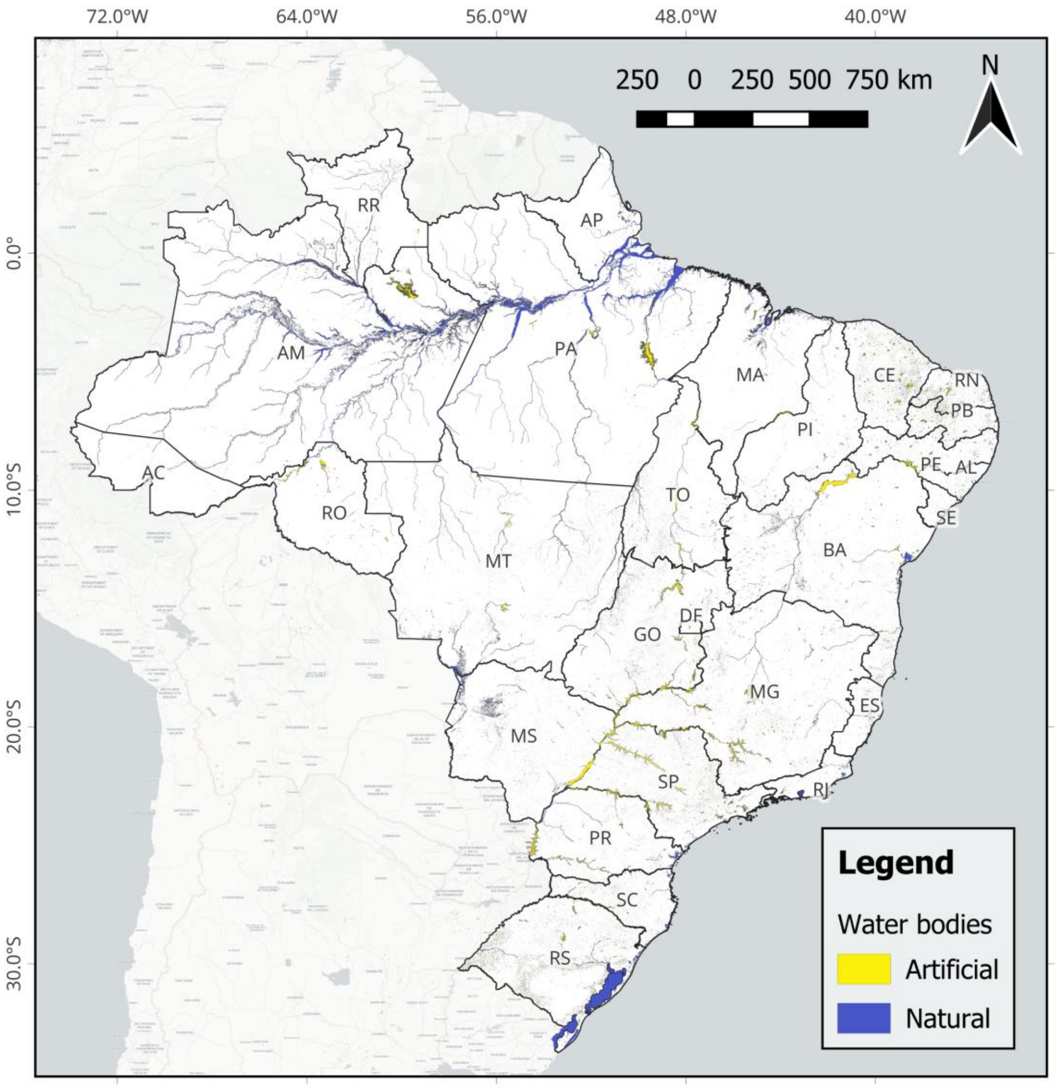

Figure 45 – Water bodies layer dataset.
Source: Own elaboration with data from [154].

Social Constraints

Urbanized Areas: Urbanized areas, as delineated by IBGE [155], are excluded from the siting of solar PV and onshore wind installations to mitigate issues related to population density, land availability conflicts, and potential adverse impacts on urban communities. Since offshore wind installations are located at sea, this constraint is not applicable.

Rural Settlements: Rural settlements, identified through INCRA [156], are excluded for SPV and onshore wind to protect the livelihoods of rural populations and to avoid conflicts with agrarian reform policies. This exclusion is not applicable for offshore wind, where the installations do not encroach on established rural communities.

Quilombola Areas: Quilombola territories, which are legally recognized and culturally significant [156], are excluded for SPV and onshore wind installations. This measure safeguards the rights and heritage of Afro-Brazilian communities. Offshore wind, being situated in the marine environment, is not subject to this constraint.

Indigenous Land: Similarly, indigenous lands are excluded for SPV and onshore wind to respect the territorial rights and cultural practices of indigenous communities [157]. Offshore wind installations are not affected by this restriction due to their non-terrestrial location. Figure 46 illustrates the dataset for the four social constraints.

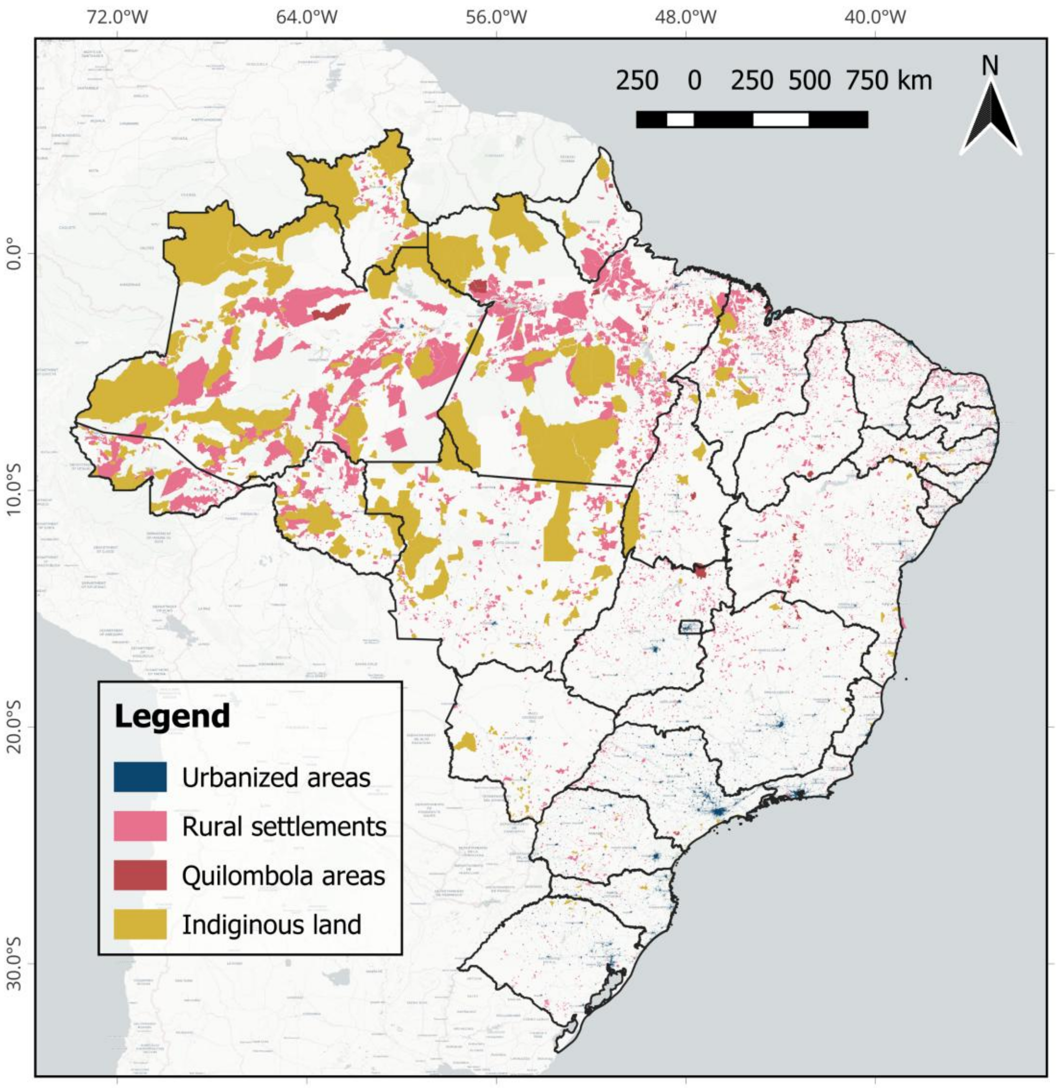

Figure 46 – Social constraints layers dataset.
Source: Own elaboration with data from [155–157].

Technical Constraints

Slope: A slope map derived from SRTM data [158] is used to identify areas where terrain steepness exceeds 75%. For solar PV and onshore wind, areas with slopes greater than 75% are excluded to ensure structural stability, ease of installation, and operational safety. This constraint is not applicable for offshore wind, where bathymetric data is more relevant.

Depth: For offshore wind, bathymetric data [159] inform the depth constraint. The threshold is set such that fixed foundation turbines are limited to depths less than 60 meters, while floating foundations are considered viable in depths ranging from 60 to 1300 meters. Areas with depths exceeding 1300 meters are excluded due to current technological limitations in constructing and maintaining turbines in such deep waters. This constraint is not applicable to SPV or onshore wind. Figure 47 illustrates the slope and ocean depth.

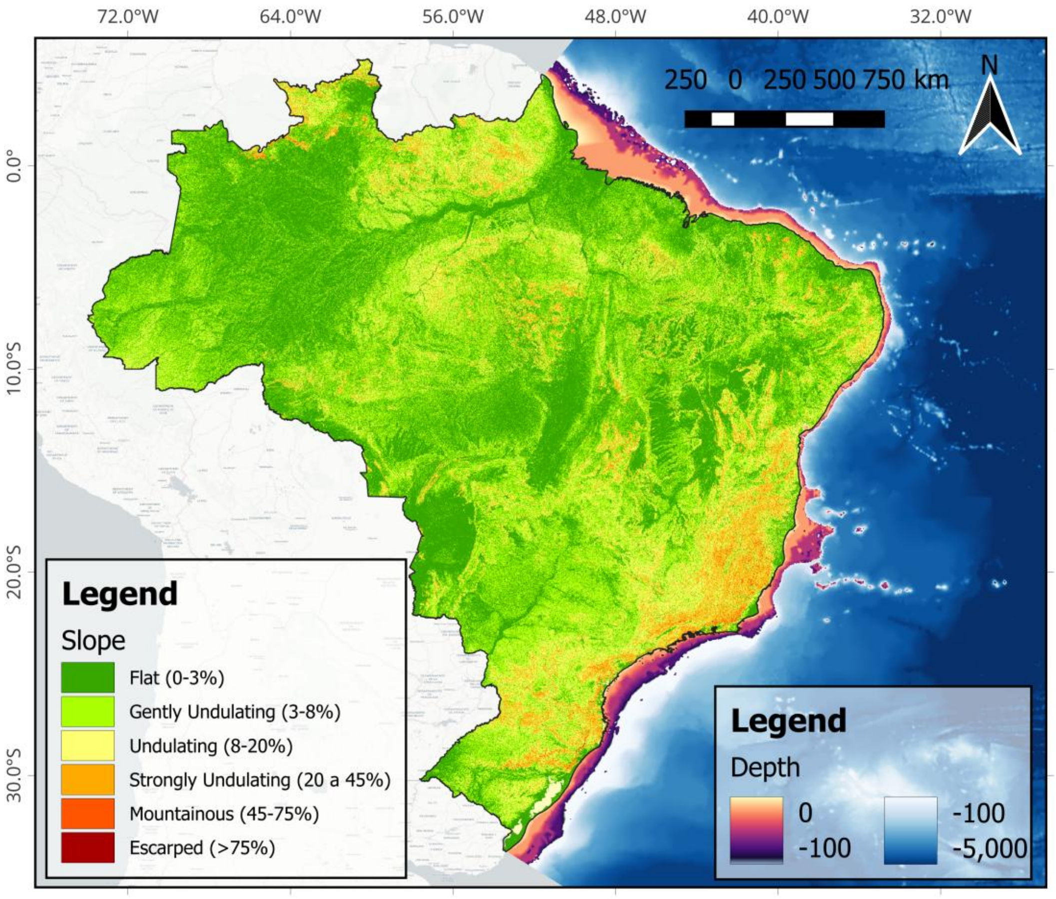

Figure 47 – Slope and depth constraints layers dataset.
Source: Own elaboration with data from [158,159].

Distance from Shore: This technical constraint is applied exclusively to offshore wind. To ensure operational feasibility and data reliability, installations are restricted to a maximum distance of 200 kilometers from the shore, corresponding to the spatial extent of the Exclusive Economic Zone (EEZ) and the coverage limits of the Global Wind Atlas [79].

Capacity Factor: Capacity factor data, modeled from the Global Solar Atlas (GSA) 2.0 for SPV and the Global Wind Atlas (GWA) 3.1 for wind, are used to assess resource quality. For solar PV, areas with capacity factors below 15% are excluded, ensuring that only regions with adequate solar irradiance are considered. For onshore wind, the threshold is set at 20%, reflecting the typically lower but still viable wind resource on land. For offshore wind, a higher threshold of 30% is applied to capture the enhanced wind performance expected over open waters. These thresholds are critical to ensure that the resulting technical potential reflects areas with high operational efficiency. The dataset for capacity factors are illustrated in Figure 4 and Figure 5 (Section 3.1).

Power Transmission Cables: Finally, the dataset on power transmission cables, maintained by EPE, informs a setback exclusion. For solar PV, a 50-meter setback is applied, whereas for both onshore and offshore wind, a 500-meter setback is required. These setbacks ensure that new installations do not interfere with existing or planned transmission infrastructure, thereby enhancing safety and reducing the risk of damage during construction or operation. Figure 48 illustrates the transmission lines data layer.

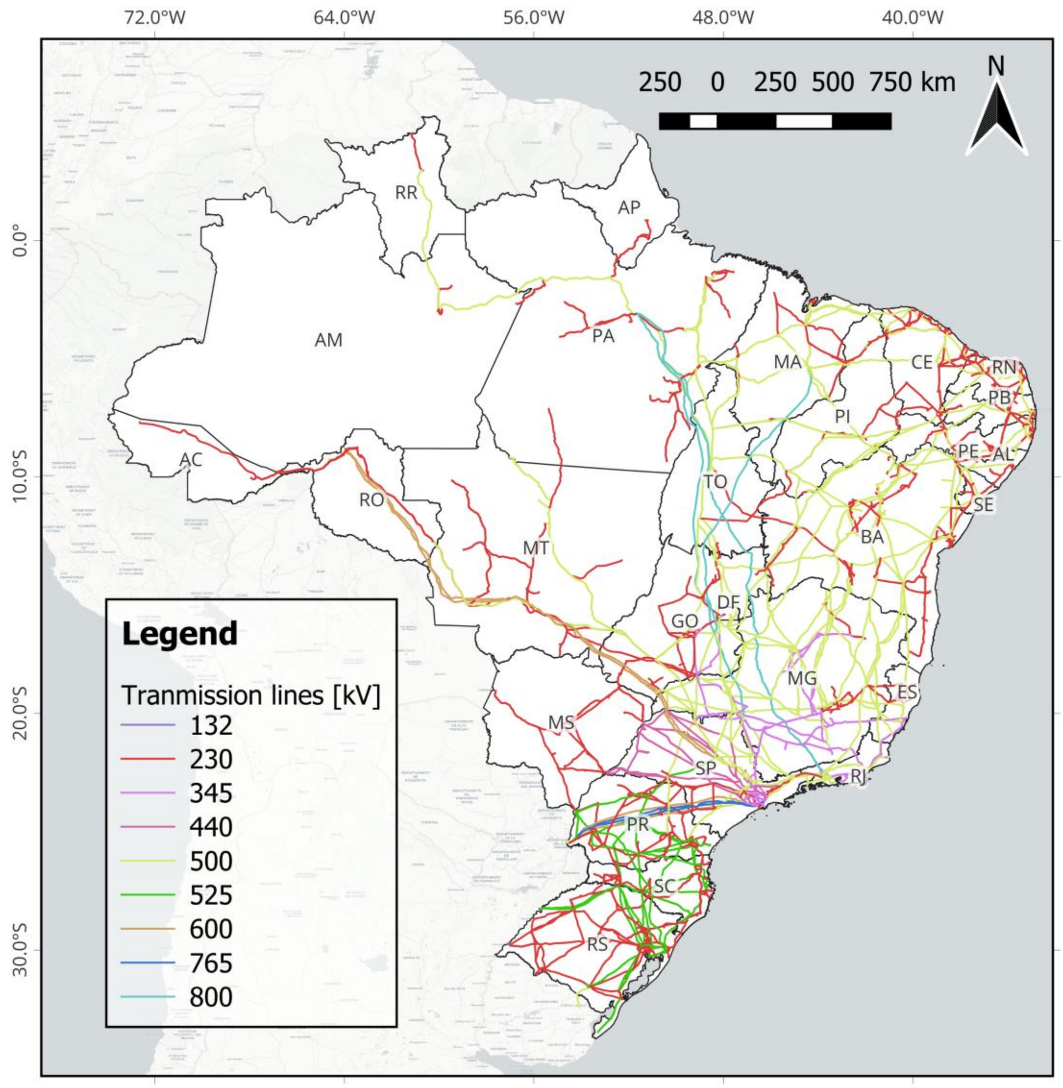

Figure 48 – Transmission lines layer dataset.
Source: Own elaboration with data from [160].

Table 39 presents the complete constraint dataset table for SPV, ONW and OSW.

Table 39 – Complete description of geospatial constraints layers applied for the technical and economic assessment of renewable energy and hydrogen production potential in Brazil.

Classification	Layer	Description and source	Solar PV	Onshore Wind	Offshore wind
Economic	Navigation routes	This dataset provides global ship traffic density raster layers, developed through a partnership between the IMF and World Bank, using AIS (Automatic Identification System) data collected hourly between January 2015 and February 2021. The dataset consists of six ship density layers, categorized by vessel type: commercial ships, fishing vessels, oil & gas platforms, passenger ships, leisure vessels, and a combined global layer representing all ship categories. Each raster grid cell measures approximately 500m x 500m at the Equator and indicates the general intensity of shipping activity, including both moving and stationary vessels [148].	N/A	N/A	Exclusion of high-density routes above 1400 ships/km2/year
Economic	Oil & Gas pipelines	This dataset is compiled and maintained by Empresa de Pesquisa Energética (EPE), with contributions from ANP and various industry operators. It covers four main types of pipelines: distribution pipelines, transportation pipelines, gathering pipelines, and oil pipelines from the Indicative Oil Pipeline Plan (PIO). The dataset includes spatial and technical details on pipeline routes, lengths, diameters, capacities, fluid types (natural gas, oil, condensate), and key origin-destination points such as production fields, processing plants, and consumer delivery points [149].	100 m setback exclusion	100 setback exclusion	100 setback exclusion
Economic	Oil & Gas fields	This dataset provides georeferenced information on exploratory blocks and production fields under contract in Brazil. Maintained by the Superintendência de Dados Técnicos (SDT) of ANP, it includes data related to exploration blocks from bidding rounds, production-sharing agreements, onerous assignment areas, and permanent offers [149].	250 m setback exclusion	250 m setback exclusion	250 m setback exclusion

Classification	Layer	Description and source	Solar PV	Onshore Wind	Offshore wind
Economic	Transport infrastructure (Waterways, railways and highways)	The transportation databases provide geospatial information on key infrastructure in Brazil, covering waterways, railways, and highways. The waterways dataset (Hidrovias ANTAQ) illustrates the location of navigable rivers and their attributes, maintained by the National Waterway Transportation Agency (ANTAQ). The railway network database focuses on Brazil's operational and planned railway segments, highlighting freight and passenger rail routes. The highways dataset, updated by the National Department of Infrastructure and Transportation (DNIT), details federal, state, and municipal roads, including classification by type (radial, longitudinal, transversal, diagonal, and connector roads) and current status [150].	50 m setback exclusion	300 m setback exclusion	300 m setback exclusion
Environmental	Coastal setbacks (viewshed setbacks)	This dataset consists of a buffer layer created from the Brazilian coastal limit, based on data provided by IBGE [161]. The buffer was generated to represent a setback zone along the entire coastline of Brazil, intended to support coastal planning and spatial analyses.	N/A	N/A	Exclusion of 12 nautical miles (22 km) from the coast
Environmental	Conservation Units	This dataset from the Ministério do Meio Ambiente provides comprehensive information on active Conservation Units (UCs) registered in the National Register of Conservation Units (CNUC), including their number and area by biome and management category. Key attributes include the identification code and name of each UC, administrative level (federal, state, or municipal), management category as per Law 9.985/2000, equivalent IUCN category, creation year, legal acts defining the UCs, and geographic coverage by state and municipality [153].	Exclusion	Exclusion	Exclusion

Classification	Layer	Description and source	Solar PV	Onshore Wind	Offshore wind
Environmental	Priority Areas for Biodiversity Conservation	The dataset presents the 2nd Update of Priority Areas for Conservation, Sustainable Use, and Benefit Sharing of Biodiversity in Brazil, coordinated by the Brazilian Ministry of the Environment (MMA). It identifies 2,081 priority areas across Brazil's major biomes—Amazon, Caatinga, Cerrado, Pantanal, Mata Atlântica, Pampa—and the Coastal and Marine Zone. These areas are classified into four priority levels: Extremely High, Very High, High, and Insufficiently Known, based on their biodiversity significance, conservation importance, and socio-environmental context. This classification aims to guide national conservation efforts, restoration activities, and sustainable development policies in line with international biodiversity commitment [152].	Exclusion	Exclusion	Exclusion
Environmental	Archaeological sites	This dataset contains geospatial polygons representing archaeological sites in Brazil, managed and safeguarded by the *Instituto do Patrimônio Histórico e Artístico Nacional* (IPHAN). These sites, classified as federal cultural heritage under the Constitution of the Federative Republic of Brazil of 1988 (Article 216) and Law No. 3,924 of July 26, 1961, include vestiges and locations linked to historical human settlements that contributed to the country's cultural identity. The dataset supports archaeological research, environmental licensing, heritage conservation, and land-use planning. As per Law No. 13,653 of 2018, any intervention in these sites requires prior authorization from IPHAN to prevent unauthorized exploitation, destruction, or alteration, ensuring compliance with national and international heritage preservation frameworks [151].	Exclusion	Exclusion	N/A
Environmental	Water bodies	The ANA Water Bodies Dataset provides a comprehensive mapping of Brazil's natural and artificial water bodies, including lakes, lagoons, reservoirs, dams, and estuaries. This geospatial dataset, maintained by the Brazilian National Water Agency (ANA), supports planning and management actions in the water resources sector and integrates the National Water Resources Information System (SNIRH). Updated in 2020, the dataset includes over 180,000 features and 23 attributes, with spatial representation in vector format and a continuous update status [154].	Exclusion	Exclusion	N/A

Classification	Layer	Description and source	Solar PV	Onshore Wind	Offshore wind
Social	Urbanized areas	This dataset provides a geospatial representation of various types of urban and peri-urban areas in Brazil, categorized by IBGE's 'Urbanized Areas of Brazil 2019' classification [155]. It includes polygons of densely and sparsely populated urban areas, approved but undeveloped subdivisions, intraurban voids (non-built areas such as parks and water bodies), remaining intraurban voids (smaller voids resulting from urban expansion), and other urban equipment (non-residential facilities such as airports, ports, and industrial sites located near urban areas).	Exclusion	Exclusion	N/A
Social	Rural settlements	This dataset consists of geospatial polygons representing rural settlement areas in Brazil, primarily established through the agrarian reform program led by INCRA (National Institute for Colonization and Agrarian Reform). These settlements are large-scale, socio-economic initiatives aimed at providing land access to landless rural workers while promoting sustainable production systems [156]**.**	Exclusion	Exclusion	N/A
Social	Quilobola areas	This dataset consists of geospatial polygons representing quilombola territories across Brazil, as recognized under national legislation and formalized by the National Institute for Colonization and Agrarian Reform (INCRA). These territories are historically significant areas, occupied by Afro-Brazilian communities descended from escaped enslaved people and others who established themselves through subsistence farming, inheritance, or peaceful land possession. The dataset is essential for territorial planning, socio-environmental studies, and ensuring the rights and cultural preservation of quilombola communities, as guaranteed by Brazil's 1988 Constitution and subsequent regulations, including Decree 4.887/2003 [156]**.**	Exclusion	Exclusion	N/A
Social	Indigenous land	This dataset comprises geospatial polygons and point features delineating Brazil's officially recognized Indigenous Lands, villages, and regional/local coordination zones, as maintained by the National Indian Foundation (FUNAI) through its Geoprocessing Coordination. It reflects the legally demarcated territories of Brazil's diverse Indigenous peoples—lands protected under Article 231 of the 1988 Constitution and subsequent FUNAI regulations [157]**.**	Exclusion	Exclusion	N/A

Classification	Layer	Description and source	Solar PV	Onshore Wind	Offshore wind
Technical	Slope	This dataset consists of a slope map of the Brazilian terrain, developed using SRTM (Shuttle Radar Topography Mission) data as a base. The slope classification follows the standards of IBGE and EMBRAPA, categorizing relief into six classes: Flat (0-3%), Gently Undulating (3-8%), Undulating (8-20%), Strongly Undulating (20-45%), Mountainous (45-75%), and Steep (>75%) [158].	Exclusions of slopes >75%	Exclusions of slopes >75%	N/A
Technical	Depth	This dataset comprises vector files (shapefiles) representing Brazil's bathymetry, developed under a Technical Cooperation Agreement between CPRM and ANP. It utilizes data from the General Bathymetric Chart of the Oceans (GEBCO) with a spatial resolution of 925 meters, derived from interpolated ship-based soundings and satellite gravity data [159].	N/A	N/A	Exclusion of deaphs > 1300 m
Technical	Distance from shore	Restricted to a range of 200 km owing to the technical challenges and the insufficiency of wind potential database [79].	N/A	N/A	Maximum of 200km from the shore in the EEZ.
Technical	Capacity Factor	This dataset provides modeled capacity factor values for renewable energy systems across Brazil. It combines data from the Global Solar Atlas (GSA) 2.0 for solar PV and the Global Wind Atlas (GWA) 3.1 for onshore and offshore wind [76,79].	Exclusion of areas <15% capacity factor	Exclusion of areas <20% capacity factor	Exclusion of areas <30% capacity factor
Technical	Power transmission cables	This dataset provides geospatial data on Brazil's energy transmission lines, both planned and in operation, maintained by the Empresa de Pesquisa Energética (EPE). It includes polyline geometries representing transmission line routes with detailed attributes such as name, owner (concessionaire), voltage level (ranging from 132 kV to 800 kV), operational or planned year, and length [160].	50 m setback exclusion	500 m setback exclusion	500 m setback exclusion

Source: Own elaboration through references indicated in the table.

C – Default assumptions and user-definable input data for GeoH$_2$-FAT

Table 40 - Example of default and user-definable assumptions for the GeoH$_2$-FAT.

Category	*Parameter*	*Unit*	*Value*
General	Construction period	months	18
	Projection start date	dd/mm/yyyy	01-Dec-22
Energy Generation	PV plant – DC/AC ratio	Wp/W	1.30
	PV modules degradation rate	%/year	0.5 %
	PV global performance ratio	%	80.0 %
	Wind complex – performance reduction rate	%/year	1.0 %
Hydrogen Production	Electrolyser degradation rate	%/year	1.0 %
Capital Expenditure (CAPEX)	Electrolyser overhaul cost	% of electrolyser CAPEX	35.0 %
	PV specific CAPEX	R$/W	4.00
	PV module share	% of PV specific CAPEX	42.0 %
	Inverter share	% of PV specific CAPEX	23.0 %
	Mounting & installation share	% of PV specific CAPEX	18.0 %
	Engineering services share	% of PV specific CAPEX	17.0 %
	PV CAPEX – auxiliary equipment & systems	% of PV CAPEX	72.0 %
	PV CAPEX – connection & transmission	% of PV CAPEX	12.0 %
	PV CAPEX – civil works	% of PV CAPEX	8.0 %
	PV CAPEX – land & environmental measures	% of PV CAPEX	1.0 %
	PV CAPEX – other	% of PV CAPEX	7.0 %
	Wind specific CAPEX	R$/W	4.75
	Other costs	% of main CAPEX	0.10 %
	Contingencies	% of main CAPEX	0.50 %
	CAPEX in year 1 of construction	% of final CAPEX	60.0 %
	Residual value – main equipment	% of main CAPEX	60.0 %
	Residual value – remaining assets	% of remaining CAPEX	80.0 %
Operational Expenditure (OPEX)	H_2 production O&M	% of electrolyser CAPEX	3.0 %
	PV O&M	R$/kW·yr	60.00
	Wind O&M	R$/kW·yr	65.00
ACL & I-REC	I-REC admission fee	R$/yr	1,300.00
	I-REC annual fee	R$/yr	12,000.00
	I-REC platform admission	R$	15,000.00
	I-REC certificate issuance cost	R$/MWh	0.27
	I-REC certificate transaction fee	R$/MWh	0.36
	ACL standard tariff	R$/MWh	231.01
Transmission Charges (EOL & UFV)	TUST	R$/kW·month	7.00
Operation	Working capital	% of OPEX	1.00 %
	Ramp-up time	months	12
	Ramp-up production	% of max production	50.0 %
	Overhaul interval	months	120
Economic & Financial	Exchange rate	BRL/USD	5
	Price adjustment base date	dd/mm/yyyy	01-Dec-22

Category	Parameter	Unit	Value
	PIS	% of gross revenue	1.15 %
	COFINS	% of gross revenue	5.30 %
	Fixed component of TLP	%/yr	2.94 %
Financing – Loan 1	Share	% of final CAPEX	25.00 %
	Base interest rate	%/yr	1.30 %
	Amortisation term	months	240
	Risk spread	—	1.50 %
	Grace period after construction	months	6
	Amortisation method	—	SAC
	Amortisation frequency	—	Monthly
Financing – Loan 2	Share	% of final CAPEX	15.00 %
	Base interest rate	%/yr	1.30 %
	Amortisation term	months	216
	Risk spread	—	1.50 %
	Grace period after construction	months	6
	Amortisation method	—	SAC
	Amortisation frequency	—	Monthly
Financing – Grants	Share	% of final CAPEX	10.00 %

Source: Own elaboration.

Table 41 - Example of user-definable inputs, support results, and supporting information for the GeoH$_2$-FAT.

Category	Parameter	Unit	Entry
General	Commercial operation start date	dd/mm/yyyy	01-Jan-25
	Project lifetime	years	20
	Commercial operation end date	dd/mm/yyyy	31-Dec-44
	Construction start date	dd/mm/yyyy	01-Jul-23
Energy	**Photovoltaic plant (UFV)**		
	DC capacity	kWp	30,000
	AC capacity	kW	23,077
	State	–	Bahia
	Municipality	–	Candeias
	Latitude	decimal degrees	–12.6711
	Longitude	decimal degrees	–38.5405
	Module model	–	DAH DHM-72X10-530W
	Specific CAPEX	R$/W	4.00
	Annual average generation	MWh/yr	41,782
	Wind complex (EOL)		
	Capacity	kW	18,000
	State	–	Bahia
	Municipality	–	Candeias
	Latitude	decimal degrees	–12.6711
	Longitude	decimal degrees	–38.5405
	Turbine model	–	Vestas V90-2.0
	Specific CAPEX	R$/W	4.75
	Annual average generation	MWh/yr	33,924
Hydrogen Production	State	–	Bahia
	Municipality	–	Candeias
	Electrolyser model	–	SiLYZER 300
	Capacity	kW (H_2)	10,000
	Capacity factor	%	80 %
	Production mode	–	CONSTANT PRODUCTION
	Annual average consumption	MWh/yr	66,361
H_2 Storage	Physical storage state	–	Gaseous

	Storage type	–	Pressurized tanks
	Maximum storage cost	R$/yr	991,050.34
H_2 Transport	Destination state	–	Bahia
	Destination municipality	–	Camaçari
	Transport distance	km	30.5
	Maximum transport cost	R$/yr	6,259,265.28
CAPEX	Main CAPEX	R$	222,084,001.30
	Electrolyser CAPEX	R$	44,276,308.99
	PV CAPEX	R$	92,307,692.31
	Wind CAPEX	R$	85,500,000.00
	Other costs	% of main CAPEX	0.10 %
	Contingencies	% of main CAPEX	0.50 %
	Final CAPEX	R$	223,416,505.30
	CAPEX in year 1 of construction	% of final CAPEX	50.00 %
	Residual value – main equipment	% of main CAPEX	50.00 %
	Residual value – remaining assets	% of remaining CAPEX	60.00 %
Operation	Working capital	% of OPEX	1.00 %
	Levelised cost of H_2 (production + transport)	R$/kg H_2	30.37
	Arbitrated selling price	R$/kg H_2	51.00
	Ramp-up time	months	12
	Ramp-up production	% of max production	50.00 %
	Overhaul interval	months	96
	ACL selling/purchase price	R$/MWh	70.00
Fiscal & Tax	Exchange rate	BRL/USD	5.00
	ICMS	% of gross revenue	23.40 %
	IRPJ/CSLL	% of profit before tax	34.00 %
	Long-term inflation rate	% per year	5.00 %
Financing – Loan 1	Share	% of final CAPEX	60.00 %
	Base interest rate	% per year	1.30 %
	Total financing cost	% per year	2.80 %
	Amortisation term	months	200
	Risk spread	–	1.50 %
Financing – Loan 2	Share	% of final CAPEX	0.00 %
	Base interest rate	% per year	1.30 %
	Fixed component of TLP rate	% per year	0.00 %
	Total financing cost	% per year	0.00 %
	Amortisation term	months	216
	Risk spread	–	1.50 %
Financing – Grants	Share	% of final CAPEX	0.00 %
Financing – Equity	Share	% of final CAPEX	40.00 %
	Cost of equity	% per year	5.00 %
Totals	Average real debt cost (with tax benefit)	% per year	1.85 %
	Average real equity cost (with tax benefit)	% per year	3.11 %

Source: Own elaboration.

D – Reference emissions for environmental comparison results

Table 42 - Emissions associated with different combustion-based technologies and transport applications

Ref.	***Application / Vehicle***	***Fuel (origin)***	***Power-train / Technology***	***H_2 / other-fuel consumption(g/(t.km))***	***GHG emissions (kg CO_2eq / (FU)***
[127]	Marítima (carga - 51500 t)	Amônia verde (Eólico)	95% ICE + 5% turbina a vapor	*0 / 7,1 (g/(t.km))*	*0,0053 (kg CO_2eq / (t.km)*
[127]	Marítima (carga - 51500 t)	Amônia verde (Hídrica)	95% ICE + 5% turbina a vapor	*0 / 7,1 (g/(t.km))*	*0,0049 (kg CO_2eq / (t.km))*
[127]	Marítima (carga - 51500 t)	HFO (diesel marítimo pesado)	95% ICE + 5% turbina a vapor	*0 / 0,85 (g/(t.km))*	*0,0108 (kg CO_2eq / (t.km))*
[127]	Marítima (carga - 51500 t)	Hidrogênio (Eólico)	95% ICE + 5% turbina a vapor	*1,1 / 0 (g/(t.km))*	*0,0024 (kg CO_2eq / (t.km))*
[127]	Marítima (carga - 51500 t)	Hidrogênio (Eólico) + Diesel marítimo (50:50 em base energética)	95% ICE + 5% turbina a vapor	*0,55 / 0,42 (g/(t.km))*	*0,0064 (kg CO_2eq / (t.km))*
[127]	Marítima (carga - 51500 t)	Hidrogênio (Hídrica)	95% ICE + 5% turbina a vapor	*1,1 / 0 (g/(t.km))*	*0,0020 (kg CO_2eq / (t.km))*
[127]	Marítima (carga - 51500 t)	Hidrogênio (Hídrica) + Diesel marítimo (50:50 em base energética)	95% ICE + 5% turbina a vapor	*0,55 / 0,42 (g/(t.km))*	*0,0061 (kg CO_2eq / (t.km))*
[132]	Marítima (ferry - 12000 t)	Gás natural	ICE	*0 / 2,0 (g/(t.km))*	*0,0112 (kg CO_2eq / (t.km))*
[132]	Marítima (ferry - 12000 t)	MGO (gasolina marítima)	ICE	*0 / 2,0 (g/(t.km))*	*0,0115 (kg CO_2eq / (t.km))*
[127]	Marítima (tanker– 100000t)	Amônia verde (Eólico)	38% ICE + 62% turbina a vapor	*0 / 1,9 (g/(t.km))*	*0,0020 (kg CO_2eq / (t.km))*
[127]]	Marítima (tanker - 100000t)	Amônia verde (Hídrica)	38% ICE + 62% turbina a vapor	*0 / 1,9 (g/(t.km))*	*0,0018 (kg CO_2eq / (t.km))*
[127]	Marítima (tanker - 100000t)	HFO (diesel marítimo pesado)	38% ICE + 62% turbina a vapor	*0 / 0,85 (g/(t.km))*	*0,0055 (kg CO_2eq / (t.km))*
[127]	Marítima (tanker - 100000t)	Hidrogênio (Eólico)	38% ICE + 62% turbina a vapor	*0,29 / 0 (g/(t.km))*	*0,0012 (kg CO_2eq / (t.km))*
[127]	Marítima (tanker - 100000t)	Hidrogênio (Eólico) + Diesel marítimo (50:50 em base energética)	38% ICE + 62% turbina a vapor	*0,14 / 0,42 (g/(t.km))*	*0,0033 (kg CO_2eq / (t.km))*
[127]	Marítima (tanker - 100000t)	Hidrogênio (Hídrica)	38% ICE + 62% turbina a vapor	*0,29 / 0 (g/(t.km))*	*0,0011 (kg CO_2eq / (t.km))*
[127]	Marítima (tanker - 100000t)	Hidrogênio (Hídrica) +	38% ICE + 62%	*0,14 / 0,42 (g/(t.km))*	*0,0032(kg CO_2eq / (t.km))*

		Diesel marítimo (50:50 em base energética)	turbina a vapor		
[122]	Rodoviária (127 kW)	Diesel	Hybrid ICE	-	0,2170 (kg CO_2eq/km)
[122]	Rodoviária (118 kW)	Diesel	ICE	-	0,2530 (kg CO_2eq / km)
[135]	Rodoviária (não especificado)	Etanol de cana de açúcar	ICE	0 / 96,7 (g/km)	0,1090 (kg CO_2eq / km)
[134]	Rodoviária (80 kW)	Gás natural	Hybrid ICE	0 / 23,1 (g/km)	0,1004 (kg CO_2eq / km)
[122]	Rodoviária (121 kW)	Gás natural	ICE	-	0,2410 (kg CO_2eq / km)
[134]	Rodoviária (80 kW)	Gás natural	ICE	0 / 39,1 (g/km)	0,1317 ± 0,0282 (kg CO_2eq / km)
[122]	Rodoviária (126 kW)	Gasolina	Hybrid ICE	-	0,2500 (kg CO_2eq / km)
[122, 124,125,135]]	Rodoviária (117 kW; 130 kW; não especificado)	Gasolina	ICE	-	0,2999 (kg CO_2eq / km)
[134]	Rodoviária (80 kW)	Hidrogênio + Gás natural (hidrogênio: 20%vol ou 7,3% da energia)	ICE	0,84/28,2 (g/km)	0,1106 (kg CO_2eq / km)
[134]	Rodoviária (80 kW)	Hidrogênio + Gasolina (hidrogênio: 7,3% da energia)	ICE Dual fuel	0,91/31,0 (g/km)	0,1301 (kg CO_2eq / km)
[134]	Rodoviária (80 kW)	Hidrogênio verde	Hybrid ICE	12,7 / 0 (g/km)	0,0410 (kg CO_2eq / km)
[134]	Rodoviária (80 kW)	Hidrogênio verde	ICE	16,8 / 0 (g/km)	0,0434 (kg CO_2eq / km)

Source: Own elaboration.

Table 43 - Emissions associated with different electric-powertrain technologies and applications.

Ref.	***Application / Vehicle***	***Fuel (origin)***	***Power-train / Technology***	***H_2 / other-fuel consumption (g/km ou g/(t.km) ou kWh/km)***	***Equivalent cradle-to-grave emissions (kgCO2eq/FU)***
[132]	Marítima (ferry - 12000 t)	Hidrogênio verde	PEMFC	2,0 / 0 (g/(t.km))	0,0105 (kg CO2eq / (t.km))
[135]	Rodoviária (56 kW)	Etanol de cana de açúcar	SOFC	0 / 39,5 (g/km)	0,1640 (kg CO2eq / km)
[135]	Rodoviária (56 kW)	Etanol de milho	SOFC	0 / 39,5 (g/km)	0,1790 (kg CO2eq / km)
[122]	Rodoviária (145 kW)	Hidrogênio (Eólico)	PEMFC	13,6 / 0 (g/km)	0,0992 ± 0,0429 (kg CO2eq / km
[135]	Rodoviária (80 kW)	Hidrogênio (matriz elétrica brasileira 2019)	PEMFC	10,5 / 0 (g/km)	0,3010 (kg CO2eq / km
[122,124]	Rodoviária (40;145 kW)	Hidrogênio (Solar)	PEMFC	11,9 / 0 (g/km)	0,1423 (kg CO2eq / km
[134]	Rodoviária (80 kW)	Hidrogênio verde	PEMFC	7,6 / 0 (g/km)	0,0560 (kg CO2eq / km

Source: Own elaboration.